High Resolution Laser Spectroscopy of the ν_8 Vibrational Band of Sulfuryl Fluoride

by

Vernon Thomas Davis

B.S. United States Military Academy

(1981)

Submitted to the Department of Physics

in partial fulfillment of the requirements for the degree of

Master of Science in Physics

at the

MASSACHUSETTS INSTITUTE OF TECHNOLOGY

June 1991

Signature of Author.....

Department of Physics

June 5, 1991

Certified by.....

Ali Javan

Professor of Physics

Thesis Supervisor

Accepted by.....

George F. Koster

Chairman, Departmental Committee on Graduate Students

High Resolution Laser Spectroscopy of the ν_8 Vibrational Band of Sulfuryl Fluoride

by

Vernon Thomas Davis

Submitted to the Department of Physics

on June 5, 1991, in partial fulfillment of the

requirements for the degree of

Master of Science in Physics

Abstract

A tunable diode laser is used to investigate the ν_8 vibrational band of Sulfuryl Fluoride in the 11 μ region. Although the absorption spectrum is doppler-limited, the resolution is high enough to observe previously unresolved lines and therefor determine the band center and other excited state molecular constants.

The band constants are determined by a least squares fit computer program using an S Reduced hamiltonian to model the molecular vibration-rotation. The molecule is slightly aspherical and requires curve fitting to thousands of lines.

The S Reduced hamiltonian, as well as other pertinent theoretical topics are discussed.

Thesis Supervisor: Ali Javan

Title: Professor of Physics

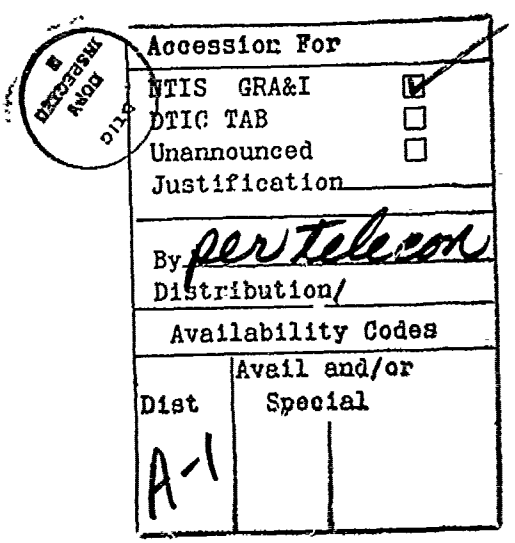

Acknowledgments

There are many individuals who, in no small part, played a role in the completion of this experiment and the preparation of this thesis. In particular I would like to recognize the following persons:

Jody Klaassen , Charlotte Flannery and the other denizens of the "Steinfeld Lounge" for the assistance they gave me in maintaining the equipment and running the experiment.

My fellow "dungeon dwellers" and office mates of Room 6-005 for two years of inspiration, support and help with problem sets. I couldn't have made it through MIT without them.

Tim Creamer for sacrificing hours of his time preparing the diagrams that went into this thesis and teaching me how to use microsoft word 4.

I would also like to thank my thesis advisor, Professor Ali Javan for granting me the honor and privilege of working with him.

I am especially grateful for the efforts of Dr. Michael Otteson. He set up the experiment, taught me how to run the equipment, wrote all the computer routines that I used to present the data, taught me the necessary theory and, in general, nursemaided me through the entire year of the experimental project. He displayed an incredible amount of patience and good humor while taking an ignorant army officer and turning him into an experimentalist. To say that this thesis is as much his as it is mine would not be an exaggeration.

To my wife I can only say thanks for putting up with me while I struggled with this project. As usual there are not enough words to express my appreciation for her infinite patience and understanding.

Contents

Chapter 1

Introduction

The advent of infrared lasers has led to unprecedented high-resolution spectroscopy in the middle IR region. The importance of the laser in spectroscopy is evident in the study of the molecule Sulfuryl Fluoride (SF_2O_2). The availability of high-resolution data allows us to observe previously unresolved structure, and for the first time, observe such effects as asymmetric K splitting and the impact of nuclear spin statistics in this molecule, as well as determine band centers and upper state molecular constants to a high degree of accuracy. In this experiment a tunable diode laser (TDL) was used to map the spectrum of SF_2O_2 in the 11 μ range.

1.1 Previous Studies of SF_2O_2

Microwave studies of SF_2O_2 have revealed seven lines in the 20 to 30 thousand Mhz region. Six of these lines were assigned to the rotational transitions $J = 1 \rightarrow 2$ and $J = 2 \rightarrow 3$ of $^{32}SF_2O_2$ and one line to the rotational transition $J = 1 \rightarrow 2$ of the $^{34}SF_2O_2$ isotope. With this data, and assuming C_{2v} symmetry, the structure of SF_2O_2 was determined and the ground state molecular constants estimated. Microwave studies have also determined that SF_2O_2 is slightly asymmetrical. However, due to the smallness of deviation from sphericity of SF_2O_2, the b and c axes (principle axes of intermediate and greatest moments of inertia respectively) could not be unambiguously assigned to their respective molecular axes. In addition the microwave data obtained was not detailed enough to determine molecular distortion parameters [14].

There has also been infrared spectroscopy performed on SF_2O_2 in which band centers of fundamental and combination vibrations have been recorded, but the transition lines themselves were unresolved [11] [12] (see Figure 1).

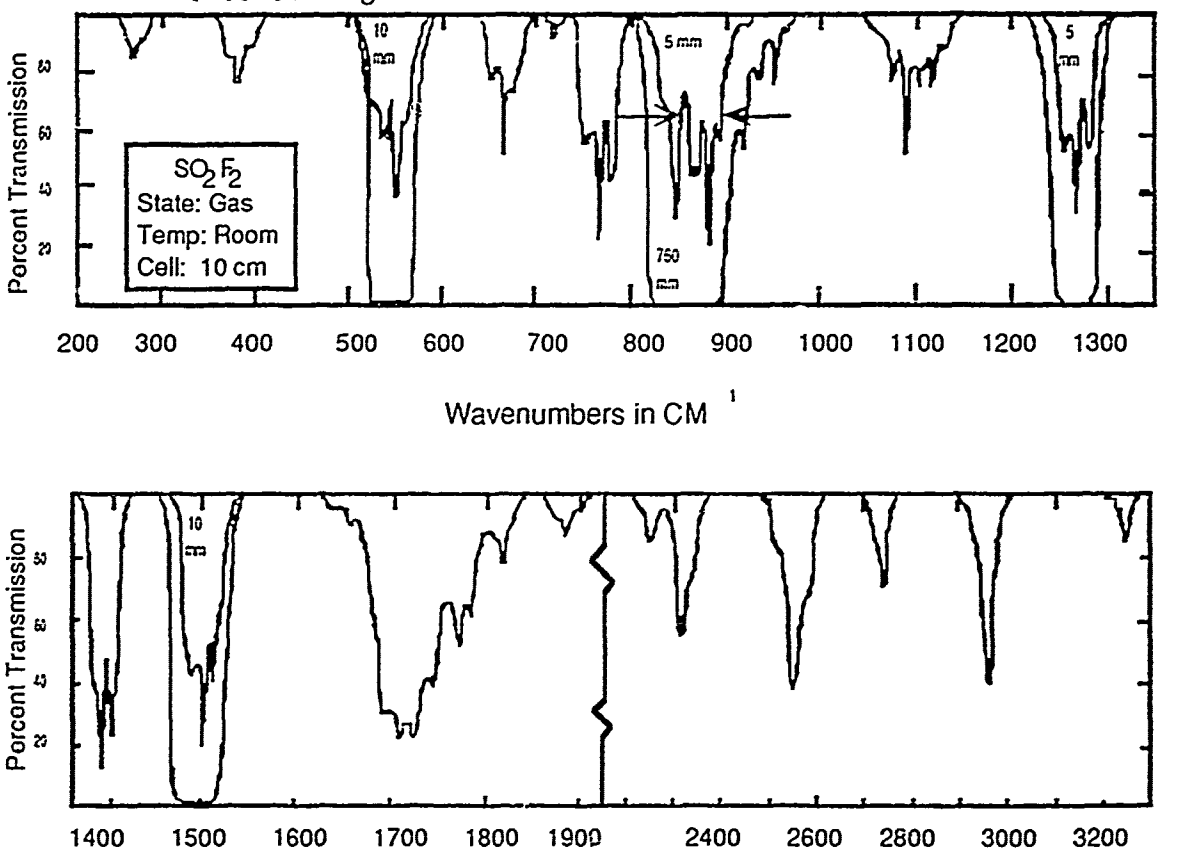

Figure 1-- Infrared Spectrum of SF_2O_2 between 250 cm^{-1} and 4000 cm^{-1}. From [12] [p. 571].

This spectrum, recorded in 1960, fails to resolve any but the coarsest of features. This means that, in the ν_8 vibrational band for example (depicted between the arrows in Figure 1), there are approximately 250 transitions and thousands of strong lines that lie entirely below the instrumental resolution of the times. The power of our technique lies in our ability to take a segment of this previously recorded spectrum and resolve completely all the transitions and strong lines. In particular, our work resolves transitions over a wide range extending from J = 30 of the R-branch to J = 16 of the P-branch of the ν_8 vibrational band. The significance and

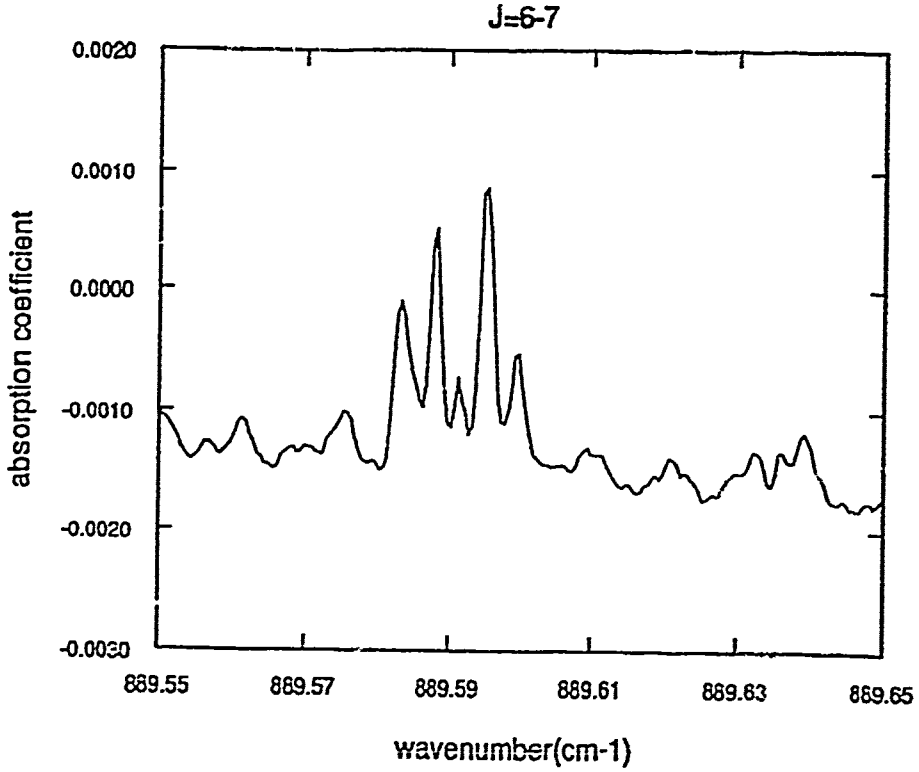

Figure 2 -- Experimental Spectra. The Resolution is about 60 MHz

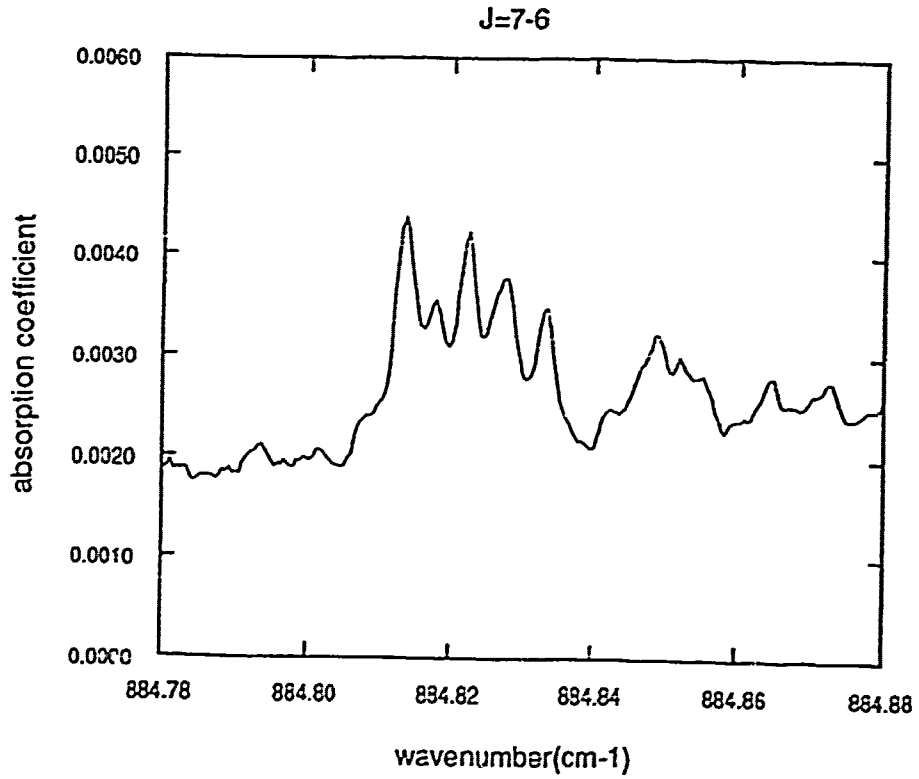

resolution of our IR data (see Figure 2 and results in Chapter 5) is apparent when compared to the previously recorded IR spectra shown in Figure 1.

In addition to our achieved resolution (which is doppler-limited to about 60 Mhz at room temperature), we have identified thousands of lines using a computer generated least squares fit. Using the fit, we have been able to clarify the assignments of the b and c axes to the appropriate SF_2O_2 molecular axes and determine the excited state inertial constants A, B and C, the ν_8 band center, and the excited state distortion parameters. None of this information had been previously available except for the ν_8 band center, which had been estimated (to the nearest wavenumber) at 885 cm^{-1}. To illustrate, some of the measured values from this experiment are given in Table 1.

Table 1

Measured Excited State Band Constants and ν_8 Band Center

Band Constant (cm^{-1})	Measured Value (cm^{-1})	Estimated Standard Deviation (cm^{-1})
Band Center	887.2185	$.2513 \times 10^{-3}$
A	.1710	$.2376 \times 10^{-5}$
B	.1691	$.2624 \times 10^{-4}$
C	.1681	$.4281 \times 10^{-4}$

1.2 Thesis Organization

The purpose of this thesis is to identify completely the P and R-branch lines covering a 15 cm^{-1} range around the Q-branch of the ν_8 vibrational band of SF_2O_2, and determine the upper state rotational and centrifugal band constants as well as the ν_8 vibrational band center.

Normally one might expect to perform an experiment to check the validity of theoretically derived parameters. In this experiment we have the opposite situation. Here we are empirically deriving values from observed spectral frequencies which are then placed into the theoretical equation. This technique is described as a reverse stochastic process in which asymmetric rotor quantum numbers are assigned to observed transitions using available theory. Once quantum numbers are assigned, band constants are determined by curve fitting using a computerized least squares routine[30]. The curve to be fitted is the S-reduced hamiltonian derived in Appendix A.

There are several steps in identifying and fitting the SF_2O_2 spectra. These steps are covered in the various chapters of this thesis.

Chapter 2 outlines the basic theory of asymmetric molecules and establishes the notations and conventions used in the thesis.

Chapter 3 explains the experimental setup and the procedure used to collect the spectra. Also covered is the application of the basic theory to the interpretation and analysis of the experimental spectra.

Chapter 4 covers error analysis.

The final results of the experiment are given in Chapter 5. Over 4600 lines were fitted by the least squares fitting routine[30]. Instead of listing all 4600 lines,several representative P and R-branch transitions are presented in graphical form.

The development of the S Reduced hamiltonian and the wave equation solution for the symmetric rotor are the subjects of Appendix A and B respectively

Chapter 2

Basic Theory

The original contribution of this thesis begins in Chapter 3 on page 36. But first, the basic theory of asymmetric vib-rotors is given in this chapter, as follows.

2.1 The Rigid Rotor-Harmonic Oscillator Approximation[1]

To begin determining the band constants and fitting the observed spectra, it is necessary to use any good approximation that is available. Oftentimes approximations can lead to reliable estimates of such quantities as band constants or transition spacings, which can then be inserted into a least-squares program to begin the fitting procedure from which accurate molecular parameters are determined. Estimated quantities can also serve as a reliable means of calculating errors and ensuring the fitting process stays accurate.

The best approximation is called the rigid rotor-harmonic oscillator approximation. This approximation begins with the hamiltonian below (see Appendix A)

$$H = \frac{(P_x - p_x)^2}{2I_{xx}} + \frac{(P_y - p_y)^2}{2I_{yy}} + \frac{(P_z - p_z)^2}{2I_{zz}} + \frac{1}{2}\sum_k p_k^2 + V \qquad (1)$$

P_x, P_y and P_z are components of the total angular momentum, p_x, p_y and p_z are components of the internal angular momentum, p_k is the momentum associated with the kth normal vibrational mode, and V represents the overall molecular potential. The first three terms represent the

[1]The theory of Section 2.1 is taken from the following References.[3] [pp. 7-9]; [2] [pp. 83-84]; [25] [pp. 266-267]; [7] [pp. 28-34].

rotational energy and the interaction of the rotational and internal angular momentum. The last two terms are pure functions of the molecular vibrations.

One can make further approximations by neglecting the internal (vibrational) angular momentum and approximating the vibrational part of the hamiltonian as a harmonic oscillator potential which can be solved exactly. In this way the rotational and vibrational energies are completely separable and are represented by the energy levels of a rigid rotor and a harmonic oscillator. In this experiment the energy solution to the vibrational part of the hamiltonian is represented by the band center ν_0. The remaining (rotational) part of the hamiltonian is the problem we now solve.

The energy levels of a rigid rotor are found by solving the Schroedinger equation:

$$H_R \Psi_{JM(\theta,\phi,\chi)} = E \Psi_{JM(\theta,\phi,\chi)} \tag{2}$$

where, with all the above approximations, we now have

$$H_R = \frac{J_x^2}{2I_{xx}} + \frac{J_y^2}{2I_{yy}} + \frac{J_z^2}{2I_{zz}} \tag{3}$$

where J now symbolizes the total angular momentum and I designates the rigid moment of inertia about the indicated axis. An asymmetric top is defined by the relation

$$I_{xx} \neq I_{yy} \neq I_{zz} \tag{4}$$

This relation removes the K-degeneracy of the symmetric rotor and, as a result, complicates the rigid rotor spectrum. Since the total angular momentum J and its projection M on a space-fixed axis are constants of the motion, they are good quantum numbers and can be used to specify the state. However, the projection of J on a molecule-fixed axis is no longer constant and therefore we can not use K to specify the state. Instead we create a parameter to indicate various degrees of deviation from the symmetric prolate (axis of symmetry is the axis of least moment of inertia)

and symmetric oblate (axis of symmetry is the axis of greatest moment of inertia) limits. The most common parameter is the asymmetry parameter

$$\kappa = \frac{2B - A - C}{A - C} \tag{5}$$

which varies from -1 for a prolate symmetric top (B=C) to 1 for an oblate symmetric top (B=A). The quantities A, B and C are constants inversely proportional to the least, intermediate and greatest moments of inertia respectively. They are defined in Appendix B (see p. 117). Energy levels are specified by the symbol $J_{K_{-1}K_1}$. This level represents a rotational level of J which in the limiting case connects a prolate symmetric top level of K_{-1} with an oblate symmetric top level of K_1 (see Figure 3).

We now expand the asymmetric top eigenfunctions in combinations of symmetric top basis functions

$$\Psi_{JM(\theta,\phi,\chi)} = \sum_k A_k |JKM\rangle \tag{6}$$

Where $|JKM\rangle$ represents the symmetric top wave function of Equation (B-15) (see p. 117). Substituting Equation (6) into Equation (2) yields

$$\sum_k A_k H_R |JKM\rangle = E \sum_k A_k |JKM\rangle \tag{7}$$

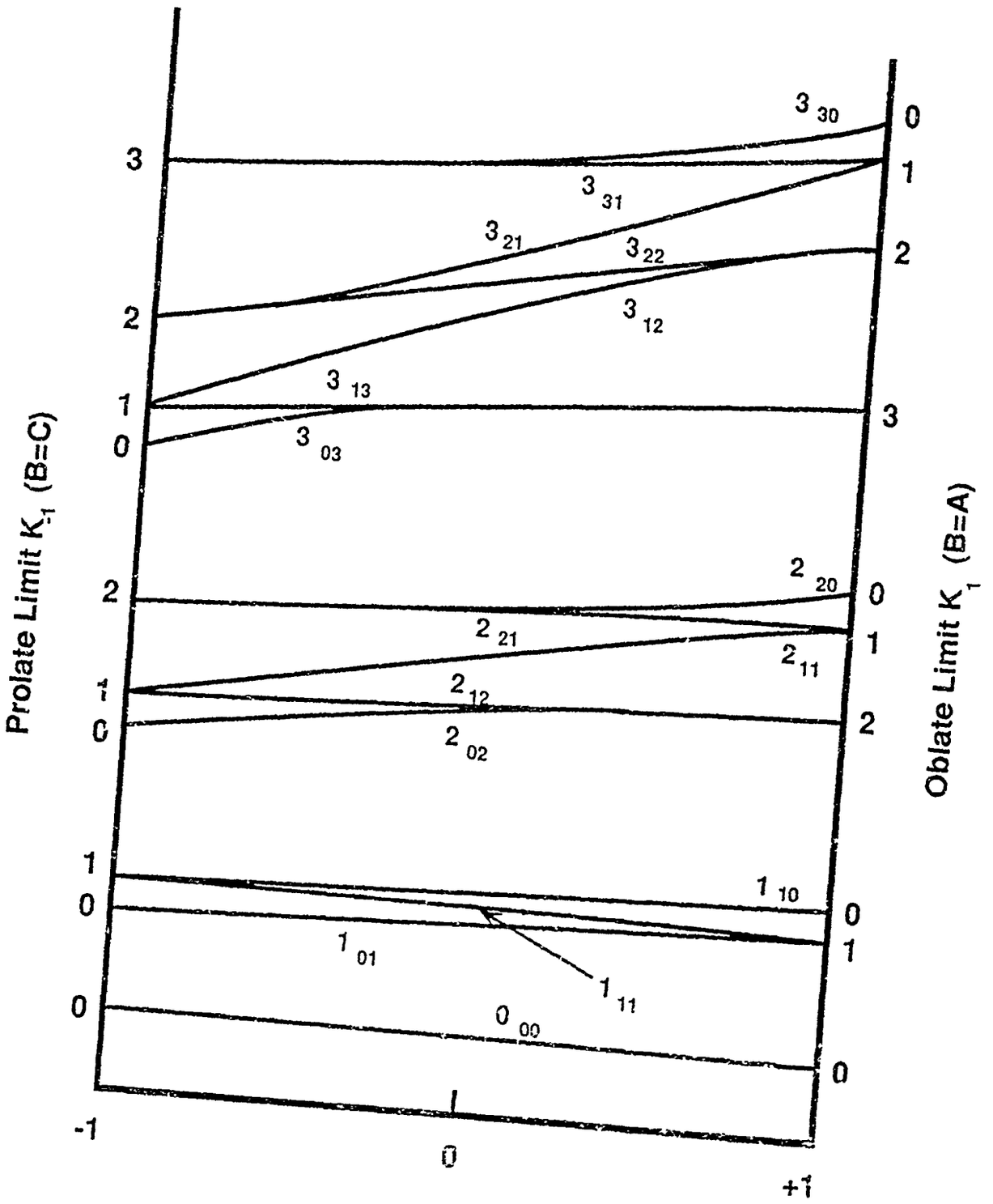

Figure 3 --Typical Qualitative Behavior of Asymmetric Rotor Energy Levels. From [25] [p. 276].

(The horizontal axis represents the entire range of values for the asymmetry parameter κ)

The energies are the roots of the $(2J+1) \times (2J+1)$ secular determinant

$$\left|H_{KK'} - E\delta_{KK'}\right| = 0 \tag{8}$$

where

$$H_{KK'} = \langle JK'M|H_R|JKM\rangle \tag{9}$$

At this point it is helpful to investigate the symmetry properties of the wave functions. For this we resort to group theory. In group theoretical nomenclature, all rigid rotor wave functions belong to representations called the external rotation group. These representations are characterized by J and M and correspond to an infinitely large amount of possible rotations of the space-fixed system that leave the energy invariant. The symmetric rotor, described by the body-fixed axes, belongs to the internal rotation group D_∞, characterized by the quantum numbers J and K. For the asymmetric rotor, the hamiltonian has the character that a rotation of $180°$ about any axis leaves the hamiltonian unchanged [see Equation (3)]. The asymmetric top is therefore classified as a member of the point group D_2, also known as the Viergruppe (V) group. This group is characterized by twofold rotations about the a, b and c axes denoted by $C_{2(a)}$, $C_{2(b)}$ and $C_{2(c)}$ and the identity E (see Table 2).

Table 2
Group Characters for the D_2(V) Group. From [25] [p. 268].

Group Operations				Quantum Numbers
E	C2(c)	C2(b)	C2(a)	$K_{-1}K_1$
1	1	1	1	ee
1	1	-1	-1	oe
1	-1	1	-1	oo
1	-1	-1	1	eo

Here a, b and c represent principle molecular axes of least, intermediate and greatest moments of inertia respectively. They correspond to the inertial constants A, B and C defined in Equation (B-1) (see p. 117). The letters "e" and "o" in Table 2 stand for even and odd respectively.

Now we examine how the $|JKM\rangle$ transform under the operations of the V group. First we note that for SF_2O_2, κ = -.5 [14], which approaches the symmetric prolate limit. Therefore it is natural to identify the X, Y, Z axes with the b,c,a axes respectively (see Table 3).

Table 3
Possible Identification of Principle Axes a, b, c with Body-fixed Coordinates x, y, z.
From [25] [p. 268].

Body-fixed coordinates	Representation		
	I[a]	II[b]	III[c]
x	b	c	a
y	c	a	b
z	a	b	c

[a] most natural limit of a prolate symmetric rotor
[b] most natural for a rotor intermediate between the two limiting symmetric rotor cases
[c] most natural limit of an oblate symmetric rotor

The effect of the V group operations on the $|JKM\rangle$ is determined by their effect on the Euler angles. We use the direction cosine matrix $\Phi_{F(\theta,\phi,\chi)}$ of Table B-1 to determine the effects of each of the four operations on the Euler angles. The results are summarized in Table 4.

Table 4
Cartisian Coordinate and Euler Angle Transformations Under Operations of the $D_2(V)$ group.
From [25] [p. 269].

Group Operation	Cartisian Coordinate Transformation	Euler Angle Transformation
E	$x \to x$	$\phi \to \phi$
	$y \to y$	$\theta \to \theta$
	$z \to z$	$\chi \to \chi$
$C_{2(a)}$	$x \to -x$	$\phi \to \phi$
	$y \to -y$	$\theta \to \theta$
	$z \to z$	$\chi \to \pi + \chi$
$C_{2(c)}$	$x \to -x$	$\phi \to \phi + \pi$
	$y \to y$	$\theta \to \pi - \theta$
	$z \to -z$	$\chi \to \pi - \chi$
$C_{2(b)}$	$x \to x$	$\phi \to \pi + \phi$
	$y \to -y$	$\theta \to \pi - \theta$
	$z \to -z$	$\chi \to -\chi$

In particular, we find

$$c_{2(a)}|JKM\rangle \propto e^{iM\phi}\Theta_{(\theta)}e^{iK(\pi+\chi)} = (-1)^K|JKM\rangle$$

$$c_{2(c)}|JKM\rangle \propto e^{iM(\phi+\pi)}\Theta_{(\pi-\theta)}e^{iK(\pi-\chi)} = (-1)^{J-K}|JKM\rangle \qquad (10)$$

$$c_{2(b)}|JKM\rangle \propto e^{iM(\phi+\pi)}\Theta_{(\pi-\theta)}e^{iK(-\chi)} = (-1)^J|JKM\rangle$$

The relations in Equation (10) tell us that we cannot use the expansion (6). Instead we must construct a basis from linear combinations of $|J,\pm K,M\rangle$ whose symmetry causes them to transform the same way under the operations of the V group. If we define

$$|JKMs\rangle = \frac{1}{\sqrt{2}}\left[|JKM\rangle + (-1)^s|J,-K,M\rangle\right] \text{ for } K \neq 0 \text{ and } s = 0,1 \qquad (11)$$

and

$$|J0Ms\rangle = (-1)^{s}|J0M\rangle = |J0M\rangle \text{ for } K = 0 \text{ and } s = 0 \tag{12}$$

then we get

$$E|JKMs\rangle = |JKMs\rangle$$

$$c_{2(a)}|JKMs\rangle = (-1)^{K}|JKMs\rangle$$

$$c_{2(c)}|JKMs\rangle = (-1)^{J-K+s}|JKMs\rangle \tag{13}$$

$$c_{2(b)}|JKMs\rangle = (-1)^{-J+s}|JKMs\rangle$$

Hence the factors of Equation (8) are divided into four sub-blocks and the eigenvectors and eigenfunctions of each sub-block correspond to one of the symmetry operations of the V group (see Table 5).

Table 5
Asymmetric Rotor Symmetry Operations. From [25] [p. 271].

Secular Determinant	Symmetry Designation			
	K	s	J even	J odd
E^+	Even	0	A	B_z
E^-	Even	1	B_z	A
O^+	Odd	0	B_x	B_y
O^-	Odd	1	B_y	B_x

Now we must calculate the matrix elements of H_R that appear in our sub-blocks. The commutation rules $[J_i, J_j] = \varepsilon_{ijk} J_k$ give us

$$\langle JKM|J_x|J,K \pm 1,M\rangle = \tfrac{1}{2}[J(J+1) - K(K+1)]^{\frac{1}{2}}$$

$$\langle JKM|J_y|J,K \pm 1,M\rangle = \mp \tfrac{i}{2}[J(J+1) - K(K \pm 1)]^{\frac{1}{2}} \qquad (14)$$

$$\langle JKM|J_z|JKM\rangle = K$$

which imply

$$\langle JKM|J_x^2|JK'M\rangle = \sum_{K''}\langle JKM|J_x|JK''M\rangle\langle JK''M|J_x|JK'M\rangle \qquad (15)$$

$$= \tfrac{1}{2}[J(J+1) - K^2]\delta_{KK'} + \tfrac{1}{4}[J(J+1) - (K \pm 1)]^{\frac{1}{2}}[J(J+1) - (K \pm 1)(K \pm 2)]^{\frac{1}{2}}\delta_{K,K'\pm 2}$$

Similarly

$$\langle JKM|J_y^2|JK'M\rangle = \tfrac{1}{2}[J(J+1) - K^2]\delta_{KK'}$$

$$- \tfrac{1}{4}[J(J+1) - (K \pm 1)]^{\frac{1}{2}}[J(J+1) - (K \pm 1)(K \pm 2)]^{\frac{1}{2}}\delta_{K,K'\pm 2} \qquad (16)$$

$$\langle JKM|J_z^2|JK'M\rangle = K^2\delta_{KK'} \qquad (17)$$

and finally, for an asymmetric rotor in the prolate limit

$$H_{KK'} = \left\{\frac{1}{2}(B+C)[J(J+1)-K^2]+AK^2\right\}\delta_{KK'}$$

$$+\left\{\frac{1}{4}(B-C)[J(J+1)-K(K\pm 1)-(J+1)-(K\pm 1)(K\pm 2)]^{\frac{1}{2}}\right\}\delta_{K,K'\pm 2} \tag{18}$$

Note that for a prolate symmetric top (B = C), $H_{KK'}$ is diagonal.

Now let σ and ρ be scalar quantities, then we can say

$$H_{R(\sigma A+\rho,\sigma B+\rho,\sigma C+\rho)} = (\sigma A+\rho)J_a^2 + (\sigma B+\rho)J_b^2 + (\sigma C+\rho)J_c^2$$

$$= \sigma\left(AJ_a^2 + BJ_b^2 + CJ_c^2\right) + \rho\left(J_a^2 + J_b^2 + J_c^2\right) = \sigma H_{R(ABC)} + \rho J^2 \tag{19}$$

with the eigenenergies

$$E_{(\sigma A+\rho,\sigma B+\rho,\sigma C+\rho)} = \sigma E_{(abc)} + \rho j(J+1) \tag{20}$$

Now let

$$\sigma = \frac{2}{A-C} \tag{21}$$

and

$$\rho = \frac{-(A+C)}{(A-C)} \tag{22}$$

which imply

$$\sigma A + \rho = 1$$

$$\sigma B + \rho = \frac{(2B - A - C)}{(A - C)} \tag{23}$$

$$\sigma C + \rho = -1$$

and give us, for Equation (20)

$$E_{(\sigma A+\rho,\sigma B+\rho,\sigma C+\rho)} = E_{(1,\kappa,-1)} \equiv E_\kappa = \frac{2}{(A-C)} E_{(abc)} - \frac{(A+C)}{(A-C)} J(J+1) \tag{24}$$

or

$$E_{(abc)} = \frac{1}{2}(A + C)J(J + 1) + \frac{1}{2}(A - C)E_\kappa \tag{25}$$

We can now find the energies $E_{(abc)}$ of the rigid asymmetric rotor as follows; we still must evaluate the secular determinant in Equation (8), but we must first identify to which group operation the $J_{K_{-1}K_1}$ level belongs (see Table 2). In Equation (8), $H_{KK'}$ now refers to the hamiltonian in Equation (18), and instead of $|JKM\rangle$ use $|JKMs\rangle$ from Equation (11) or Equation (12). To find E_κ use the same procedure, but substitute A = 1, B = κ and C = -1.

2.2 Line Strengths[2]

We begin our discussion using the rigid rotor-harmonic oscillator approximation. This approximation assumes the hamiltonian can be written as

$$H = H_V + H_R \tag{26}$$

[2]The theory of Section 2.2 is taken from the following References. [3] [pp. 94-95], [26] [p. 32]; [25] [p.82,290].

and therefore the vibrational and rotational energies as

$$E = E_v + E_r \tag{27}$$

This type of separation also leads to the form of the total wave function as a superposition of two different wave functions:

$$\Psi_{VR} = \Psi_V \Psi_R \tag{28}$$

To find selection rules and line strengths, the matrix elements of the electric moments connecting the vibrational-rotational states V'R' to V"R" within the same electronic states are considered. Microwave studies have shown that, for this molecule, the permanent electric moment lies along the axis of symmetry, which for a I^r group representation, can be designated as the a axis (axis of least moment of inertia). If we call this axis the z axis, then both sets of axes: x,y,z and X,Y,Z, representing axes fixed in the molecular and lab frames respectively, are needed to formulate the problem.

The electric moment relative to the body-fixed z axis can be written as

$$M_z = (M_z)_o + \sum_k \left(\frac{\partial M_z}{\partial Q_k}\right)_{Q_k=0} Q_k + \cdots \tag{29}$$

where $(M_z)_o$ is the permanent electric moment and Q_k is the kth normal coordinate of the vibrational movement.

The component of the electric moment along the lab-fixed Z axis would be

$$M_Z = M_x \cos xZ + M_y \cos yZ + M_z \cos zZ \tag{30}$$

where the direction cosines between the two coordinate systems are functions of the rotational coordinates alone. Generalizing, we say

$$M_F = \sum_g \Phi_{Fg(\theta,\phi,\chi)} M_g \quad ; \quad F = X,Y,Z \quad ; \quad g = x,y,z \tag{31}$$

$\Phi_{Fg(\theta,\phi,\chi)}$ are the direction cosines of the rotating molecule whose molecule-fixed frame is described by the Euler angles θ,ϕ,χ.

The matrix elements of the electric moment are

$$\langle V'R'|M_F|V''R''\rangle = \int \psi'^*_V \psi'^*_R M_F \psi_{V''} \psi_{R''} d\tau \tag{32}$$

Substituting Equation (31) and the generalized form of Equation (29) into Equation (32) enables the separation of Equation (32) into two independent parts:

$$\langle V'R'|M_F|V''R''\rangle = \sum_g (M_g)_0 \int \psi'^*_R \Phi_{Fg} \psi_{R''} d\tau = \sum_g (M_g)_0 \langle V'R'|\Phi_{Fg}|V''R''\rangle \tag{33}$$

and

$$\langle V'R'|M_F|V''R''\rangle = \sum_g \int \psi'^*_V \sum_k \frac{\partial M_g}{\partial Q_k} Q_k \psi_{V''} - \int \psi'^*_R \Phi_{Fg} \psi_{R''} d\tau = \sum_g \langle V'|M_g|V''\rangle \langle R'|\Phi_{Fg}|R''\rangle \tag{34}$$

$\langle R'|\Phi_{Fg}|R''\rangle$ represents the matrix element in the F-direction corresponding to a unit electric moment along the g-direction associated with the change in rotational quantum numbers from R' to R''. As such it is independent of the vibrational normal coordinates of the system. $\langle V'|M_g|V''\rangle$ are the matrix elements of the electric moment along g associated with a change in vibrational quantum numbers from V' to V''. For the harmonic oscillator approximation the eigenfunctions, the Hermite polynomials, are odd, so the matrix elements are only non-zero for a change in vibrational quantum numbers of $\Delta v = \pm 1$. Such transitions are called fundamental transitions because they are the most intense. To obtain overtone transitions for which $\Delta v > 1$ or combination bands in which the quantum numbers associated with more than one normal mode of vibration changes, it is necessary to include higher order terms in the normal mode expansion (29). Coupling between normal modes caused by anharmonic terms is zero unless v'=v" (direction

cosines are even functions). Equation (33) represents the matrix elements for pure rotational spectra, that is, transitions between rotational states in the same vibrational level. These types of transitions give rise to microwave spectra, and are functions of the permanent electric moment of the molecule.Equation (34) represents the matrix elements for simultaneous changes in both vibrational and rotational states.

In the analysis of the vibration-rotation spectra, absolute intensities are not necessary, only the relative intensities are important. Therefore it is not necessary to know the exact form of $\langle V'|M_g|V''\rangle$, only that it is non-zero. Hence we are left with the quantity $\sum_{F,g}\left|\langle R'|\Phi_{Fg}|R''\rangle\right|^2$, the line strength, which along with weight factors to be discussed later, defines the relative transition intensities.

2.3 Symmetric Rotor Selection Rules[3]

Before we attack the transition intensities, we first address the selection rules by examining the matrix elements $\langle R'|\Phi_{Fg}|R''\rangle$ for an asymmetric rotor. The selection rules for a slightly asymmetric vibrating-rotating molecule can be best understood by first considering the selection rules for a symmetric rotor. This is because for a symmetric rotor, K is a good quantum number (see Appendix B) and we can derive exact selection rules for K in the symmetric limit.

We start by realizing that angular momentum will transform from the lab frame to the fixed molecule frame exactly as the coordinates transformed under rotation

$$P_g = \sum_F \Phi_{Fg(\theta,o,\chi)} P_F \qquad (35)$$

Note that everything is done in the representation for which the energy of the symmetric rotor is diagonal in J and K. In this representation we have

[3]The theory of Section 2.3 is taken from Reference [3] [pp. 95-98];

$$\langle JKM|P_z|J'K'M'\rangle = K\delta_{JJ'}\delta_{KK'}\delta_{MM'} \tag{36}$$

and

$$\langle JKM|P^2|J'K'M'\rangle = J(J+1)\delta_{JJ'}\delta_{KK'}\delta_{MM'} \tag{37}$$

Consider

$$\left[P^2,\left[P^2,\Phi\right]\right] = P^4\Phi - 2P^2\Phi P^2 + \Phi P^4 \tag{38}$$

Repeated application of the commutation rules $\left[P_i,P_j\right] = \varepsilon_{ijk}P_k$ gives

$$P^4\Phi - 2P^2\Phi P^2 + \Phi P^4 = 2h^2\left(P^2\Phi + \Phi P^2\right) - 4h^2P(P\cdot\Phi) \tag{39}$$

This means that

$$\langle J'K'M'|P^4\Phi - 2P^2\Phi + \Phi P^4|JKM\rangle = 2h^2\langle J'K'M'|P^2\Phi + \Phi P^2|JKM\rangle$$

$$- 4h^2\langle J'K'M'|P(P\cdot\Phi)|JKM\rangle \tag{40}$$

which implies

$$h^4\left[J'^2(J'+1)^2 - 2J'(J'+1)J(J+1) + J^2(J+1)^2\right]\langle J'K'M'|\Phi|JKM\rangle$$

$$= 2h^4\left[J'(J'+1) + J(J+1)\right]\langle J'K'M'|\Phi|JKM\rangle - 4h^2\langle J'K'M'|P(P\cdot\Phi)|JKM\rangle \tag{41}$$

For $J'\neq J$ the last term on the R.H.S. of Equation (41) vanishes. For the other factor on the R.H.S. of Equation (41) we write

$$2\left[J'(J'+1) + J(J+1)\right] = (J'+J+1)^2 + (J'-J)^2 - 1 \tag{42}$$

The term on the L.H.S. is factored to give

$$\left[J'^2(J'+1)^2 - 2J'(J'+1)J(J+1) + J^2(J+1)^2\right] = \left[(J'-J)^2(J'+J+1)\right] \quad (43)$$

resulting in

$$\left[(J'-J)^2(J'+J+1)^2 - (J'+J+1)^2 - (J'-J) - 1\right]\langle J'K'M'|\Phi|JKM\rangle = 0 \quad (44)$$

or

$$\left[(J'+J+1)^2 - 1\right]\left[(J'-J)^2 - 1\right]\langle J'K'M'|\Phi|JKM\rangle = 0 \quad (45)$$

For a non-vanishing matrix element one of the coefficient expressions must be zero. The first term cannot be zero because, by assumption, $J' \neq J$ and $J', J \geq 0$. The second term is zero only if $J'-J = \pm 1$.

For $J = J'$, note that $P \cdot \Phi$ is a scalar operator and is therefore invariant under operations generated by P_z and P^2. Therefore we have

$$\left[P_z,(P\cdot\Phi)\right] = \left[P^2,(P\cdot\Phi)\right] = 0 \quad (46)$$

leading to the following matrix representations

$$0 = \langle J'K'M'\left[P^2,(P\cdot\Phi)\right]JKM\rangle = \langle J'K'M'|P_z(P\cdot\Phi) - (P\cdot\Phi)P_z|JKM\rangle$$

$$= (K'-K)\langle J'K'M'|P\cdot\Phi|JKM\rangle \quad (47)$$

and

$$0 = \langle J'K'M'\left[P^2,(P\cdot\Phi)\right]JKM\rangle = \langle J'K'M'|P^2(P\cdot\Phi) - (P\cdot\Phi)P^2|JKM\rangle$$

$$= \left[J'(J'+1) - J(J+1)\right]\langle J'K'M'|P\cdot\Phi|JKM\rangle \quad (48)$$

Equation (47) and Equation (48) lead to nonvanishing matrix elements only for $K' = K$ and $J' = J$. Finally we construct operator $\Phi_{Fy} \pm i\Phi_{Fx}$, which together with P_z and the commutation relations used above, show us that

$$\langle J'K'M'|\Phi_{Fy} \pm i\Phi_{Fx}|JKM\rangle = \delta_{JJ'}\delta_{KK'}\delta_{M',M\pm1} \tag{49}$$

which implies the selection rule $\Delta M = \pm 1$. Collecting the important results we have for the selection rules for the symmetric rotor in the general case $\langle V'|M_g|V''\rangle$ are

$$\Delta J = 0,\pm 1\ ,\ \Delta K = 0,\pm 1 \tag{50}$$

2.4 Asymmetric Rotor Symmetry Considerations and Selection Rules[4]

The spectrum of the asymmetric rotor will be complicated because the selection rules are more complex than in the symmetric case. This is because of the increased number of energy levels and the arbitrary direction of the changing dipole moments. Despite these problems, general statements can be made concerning selection rules for asymmetric rotors.

First, since total angular momentum is always conserved, even though the molecule is now asymmetric, the transformation matrices for the asymmetric case are diagonal with respect to J (as they are in the symmetric case). The selection rules for J are therefore the same; that is, $\Delta J = 0,\pm 1$. The selection rules for K_{-1} and K_1 can be obtained by examining the symmetry of the molecule in question.

The rotational behavior of a molecule of C_{2v} symmetry depends on the ellipsoid of inertia, which is symmetric with respect to a rotation of $180°$ about the principal axis even though the molecule itself, being asymmetric, may not be symmetric with respect to such a

[4]The theory of Section 2.4 is taken from the following References: [2] [p. 93]; [3] [pp. 106-107]; [8] [pp. 214-216].

rotation. The rotational wave function $\Psi_{JK_{-1}K_1}$ is either symmetric or antisymmetric with respect to such a rotation.

For an asymmetric rotor in the limiting prolate case, symmetry of the wave function with respect to a $180°$ rotation about the a axis (axis of least moment of inertia) which is the axis of symmetry, depends on the angle χ as in $e^{\pm iK_{-1}\chi}$. Therefore $\Psi_{JK_{-1}K_1}$ is symmetric when K_{-1} is even and antisymmetric when K_{-1} is odd. Similarly, in the limiting oblate case, $\Psi_{JK_{-1}K_1}$ is symmetric with respect to rotation about the axis of greatest moment of inertia (c axis) when K_1 is even, and antisymmetric when K_1 is odd. Since successive rotations of $180°$ about all three axes bring the molecule back to its original position, the symmetry for a rotation about the b axis is the product of the a and c axis symmetries.

Now if the changing dipole moment lies along the a axis, the matrix element, on which the relative transition intensities depend, is of the form

$$\langle R'|\Phi_{Fa}|R''\rangle = \int \psi_{J'K'_{-1}K'_1} \Phi_{Fa} \psi_{J''K''_{-1}K''_{+1}} d\tau = \int \psi_{J'K'_{-1}K'_1} \mu\cos(Fa) \psi_{J''K''_{-1}K''_1} d\tau \tag{51}$$

where $J'K'_{-1}K'_1$ and $J''K''_{-1}K''_1$ represent the quantum numbers of the initial and final rotational states, μ is the dipole moment and cos(Fa) is the cosine of the angle between a and some space-fixed axis. Since cos(Fa) changes sign for a $180°$ rotation about the c axis for example; then $\Psi_{J'K'_{-1}K'_1} \Psi_{J''K''_{-1}K''_1}$ must also change sign for the matrix element to be non-zero. Otherwise $\langle R'|\Phi_{Fa}|R''\rangle$ itself would appear to change sign, and since the ellipsoid moment of inertia is symmetric with respect to this rotation, this would imply the matrix element would have to be equal to zero to avoid a contradiction. Therefore transitions of this type can occur only when K'_1 and K''_1 are of different parity. A similar argument for rotation about the b axis shows that K'_{-1} and K''_{-1} must be of the same parity. This type of procedure is repeated for changing moments along the b and c axes to establish selection rules for all cases.

Symmetry properties for asymmetric wave functions are summarized in Table 6 and selection rules in Table 7.

Table 6

Symmetry Properties of Asymmetric Rotor Wave Functions. From [2] [p. 94].

Designation	Behavior with 180° rotation about principle axes		
K_{-1} K_1	a (least moment)	b (intermediate moment)	c (greatest moment)
e e	+	+	+
e o	+	-	-
o o	-	+	-
o e	-	-	+

Table 7

Selection Rules For Asymmetric Tops. From [2] [p. 94].

Axis Parallel to Changing Dipole Moment	Allowed Transitions
a (least)	ee ↔ eo oo ↔ oe
b (intermediate)	ee ↔ oo eo ↔ oe
c (greatest)	ee ↔ oe oo ↔ eo

Briefly, we see that the selection rules for symmetric rotors, $\Delta K = 0,\pm 1$ have been relaxed. In general we now have $\Delta K = 0,\pm 2,\pm 4,\ldots$ or $\Delta K = 0,\pm 1,\pm 3,\ldots$ that is, ΔK_{-1} and ΔK_1 are restricted to even or odd changes. However, not all numerical combinations of ΔK_{-1} and ΔK_1 are possible since $K_{-1} + K_1 = J$ for even levels (even levels defined as $K_{-1} + K_1 + J =$ even) and $K_{-1} + K_1 = J + 1$ for odd levels (odd levels defined as $K_{-1} + K_1 + J =$ odd).

2.5 Relative Intensities of Asymmetric Rotor Transitions From the Direction Cosine Line Strengths[5]

The line strengths $\sum_{Fg} \left|\langle R' | \Phi_{Fg} | R'' \rangle\right|^2$ mentioned earlier were, strictly speaking, direction cosine matrices of basis functions for a symmetric rotor described by the Euler angles. To describe the line strengths for an asymmetric rotor we just represent the asymmetric rotor wave functions as a sum of symmetric rotor basis functions which transform under rotation to the degenerate pairs to which they converge to in the limiting symmetric cases. Hence, direction cosine matrices for the asymmetric rotor can be calculated from linear combinations of values of Φ_{Fg} which give the same symmetry.

We will define transition intensities as the direction cosine line strengths as modified by the fraction of molecules available in the ground state of the particular transition. In the rigid rotor-harmonic oscillator approximation this fraction is given by

$$f = f_{JK_{-1}K_1} f_V \tag{52}$$

[5]The theory of Section 2.5 is taken from the following References; [2] [pp.100-101]; [3] [pp. 105, 110-111]; [8] [pp. 210-214].

This approximation also assumes no coupling between vibration and rotation, which is particularly true for low vibrational quantum numbers. Note we have also assumed all the electrons to be in their lowest state. The fraction of molecules in a particular vibrational state of energy $h\nu\left(n+\frac{1}{2}\right)$, $n = 0,1,2,\ldots$ is

$$f_V = \frac{\exp\left[\frac{-h\nu\left(n+\frac{1}{2}\right)}{k_B T}\right]}{\sum_{n=0}^{\infty}\exp\left[\frac{-h\nu\left(n+\frac{1}{2}\right)}{k_B T}\right]} = \exp\left[\frac{-nh\nu}{k_B T}\right]\left(1-\exp\frac{-h\nu}{k_B T}\right) \tag{53}$$

For a multi-band harmonic oscillator it is

$$\prod_m \exp\left[\frac{-n_m h\nu_m}{k_B T}\right]\left(1-\exp\frac{-h\nu_m}{k_B T}\right)^{d_m} \tag{54}$$

where d_m is the degeneracy of the vibrational mode of frequency ν_m. Since there is a $2J+1$ degeneracy from the M-quantum numbers, we have for the fraction of molecules in a particular rotational state (the asymmetry of the molecule splits the K-degeneracies of the symmetric rotor)

$$f_{JK_{-1}K_1} = \frac{(2J+1)\exp\left[\frac{-E_{(abc)}}{k_B T}\right]}{\sum_J (2J+1)\exp\left[\frac{-E_{(abc)}}{k_B T}\right]} \tag{55}$$

where $E_{(abc)}$ is the energy given in Equation (25).

In our case, the ν_8 transition is non-degenerate and the ground state has the vibrational quantum number n = 0. So in principle, we can write the intensity of a spectral transition for a single band in the rigid rotor-harmonic oscillator approximation as

$$I_{V'R',V''R''} \propto \frac{g_{V'R'}\left(1-\exp\frac{-h\nu}{k_B T}\right)\exp\left[\frac{-E_{V'R'(abc)}}{k_B T}\right]}{\sum_n g_{V'R'}\exp\left[\frac{-E_{n(abc)}}{k_B T}\right]}\left|\langle V'R'|M_F|V''R''\rangle\right|^2 \quad (56)$$

where V'R' and V"R" stand for all the vibrational-rotational quantum numbers of the lower and upper states respectively. $g_{V'R'}$ is the multiplicity of the lower state, which, since we assume all the electrons to be in the ground state, includes only the nuclear spin statistics. $E_{n(abc)}$ is the asymmetric rigid rotor energy from Equation (25), N is the number of molecules per cubic centimeter and ν is the transition frequency.

To compute relative transition intensities, we note that the denominator and the constants in Equation (56) are the same for any given molecule. Also, since the frequency from one end of a vibrational-rotational transition band to the other does not vary appreciably, $\left(1-\exp\frac{-h\nu}{k_B T}\right)$ is essentially essentially constant for a given band. And, as pointed out earlier, the purely vibrational part of $\langle V'R'|M_F|V''R''\rangle$ is not important for calculating relative intensities as long as it is not zero. Therefore the relative intensities in a vibrational-rotational band can be computed to a high degree of accuracy with knowledge of $E_{n(abc)}$, the line strengths and the nuclear spin statistics.

We finish the discussion of relative transition intensities by addressing the issue of the nuclear spin statistics.

2.6 Nuclear Spin Statistics of SF_2O_2[6]

Anytime a molecule has two identical nuclei (same isotope of the same element) which share the same electronic environment within the molecule, the nuclear spins will affect the

[6]The theory of Section 2.6 is taken from Reference [2] [pp. 102-103].

symmetry of the overall molecular wave function. The overall wave function can be approximated as the product

$$\Psi_T = \Psi_e \Psi_V \Psi_R \Psi_I \tag{57}$$

where Ψ_e, Ψ_V, Ψ_R and Ψ_I represent the parts of the wave function dependent respectively on electronic, vibrational, rotational, and spin coordinates. Naturally the behavior of Ψ_T with respect to any symmetry operation depends on the behavior of each of the four parts. The electronic wave functions for most polyatomic molecules are in the ground state (and therefore symmetric) at room temperature, and the ground vibrational state for SF_2O_2 is also symmetric in the harmonic oscillator approximation, so the symmetry of the total wave function for this transition in the SF_2O_2 spectra is determined only by the product of the rotational and nuclear spin functions. We can then write, for symmetry purposes,

$$\Psi_T = \Psi_{JK_{-1}K_1} \Psi_I \tag{58}$$

If, in a molecule, two equivalent nuclei occur, the molecule will have a twofold axis of symmetry, and consideration of the nuclear spin statistics with respect to an interchange of identical nuclei coordinates about this axis must be considered. In SF_2O_2 we have two pairs of identical nuclei, but since the oxygen nuclei have zero spin, they will not contribute to the spin statistics. Only the two fluorine nuclei, each of which has a spin of $1/2$, will affect the nuclear spin states.

The nuclear spin function can be either symmetric or antisymmetric, and is formed by taking linear combinations of the spin functions of each individual nucleus, that is

$$\psi_I = \sigma_m(1)\sigma_{m'}(2) \quad , m = m' \text{ (symmetric)}$$

$$\psi_I = \sigma_m(1)\sigma_{m'}(2) + \sigma_{m'}(1)\sigma_m(2) \text{ (symmetric)} \tag{59}$$

$$\psi_I = \sigma_m(1)\sigma_{m'}(2) - \sigma_{m'}(1)\sigma_m(2) \text{ (antisymmetric)}$$

where $\sigma_m(1)$ and $\sigma_m(2)$ are, respectively, the spin states of the first and second identical nuclei with projection m of spin I on a space-fixed axis. As usual, m takes on the $2I + 1$ values $I, I-1, I-2, \ldots, -I$. Hence there are $2I + 1$ combinations possible for the first equation of (59) and $\left[\frac{(2I+1)^2-(2I+1)}{2}\right]$ possible combinations each for the last two equations of (59). This gives us a total possible number of symmetric spin functions of

$$N_{sym} = (2I + 1)(I + 1) \tag{60}$$

and a total possible number of antisymmetric spin functions of

$$N_{antisym} = (2I + 1)I \tag{61}$$

A molecular rotation of $180°$ about the symmetry axis (a axis) in SF_2O_2 amounts to a complete exchange of molecular coordinates of the two fluorine nuclei. Since only the fluorine nuclei (which are fermions) contribute to the spin statistics, Ψ_T must obey Fermi-Dirac statistics for the exchange. Hence we must always pair an antisymmetric nuclear spin function with a symmetric rotational function to keep the nature of Ψ_T antisymmetric. Similarly, a symmetric nuclear spin function will always be paired with an antisymmetric rotational wave function for rotation with respect to the symmetry axis.

Since $I = \frac{1}{2}$ for the fluorine nucleus, Equations (60) and (61) tell us we have a total of three symmetric and one antisymmetric nuclear spin functions. So, according to Equation (56), rotational wave functions for SF_2O_2 marked with a "-" under the least moment column in Table 6

will have (all other factors aside) three times the intensity of those marked with a "+". These results are tabulated in Table 8.

Table 8
Nuclear Spin Statistics for SF_2O_2

$\Psi_{JK_{-1}K_1}$ K_{-1} K_1		Symmetry with respect to $180°$ rotation about axis of symmetry (a axis)	Statistical Weight
e	e	symmetric	1
e	o	symmetric	1
o	o	antisymmetric	3
o	e	antisymmetric	3

Chapter 3

Experimental Procedure

In this experiment, a tunable diode laser was used to generate laser light in the 11 μ range to observe the SF_2O_2 spectral profile. The laser light was transmitted through a 150 cm absorption cell and the resulting signal was chopped at 500 Hz before entering the detector. The spectral trace was recorded on a personal computer (PC).

3.1 Experimental Description

The layout of the experiment is depicted in Figure 4.

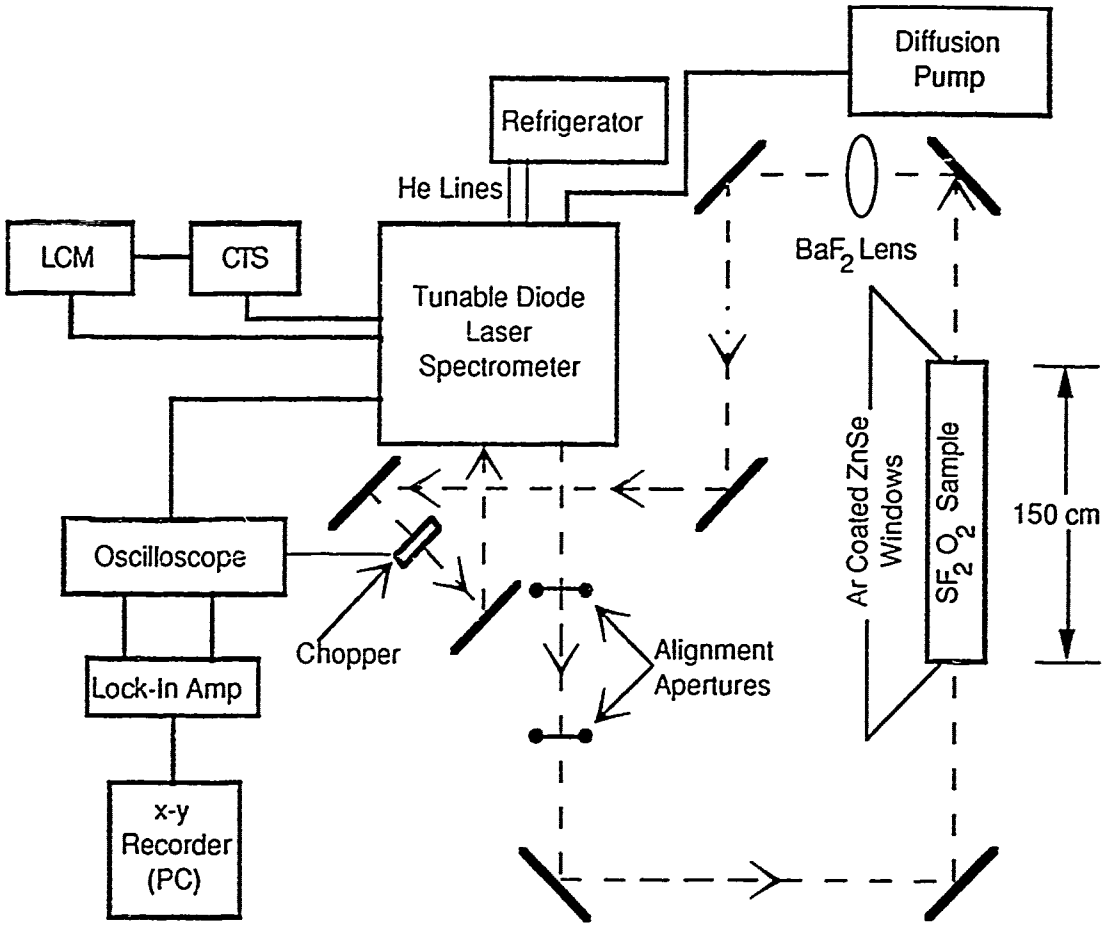

Figure 4---Experimental Layout

The source is a small (400 μ x 200 μ) crystal chip of the Pb-salt family with a typical line width of a few megahertz [16] [p. 945], [15] [p.2695]. The chip is mounted in a refrigerated dewar (cold head) and is part of an overall laser system. This system is a Laser Photonics model LS-3 laser spectrometer. In addition to the laser source, the spectrometer includes: a HgCdTe type, liquid nitrogen cooled detector with low-noise amplifier, a cryogenic temperature stabilizer (CTS); a laser control module (LCM); a grating monochromator; and various optics (see Figure 5).

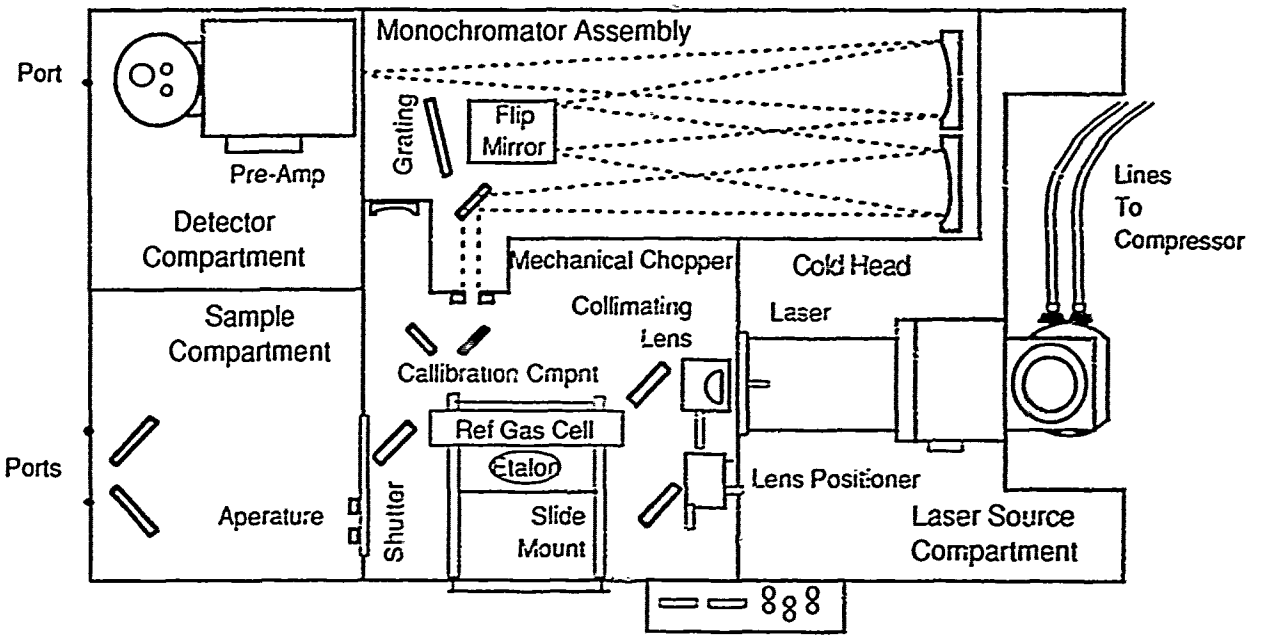

Figure 5—Tunable Diode Laser Spectrometer. From [16] [p.9-3].

The laser is cooled by a CTI-Cryogenics model 22C cryodyne refrigeration system. It operates on a high purity, closed He gas expansion cycle, and can cool the laser down to a temperature of 14°K. The CTS provides temperature stabilization of the laser cold head to the order of less than a millikelvin. At cryogenic temperatures it also provides a convenient and accurate temperature indicator for the range of operation of this experiment. Although the cold head is a closed system, interior outgassing necessitated periodic evacuation. The vacuum was maintained by a liquid nitrogen cold trapped Varien diffusion pump operating in tandem with a standard roughing pump.

The LCM provides current control of either positive or negative polarity to the laser. The current can be adjusted from zero to a limit of 2 Amps at a continuously adjustable rate from 10^{-2} to 10^{-5} Amps/sec.

The grating monochromator provides two functions. It gives absolute frequency calibration to within 0.5 cm^{-1}, and, by varying the slit width, it can act as a variable frequency bandpass filter (~0.5 cm^{-1} wide). The latter function is necessary because the laser emits

multiple modes, and high resolution spectroscopy is performed with only one mode at a time [16] [p. 948].

This method of using the monochromator and the CTS for coarse tuning and the LCM for fine tuning allows a limited tuning range of about 1 to 2 cm^{-1}. The tuning behavior results from the dependence of mode frequencies on both the energy bandgap and the refractive index of the crystal [16] [p.947].

The SF_2O_2 sample is stored at low pressure in a 150 cm stainless steel cylinder with AR coated ZnSe windows. The purity of the sample is not known.

Scans were recorded on a computer with the help of the software package that came with the Stanford Research Systems model SR510 Lock-in amplifier.

3.2 Conduct of the Experiment

From earlier experiments we knew the P and R-branches of the ν_8 vibrational band would be in the 885 cm^{-1} region [11], [12], so we ordered laser crystals which were designed to be tunable in this region. Once the laser crystals were mounted in the cold head, all modes of the laser output in this particular frequency range were identified by tuning the monochromator to the approximate wave number and using the CTS to adjust the temperature of the laser.

The laser output was observed on the oscilloscope while the LCM was used to ramp the current over the entire current range. Only those oscillating laser modes whose transmission profiles were free of mode-hops or other irregularities were selected. We then repeated this process at different temperatures until we had a collection of acceptable modes for a particular frequency setting of the monochromator. For another frequency, the monochromator was reset and the process repeated.

The procedure for actually recording spectra involved three steps. At a fixed monochromator setting and a fixed cold head temperature, the laser current current was slowly swept. First, we placed the cell containing the SF_2O_2 sample in the beam path. The cell was

then removed from the beam path and the current sweep was repeated in the exact same manner. This transmission scan provided a record of the pure laser power output profile. An air-spaced Ge fabry-perot etalon (with a free spectral range of .05 cm^{-1}) was placed in the beam path for the final scan. The etalon would hopefully provide a means to establish a relative frequency scale for each family of scans [16] [pp. 948-949], [13].

The scans were recorded in a personal computer in a volts versus time Cartesian format. This computer was hooked directly to the lock-in amplifier. The available software gave us an option of selecting a sample rate varying from 20 to 2 Hz. A standard sampling rate of 2 Hz was selected to balance the need for a high signal to noise ratio against the need for a reasonable scanning time.

Initially the SF_2O_2 sample was placed in a cell 30 cm long at 300 mTorr. This cell was small and easily handled, but did not provide for enough absorption to measure low J rotational transitions. The SF_2O_2 sample was then moved to a cell 150 cm long and kept at 900 mTorr. The pressure was gradually reduced to 150 mTorr to prevent saturation of the transition, and to ensure we were well within the doppler-broadened regime. This combination of cell length and sample pressure allowed the measurement of even the lowest J transitions, as long as the lines were not obscured by other transitions.

There are basically two methods for recording spectra with a tunable diode laser [15] [p. 2697], [13]. One method is by rapidly ramping the current over the entire current range and recording the output on a multichannel integrator. Since a multichannel integrator was not available, we relied on the more conventional lock-in method. In this method the diode current is slowly swept as the output is traced on the recorder (which in this case is the computer screen) utilizing a step and integration collection method [13]. After some trials, we decided that a current scanning rate of 10^{-4} amps/sec was ideal for the type of scans we wanted and the amount of detail needed. Faster scanning rates tended to smear away details while slower rates allowed excessive thermal and vibrational noise to obscure the spectra. The characteristics of the laser also had an impact on the data collection. A crystal with a frequency scanning rate over about 480

MHz/milliamp would force us to slow the current scanning rate below the level at which unacceptable amounts of noise would creep in.

3.3 Data Analysis

After a set of scans for a particular monochromator setting was recorded, a normalized spectrum was then created by dividing the absorption scan by the transmission scan. It was evident that the scans produced a distinct set of lines that appeared to be somewhat regularly spaced, but before those lines could be unambiguously assigned to various SF_2O_2 transitions, it was necessary to examine the available information on the molecule more closely.

Previous work in both the microwave and infrared regions has given reliable information about the structure and inertial parameters of SF_2O_2. SF_2O_2 possesses C_{2v} symmetry with a pair of oxygen atoms and a pair of fluorine atoms attached to the central sulfur atom tetrahedrally (see Figure 6) [14] [p. 4]. From previous microwave work, the three inertial constants of SF_2O_2 were found to be A = .1713 cm^{-1}, B = .1693 cm^{-1}, and C = .1686cm^{-1} [14]. The shape of the molecule suggests (and microwave measurements confirm) the assignment of the least axis of inertia (a axis) to the symmetry axis (z axis) of the molecule. However since C and B are nearly equal, the assignment of the b and c axes is not immediately obvious. Since the difference between the greatest and least inertial constants is small compared to the value of the constants themselves, SF_2O_2 is classified as a slightly aspherical asymmetric top, an uncommon type of molecule. Consequently, the asymmetric splitting will be small, and the spectrum, while still representative of an asymmetric rotor, will be simplified [14] [p. 1].

The nine normal vibrations for SF_2O_2 are given in Figure 7 along with their symmetries.

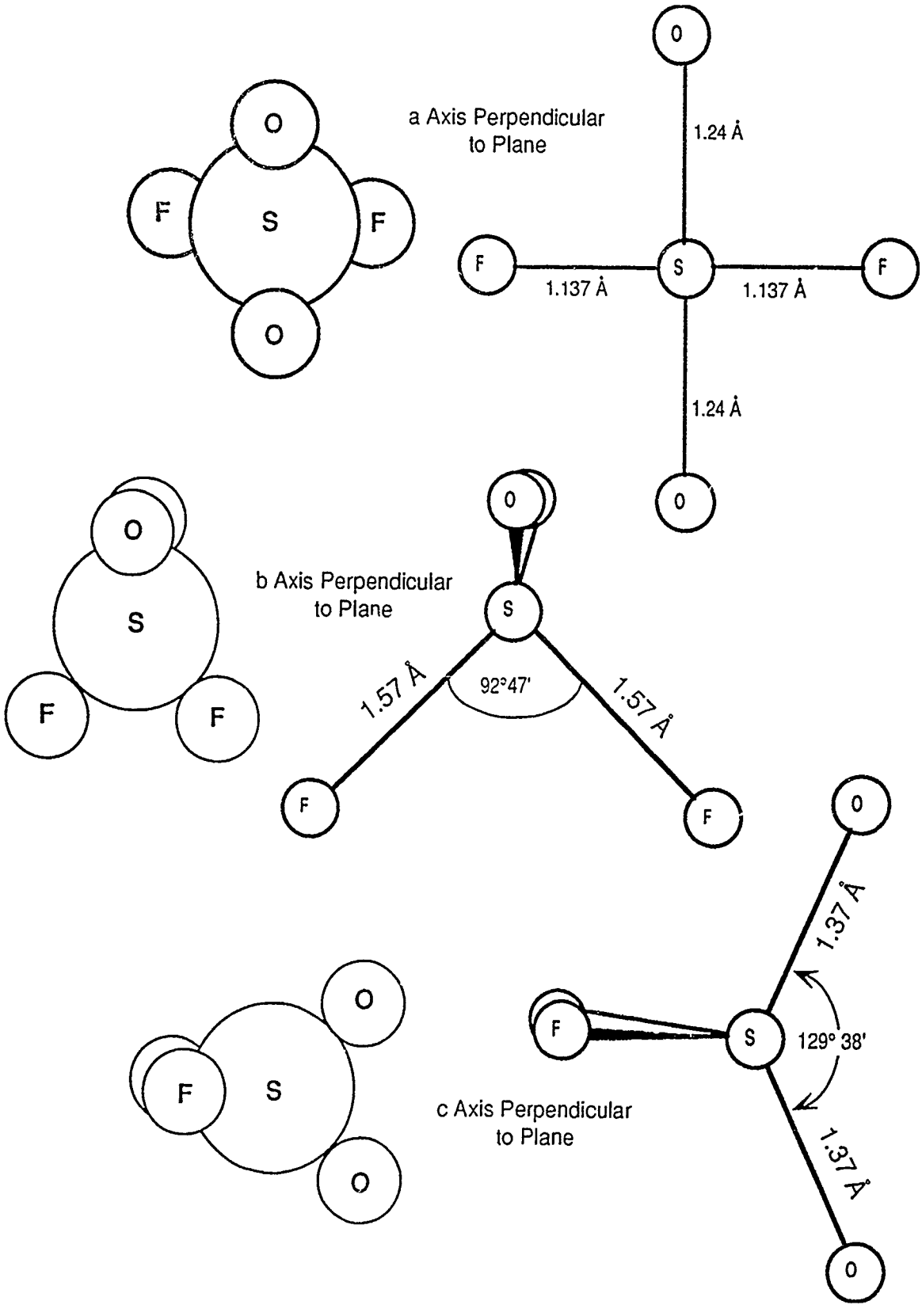
O
F
S
F
O
a Axis Perpendicular
to Plane
O
1.24 Å
F
S
F
1.137 Å
1.137 Å
1.24 Å
O
O
S
F
F
b Axis Perpendicular
to Plane
O
S
1.57 Å
92°47'
1.57 Å
F
F
O
F
S
O
c Axis Perpendicular
to Plane
O
1.37 Å
F
S
129° 38'
1.37 Å
O

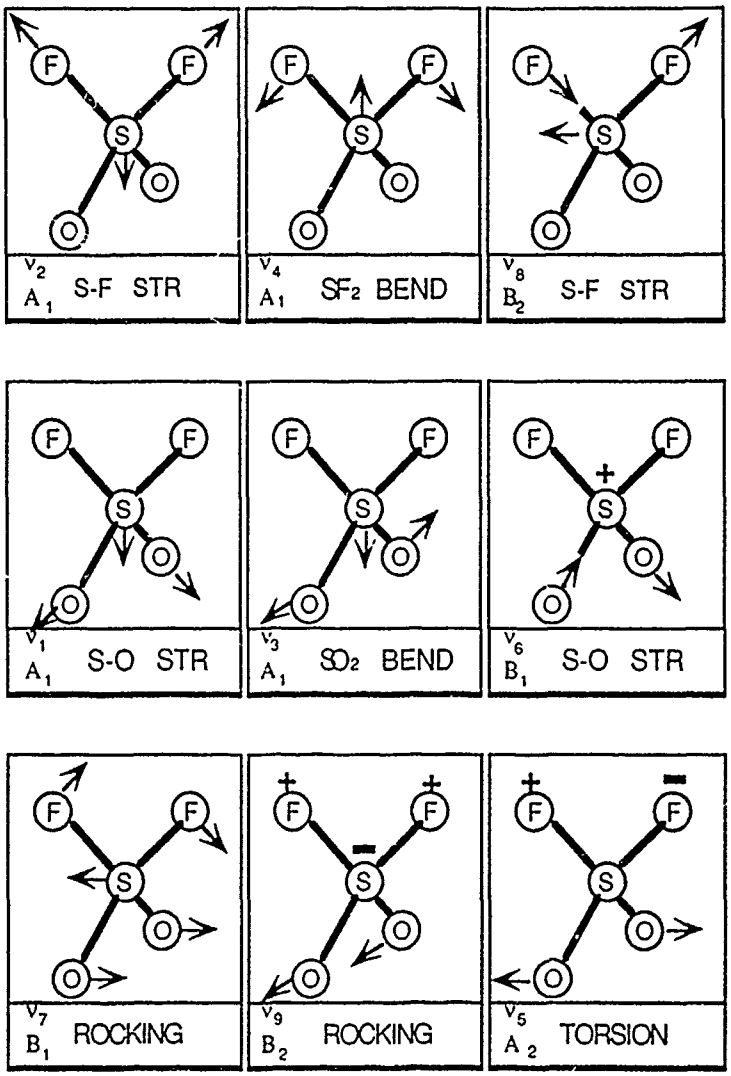

Figure 7--The Normal Vibrational Modes Of SF_2O_2. From [11] [p.1792].

Figure 6 (previous page)--Structure of SF_2O_2. From [14].

The vibration we are studying has been described as the SF_2 asymmetric stretch (ν_8 band). The schematic of the transition is given in Figure 8.

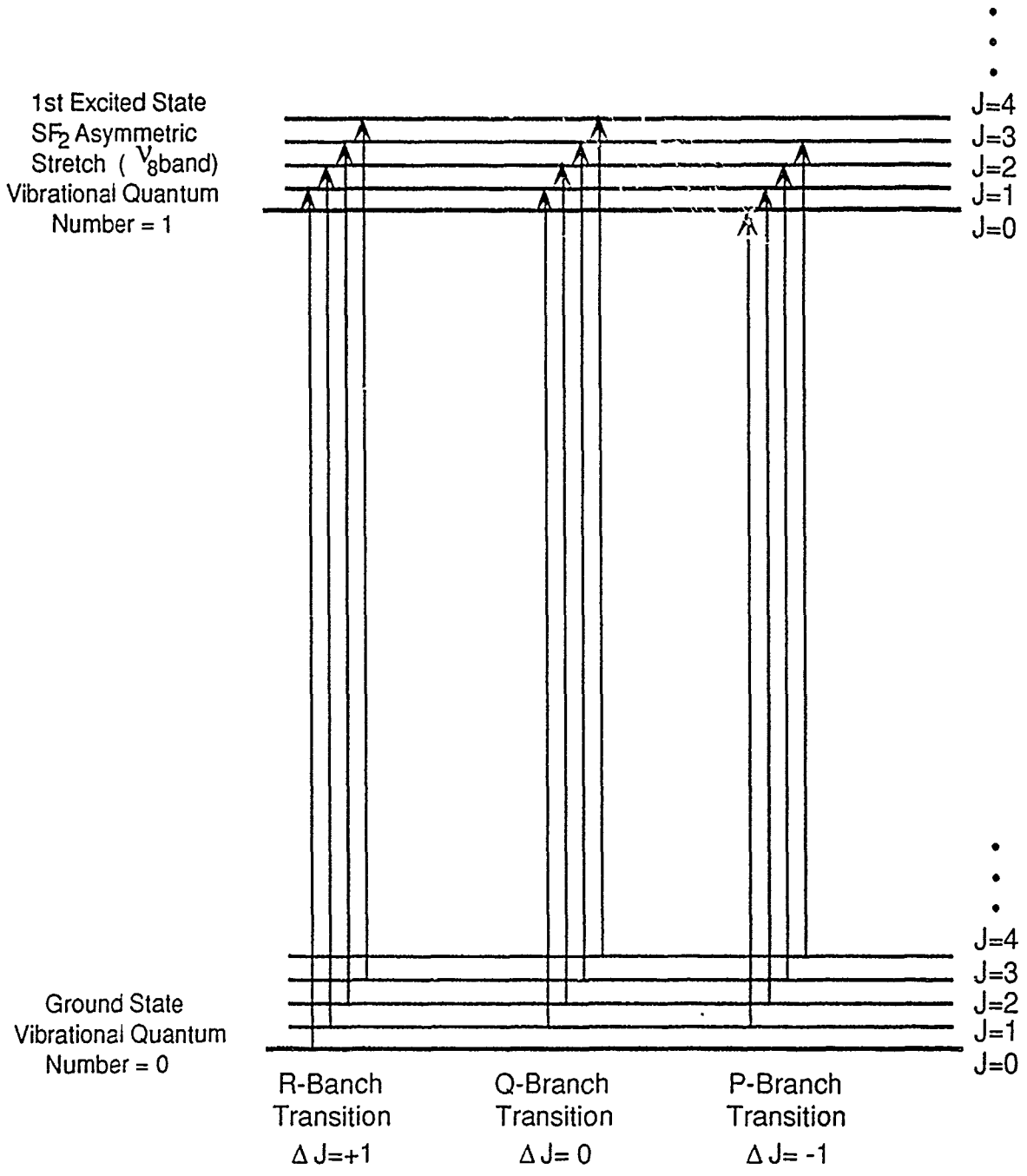

Figure 8--Schematic of the ν_8 Transition for the Slightly Aspherical Rotor SF_2O_2

The spectrum is divided into P, Q, and R -branches based on the primary selection rules for asymmetric rotors $\Delta J = -1, 0, +1$ respectively . Because SF_2O_2 is very nearly a spherical top, we should expect to see a distinct and well-defined PQR structure [11] [p. 1791].

Classically, a vibrational transition is connected with a change in the dipole moment of the molecule. For a transition to be IR active, it must have non-zero matrix elements. For any molecule of the form X_2YZ_2 having C_{2v} symmetry, the only transition that is IR inactive is the tortion oscillation of X_2 against Y_2 [26] [p. 240]. For SF_2O_2 this corresponds to the ν_5 mode (see Figure 7).

The vibrational transitions of molecules are classified into A, B, or C type bands depending on whether the change in the dipole moment lies along the a, b, or c axes. SF_2O_2 does have a permanent dipole moment of .228 $\pm$.004 Debye which lies along the symmetry axis (a axis) and points in the direction of the two fluorine atoms [14] [p. 5]. Since the ν_8 asymmetrical stretch of SF_2O_2 lies entirely in one plane, the only type of transitions we will observe will be transitions represented by changes in the dipole moment along the a axis and/or the perpendicular axis lying in the plane of the ν_8 vibration. But further examination of the molecular structure of SF_2O_2 suggests that, for the ν_8 asymmetrical stretch, the strongest dipole moment change would lie in the axis perpendicular to the a axis in the plane of the vibration. Since earlier microwave work was unable to resolve the b axis from the c axis, it was not immediately clear if we would observe B-type or C-type bands in the spectra. In any case, we can eliminate A-type bands because the structure of the spectra would be completely different from what we observe. Fortunately, it is relatively easy to distinguish between B and C type bands by examining their Q-branch structure. The Q-branch structure of a B-type band does not possess a strong central branch. Rather, the Q-branch has a central minimum and its lines tend to overlap the P and R-branches. In contrast, a C-type band of an asymmetric rotor in the prolate symmetric limit strongly resembles the perpendicular band of the symmetric rotor. This band is characterized by a strong central Q-branch of unresolved lines that are generally stronger than the P and R-branch lines [27] [p.88]. This stark difference in Q-branch structure between B and C type bands should help to determine if the observed spectral transitions are B or C type.

Finally, we can use Equation (25) to estimate the relative spacings of the transitions, at least for low values of J. If we neglect centrifugal distortion, set the inertial constants for the

excited state approximately equal to their value in the ground state, and note that $A \approx C$, we see that each transition is separated by an interval $E \approx (A + C) \approx 10.2$ GHz.

So, based on the physical properties of SF_2O_2, we are looking for a well-defined PQR structure, and a Q-branch reflecting the characteristic shape of a (B or C) type transition. The transitions should be approximately 10.2 GHz apart from one another and each transition should have a fairly regular structure due to the slightly aspherical nature of the molecule.

3.4 Determination of Relative and Absolute Frequency

To measure the spacing of the transitions, we initially used an air spaced Ge etalon with a free spectral range of .05 cm^{-1}. It was hoped this etalon would give a large number of closely spaced peaks within the range of the scan, thereby allowing a frequency scale to be established[13]. Assuming each peak was separated by .05 cm^{-1}, a linear scanning rate for each peak interval was established by dividing .05 cm^{-1} by the measured time interval between each etalon peak. The spacing of each transition was then determined by counting the number of etalon peaks between the transitions, then multiplying the determined scanning rate by the remaining fractional intervals. We were able to find that the interval between the major prominent features of each scan to be around 10 GHz, leading us to conclude that we were in fact observing transitions of the ν_8 band of SF_2O_2. However, we also measured intervals of other scans with the etalon that ranged from 8 to 12 GHz. Apparently the free spectral range of the etalon was too large to effectively linearize the diode scan. Other etalons with smaller free spectral ranges were tried, but were found to be too sensitive to vibrations to give consistent results.

This problem was corrected at the same time a way was found to determine absolute frequency. Since the monochromator could not give a precise location in frequency space, SiH_4, which has a structure that is very precisely known, was used as a reference [28]. In the experimental procedure, the etalon scan was replaced with a simultaneous scan of both the SF_2O_2 sample cell and the SiH_4 sample cell. The SF_2O_2 transitions were now superimposed on SiH_4

lines which had well known locations. Relative and absolute frequency could now be determined by measuring the time interval between the nearest two SiH_4 lines which straddled each SF_2O_2 transition. This technique did not completely account for all the error of a non-linear diode tuning rate, but results were much more self-consistent, and more consistent with the theoretical approximations. (see Table 14).

3.5 Interpreting the Spectra

An examination of the Q-branch scans showed quite clearly that we were dealing with C-type transitions. The Q-branch strongly resembles the parallel type band of a symmetric prolate rotor. This knowledge, along with the nuclear spin statistics, allowed us to immediately identify each transition with an even or odd rotational quantum number. This is because the lines of each transition of the P and R-branches (the Q-branch lines are not resolved) at some point show a regular alteration in intensity in complete agreement with the nuclear spin statistics of the two fluorine atoms. For a C-type band, even J transitions start with a weak line (on the high energy side), odd J transitions with a strong line. For the R-branch these parity assignments were confirmed when actual J-values were assigned to each transition by using the SiH_4 lines and counting the number of 10.2 GHz intervals from the edge of the Q-branch. This was not so easy on the P-Branch side because there was no definite edge to the Q-branch there, and it was clear that an unknown number of P-branch transitions were obscured by the Q-branch lines.

To be absolutely sure of the quantum number assignments on the R-branch side, and to determine how many P-branch transitions were actually hidden by Q-branch lines it was necessary to actually identify in the scans as many low J transitions as possible. This was not easy, because the low J transitions on both the P and R-branch sides were weak and it was hard to tell them apart from the noise in the scan. One way to strengthen the low J transitions was to change the Boltzman distribution of the sample. We did this by cooling the cell to dry ice temperature. Under the approximations given in Equation (57) and Equation (52), the rotational wave functions,

and hence the rotational energies, are independent from the other energies of the molecule. Therefore we can approximate the fraction of molecules in the sample at a particular rotational energy level J by Equation (55). If we approximate A ≈ C, then we have from Equation (55)

$$f_{J\,K_{-1}K_1} \approx f_J = \frac{(2J+1)\exp\dfrac{-(A+C)J(J+1)}{2k_BT}}{\sum_J (2J+1)\exp\dfrac{-(A+C)J(J+1)}{2k_BT}} \quad \text{, for A and C in units of energy} \tag{62}$$

For this molecule in the ground state $k_BT \gg \frac{1}{2}(A+C)$, even at dry ice temperatures. Thus $\sum \rightarrow \int$, and the denominator of Equation (62) becomes

$$\int_0^\infty (2J+1)\exp\frac{-(A+C)J(J+1)}{2k_BT} = \frac{2k_BT}{(A+C)} \tag{63}$$

To determine the preferred J value at any particular temperature we set

$$\frac{d(f_J)}{dJ} = 0 \tag{64}$$

which leads to

$$J_{max} = \sqrt{\frac{1}{(A+C)}(k_BT)} - \frac{1}{2} \text{ for A and C in units of energy} \tag{65}$$

For room temperature $J_{max} \approx 25$. For dry ice temperatures $(-80°C)$, $J_{max} \approx 20$. By cooling the cell with dry ice we were able to identify all R-branch transitions, and all P-branch transitions down to J=4. (the J value of this transition was later confirmed by direct association with computer generated spectra.)

Although we determined the SF_2O_2 spectra to be primarily C-type transitions, there was still some structure in the absorption scans that could not be accounted for. Since there were no B or A transitions for the ν_8 band, this additional structure could only be coming from another vibrational transition (hot band), or from an isotopic band. The only isotope that exists in any

appreciable quantity for any SF_2O_2 component is ^{34}S. Approximately 1/20 of all sulfur is ^{34}S. Therefore, if the observed structure was due to ^{34}S, we would expect to see a C-type spectrum that was 1/20 as intense as our primary spectra with the following modifications: Under the harmonic oscillator approximation, the vibrational band center would be shifted by an amount proportional to the ratios of the reduced masses; that is:

$$\mu = \frac{m_s}{m_s + 2m_f + 2m_o} = \frac{32}{32+38+32} = \frac{32}{102} \tag{66}$$

$$\mu^i = \frac{m_s^i}{m_s^i + 2m_f + 2m_o} = \frac{34}{34+38+32} = \frac{34}{104} \tag{67}$$

$^{32}SF_2O_2$ band center: $$\sqrt{\frac{\mu}{\mu^i}}(872.21) \approx 869.12\,cm^{-1} \tag{68}$$

Furthermore the transition spacings will be shifted an amount approximated to first order by

$$\left(\frac{A+C}{2}\right)\left(\frac{\mu}{\mu^i}\right) \approx 9.79Ghz \tag{69}$$

However, this type of structure was not observed. What we do see is too strong and does not follow the above patterns. Therefore we conclude that the unidentified structure is probably not due to the isotope ^{34}S.

To check the possibility that the structure may be due to a hot band, we can check Table 9 for the correct vibrational difference combinations.

Table 9
Observed Frequencies and Band Assignments for SF_2O_2. From [12] [p. 572]

ν (cm-1)	Assignments
274	ν_4
360	ν_5
386	ν_9
539	ν_7
544	$2\nu_4$
553	ν_3
668	$\nu_4 + \nu_9$
720	$2\nu_5$
769	$2\nu_9$
848	ν_2
887.2	ν_8
925	$2\nu_4 + \nu_9$
954	$\nu_6 - \nu_3$
1077	$2\nu_7$
1092	$\nu_3 + \nu_7$
1103	$2\nu_3$
1118	$\nu_2 + \nu_4$
1269	ν_1
1389	$\nu_2 + \nu_7$
1502	ν_6
1698	$2\nu_2$
1727	$\nu_2 + \nu_8$
1772	$2\nu_8$
1820	$\nu_1 + \nu_3$
1889	?
2052	$\nu_3 + \nu_6$
2115	$\nu_1 + \nu_2$
2355	$\nu_2 + \nu_6$
2536	$2\nu_1$
2760	$\nu_1 + \nu_6$
2995	$2\nu_6$

We look for difference combinations of various excited bands that come close to being separated by $887cm^{-1}$, and have an appreciable occupation at room temperature. The only likely candidates are listed in Table 10.

Table 10
Possible Hot Bands

Band	+ 887 cm-1 =	Band	+ Left-over Rotational Energy	Rotational J-values[1] to which left-over Rotational Energy Corresponds
$\nu_4 = 1$ $(274cm^{-1})$		$\nu_7 = 2$ $(1077cm^{-1})$	$84cm^{-1}$	252
$\nu_5 = 1$ $(360cm^{-1})$		$\nu_1 = 1$ $(1269cm^{-1})$	$-22cm^{-1}$	66
$\nu_9 = 1$ $(386cm^{-1})$		$\nu_1 = 1$ $(1269cm^{-1})$	$4cm^{-1}$	12

[1]Based on a spacing of approx. .34 cm^{-1} per transition

Based on the information in Table 10 we can eliminate all but the ν_9 band. The other modes involve interactions with J-values that are so high as to preclude any appreciable occupation at room temperature(for example, the J=66 rotational level has an occupation of only .028%). Therefore, if the unidentified structure is hot band activity, it is probably due to the transition $\nu_9 = 1 \rightarrow \nu_1 = 1$.

Next we use the fact that the Boltzman occupancy of the ν_9 band will change differently with temperature than the occupancy of the ν_8 band. Using Equation (52), Equation (54), Equation (62) and Equation (63) we can construct the following table

Table 11

Comparison of Fractional Occupancies ($f_V f_J$) of Typical Low-J Transitions of the ν_8 Band with Hot Band $\nu_9 = 1$ Transitions of Similar Energies

Basic Data			Comparison Of Fractional Occupancies	
Vibrational State	Fractional Occupancy at Room Temp. (T = 294 °K)	Fractional Occupancy at Dry Ice Temp. (T = 193°K)	Fractional Occupancy at Room Temp. (T = 294 °K)	Fractional Occupancy at Dry Ice Temp. (T = 193°K)
Ground State	$f_V = 43.4\%$	$f_V = 74.9\%$	$f_{ground\ state} f_{J=3} =$ .25%	$f_{ground\ state} f_{J=3} =$ .65%
$\nu_9 = 1$	$f_V = 6.6\%$	$f_V = 4.2\%$	$f_{\nu_9=1} f_{J=15} =$ .14%	$f_{\nu_9=1} f_{J=15} =$ .12%
Rotational State			$f_{ground\ state} f_{J=7} =$ .52%	$f_{ground\ state} f_{J=7} =$ 1.33%
J = 3	$f_J = .57\%$	$f_J = .87\%$	$f_{\nu_9=1} f_{J=19} =$ .16%	$f_{\nu_9=1} f_{J=19} =$ .13%
J = 7	$f_J = 1.19\%$	$f_J = 1.77\%$		
J = 15	$f_J = 2.11\%$	$f_J = 2.90\%$		
J = 19	$f_J = 2.37\%$	$f_J = 3.06\%$		

If we now go to our scans we see that in each case as we go from room temperature to dry ice temperature, the strength of the ν_8 band transition increases while that of the hot band decreases, just as predicted in Table 11. If we take the ratio of the strongest ν_8 band line to the strongest hot band line in the same scan, and compare this ratio at both temperatures, we should see that the ratio will always increase as we go from room temperature down to dry ice temperature (see Figure 9).

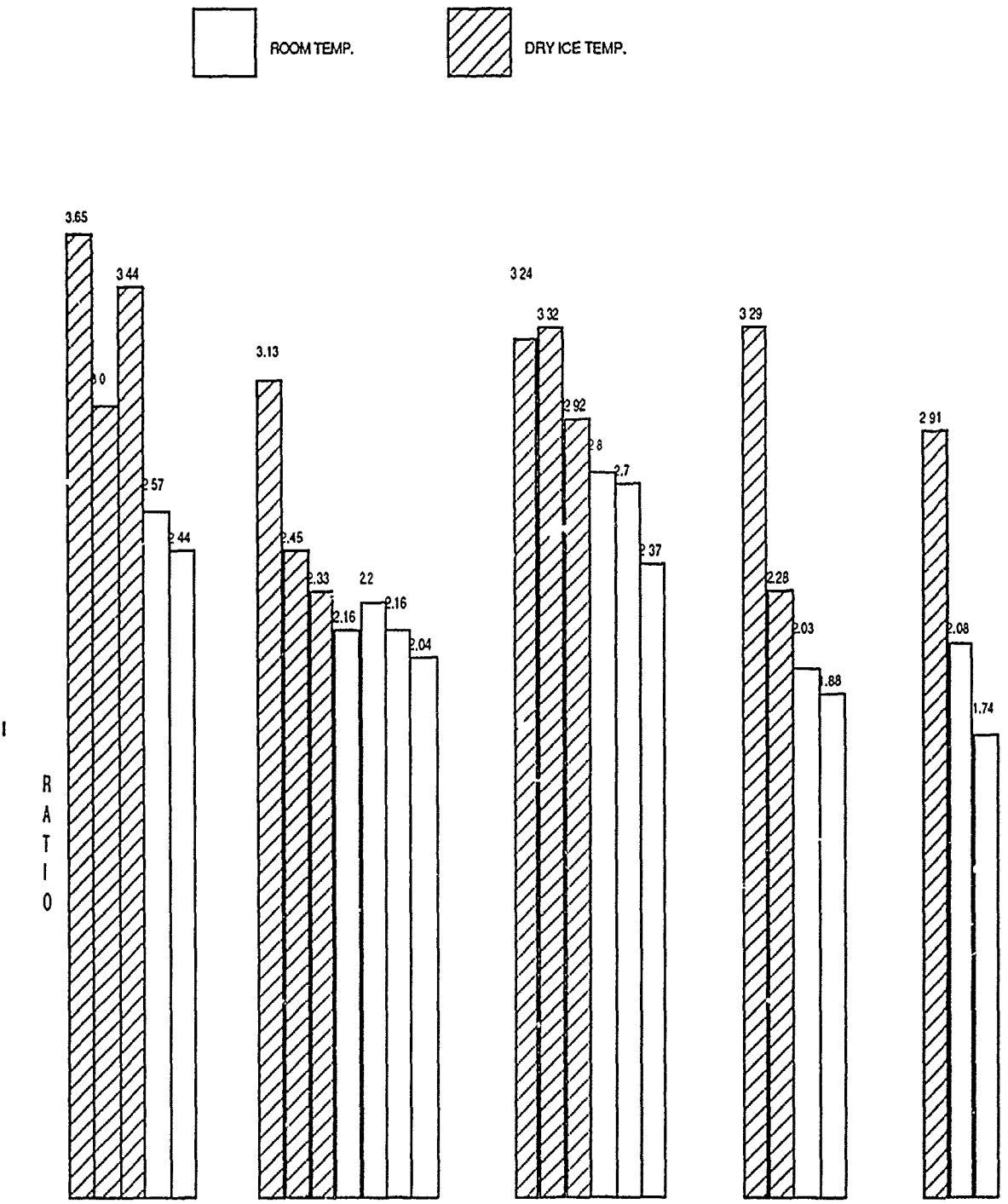

Figure 9—Comparison of Lines From the ν_8 Band to Lines from the Hot Band Transition At Room and Dry Ice Temperatures

Figure 9 shows that the experimental scans do in fact display the predicted pattern. Therefore we conclude that the unidentified structure in the scans which cannot be attributed to

the C-type transitions of the ν_8 band are most probably hot band transitions originating from the ν_9 vibrational band.

Chapter 4

ERROR ANALYSIS

The largest source of experimental error was the diode itself. Over the course of the scans, taken in the lock-in mode, small deviations in frequency output linearity were observed which did not reproduce from scan to scan [15] [p.2699]. These instabilities in the laser affected our ability to pinpoint transition frequencies, that is, repeated scans of the same transition produced different locations in frequency space for the same lines. The precision with which we could measure the frequency of a particular transition varied from transition to transition depending on the behavior of the laser and the relation of the transition line in question to the superimposed SiH_4 sample lines. These errors were accounted for by scanning each transition several times and using the sample standard deviation as a measure of the uncertainty or precision of the frequency of each line entered into the least-squares fit program. The program then assigned a relative weight factor, by standard least-squares theory, to each line based on the entered uncertainty.

The instabilities in the laser output frequency arise from the sensitivity of the laser to temperature, current and mechanical fluctuations. In each case, we were able to develop techniques for minimizing the errors produced from each source.

Of all the sources of instability, the diode is most sensitive to temperature fluctuation [15] [p. 2695]. Temperature fluctuations over the course of a scan are either instantaneous or long term. Long term temperature fluctuations (temperature drift) were detected by comparing the CTS panel readings from the beginning and the end of the scans. However, unless the CTS was monitored constantly during the scan, only cumulative temperature drift could be detected. For the CTS model used, which employed a silicon diode temperature sensor, typical temperature drifts are given in Table 12.

Table 12
Temperature Drift

	Temperature Drift	Si Diode Behavior
T>25°K	$\pm.003\frac{°K}{min}$	$2.7\frac{mV}{°K}$
T<25°K	$\pm.001\frac{°K}{min}$	$50\frac{mV}{°K}$

Table 12 also shows that the temperature is susceptible to voltage fluctuations, particularly at lower temperatures. Error due to temperature changes was minimized by rejecting all scans for which large temperature drifts were observed. The diode temperature was also allowed a period of time to stabilize to the new current setting before a scan was initiated.

Although we could eliminate a large number of scans by reading temperature drift from the CTS, not all errors from the temperature fluctuation could be eliminated this way. Instantaneous temperature variations, temperature hysteresis , and temperature drift which affected the laser but could not be measured on the CTS still influenced the scans. Temperature hysteresis results in an overall (non-reproducable) frequency shift between scans [15] [p. 2699]. This error manifests itself when the scans are normalized. Since absorption and transmission scans were not taken simultaneously, dividing them together, when one is shifted with respect to the other, may have introduced a shift in the line positions. If the right equipment is available, the shift between absorption and transmission scans can be eliminated. One way is to split the beam before it enters the sample cell. Part of the beam then travels through the sample, while the other part does not. The beams remain spatially separated through the monochromator and enter separate detectors. Since the scans are recorded simultaneously, there will be no shift.

But even if absolute shift between divided scans is eliminated, there still exists instantaneous temperature fluctuations and some temperature drift. Both drift (which has already been discussed) and fluctuations are functions of the CTS. The ability of the CTS to stabilize the temperature (and hence eliminate fluctuations) is affected in part by the sensor responsitivity. The increase in heat capacity of the sensor with temperature will slow the speed

of the cryogenic heat sink and increase the time required to stabilize the temperature as the current changes during the scan. We compensated for this as much as we could by optimizing the gain and reset controls on the CTS for each scan temperature. Another way to eliminate the effect of a temperature fluctuation would be to use the sweep integration method of recording data. Since scan times for this method of data collection are extremely fast (10 seconds or less), the laser mount temperature, once it has reached equilibrium with respect to the average current, generally remains stable over periods lasting much longer than the typical scan time [15] [p. 2697].

Fluctuations in current, or non-linear current sweeps, are also classified as instantaneous and long-term. Instantaneous fluctuations result from changes in ambient temperature and the ability of the LCM to control transient currents. For this system, typical values are given in Table 13.

Table 13
Current Stability

Current Readout Accuracy	.1mAmp
Drift	$\approx .02 \frac{\text{mAmp}}{\text{day}}$
Temperature Stability	$\approx .02 \frac{\text{mAmp}}{^{\circ}\text{C}}$
Line Voltage Stability	≈ .01 mAmp change for line voltage change up to 20%

From the table we see that the current is much more stable than the temperature. But at a typical diode tuning rate of 480 MHz/mAmp, even current fluctuations can lead to errors.

The major source of mechanical fluctuations was the refrigerator piston in the cold head. Although various methods of insulating the cold head were tried , this vibration could not be eliminated completely. This is one of the reasons the etalon was abandoned as a means of measuring relative frequency in the spectra. The jiggle in the beam as it traveled through the etalon caused the peak spacings to vary considerably within the same scan, making them almost

useless as measuring tools. The smaller the free spectral range of the etalon, the worse the effect. Besides going to the SiH_4 as a means of estimating relative frequency, the effect of the vibration was minimized by using irises to clip the perimeter of the beam, thereby eliminating the most unstable part of the beam profile.

The net effect of these error sources was to cause the current-temperature combination at each frequency to be different from scan to scan, resulting in deviations from frequency linearity down to the MHz level [16] [p.951]. Because we derived relative frequency in the spectra by estimating a linear scan rate between neighboring SiH_4 lines, transition lines which were closer to the SiH_4 lines were inherently more accurate than lines which were farther away. Lines that were far away were subject to a cumulative error as the linear estimate deviated farther and farther from the actual non-linear scan rate. This effect was manifested in larger sample variances for transitions that were positioned far away from SiH_4 lines.

As stated earlier, because these errors manifest themselves as variations in transition frequencies which are not reproducible from scan to scan,they can be treated as random errors. Therefore the sample variance is a measure of the frequency error. Table 14 lists the data from the usable scans that were actually entered into the least-squares fit program. It was assumed that all lines within the same transition shared the same variance. Each line entered into the program with its accompanying variance was assigned a weight factor by the least-squares routine. Table 14 does not represent all the scans taken. Those scans which were too noisy or otherwise distorted or smeared beyond value were eliminated from consideration . Scans which produced values which were so far off as to be obviously incorrect were discarded or retaken.

Table 14

Spectral Data For Least-Squares Fitting Routine

Observed J Transition	Sample Mean[1]	Sample Standard Deviation	Transition Spacing[2] (Ghz)
29 → 30	897.2524	≈.0001	
			9.67
28 → 29	896.9300	.0005	
			9.97
27 → 28	896.5976	.0010	
17 → 18	893.2986	.0002	
			10.21
16 → 17	892.9582	.0015	
12 → 13	891.6268	.0006	
			10.13
11 → 12	891.2891	.0004	
			10.12
10 → 11	890.9517	≈.0001	
			10.08
9 → 10	890.6156	.0003	
			10.09
8 → 9	890.2792	.0028	
			10.20

Table 14 (cont)

7 → 8	889.9391	.0018	10.20
6 → 7	889.5990	.0016	10.12
5 → 6	889.2617	.0014	10.18
4 → 5	888.9225	.0005	10.22
3 → 4	888.5818	.0006	10.22
2 → 3	888.2412	.0012	10.21
1 → 2	887.9008	.0001	
5 → 4	885.5030	.0013	10.20
6 → 5	885.1631	.0004	10.23
7 → 6	884.8220	.0005	
13 → 12	882.7302	.0001	
16 → 15	882.6873	.0007	

[1]Reflects value of first line on high energy side of transition

[2] Rigid Rotor approximation predicts a transition interval of ≈ 10.2 Ghz for low-J transitions.

The basis of accuracy in this experiment comes from the SiH_4 lines. They are given to an accuracy of .0001 cm^{-1} [28]. Our accuracy may have also been affected by the sample rate. Linear estimates of scan rates varied typically from 20-40 MHz/sec. A sample rate of 2 Hz may have introduced errors into the absolute frequency measurements. However the net effect of the low sample rate over our entire scan should cancel itself out, and this effect can be ignored.

Since we were operating with a sample pressure of 150 mTorr , we were well into the doppler-broadened regime. The broadening of the lines is given by

$$FWHM = \frac{214}{\lambda}\sqrt{\frac{T}{M}} \tag{70}$$

where FWHM is the full width of the transition line at half-maximum in MHz, λ is the frequency of the laser in microns, T is the sample temperature in °K, and M is the mass of the sample in atomic mass units. For SF_2O_2, we get a width of FWHM = 57 MHz at room temperature. This amount of width did not prevent us from determining line centers to any significant degree.

The least squares fitting routine relies on the ground state inertial constants as starting points in the fitting process. For the fitting process, the ground state inertial constants from the previous microwave experiments were used. We can use the rigid rotor approximation and our experimental data to calculate the ground state inertial constants and verify the accuracy of the constants used[7]. We start with the general rigid rotor hamiltonian for an asymmetric molecule in the prolate limit

$$H_R = AJ_a^2 + BJ_b^2 + CJ_c^2 \tag{71}$$

which means

$$E_{(abc)} = \langle H_R \rangle = A\langle J_a^2 \rangle + B\langle J_b^2 \rangle + C\langle J_c^2 \rangle \tag{72}$$

[7]The theory of this portion of Chapter 4 is taken from the following References: [3] [pp. 43-44,188-189,204-205]; [29] [p. 738]; [9] [p. 1578].

where $\langle\ \rangle$ stand for the diagonal elements (average values) of the enclosed operators in the basis which diagonalizes H_R.

Now let H_R be perturbed by a small change in C, denoted by δC, and let the perturbation be given by the operator

$$H' = \delta C J_c^2 \tag{73}$$

Then if $E_{(abc)}$ is the energy eigenvalue of the unperturbed operator, we can denote the first order correction due to the perturbation as

$$E = \langle \delta C J_c^2 \rangle \tag{74}$$

Let $E_{(a,b,c+\delta c)}$ be the eigenvalue of the hamiltonian

$$H = AJ_a^2 + BJ_b^2 + (C + \delta C)J_c^2 \tag{75}$$

and define an ε such that

$$E_{(a,b,c+\delta c)} = E_{(abc)} + E' + \varepsilon \tag{76}$$

then

$$\frac{\partial E_{(abc)}}{\partial C} = \lim_{\delta C \to 0} \frac{E'+\varepsilon}{\partial C} \tag{77}$$

But since $\varepsilon \approx O(\delta C^2)$ then

$$\frac{\partial E_{(abc)}}{\partial C} = \langle J_c^2 \rangle \tag{78}$$

In this vein, we can, using Equation (25) and Equation (5),define the following quantities

$$\alpha = \frac{\partial E_{(abc)}}{\partial A} = \frac{1}{2}J(J+1) + \frac{1}{2}E_\kappa - \frac{(\kappa+1)}{2}\frac{\partial E_\kappa}{\partial \kappa}$$

$$\beta = \frac{\partial E_{(abc)}}{\partial B} = \frac{\partial E_\kappa}{\partial \kappa} \tag{79}$$

$$\gamma = \frac{\partial E_{(abc)}}{\partial C} = \frac{1}{2}J(J+1) - \frac{1}{2}E_\kappa - \frac{(1-\kappa)}{2}\frac{\partial E_\kappa}{\partial \kappa}$$

and we can write Equation (72) as

$$E_{(abc)} = \alpha A + \beta B + \gamma C \tag{80}$$

Values for α, β and γ are compiled in Table 15, for various $J_{K_{-1}K_1}$ levels.

Table 15

Approximate Energy Derivatives of a Rigid Asymmetric Rotor (for $\kappa \sim -0.5$). From [3] [p. 190]

$J_{K_{-1}K_1}$	α	β	γ
3_{30}	8.953	1.838	1.209
4_{40}	15.950	2.368	1.681
5_{50}	24.941	2.936	2.122
5_{51}	24.928	2.990	2.082
5_{41}	15.784	8.668	5.583
5_{42}	15.785	8.492	5.723
5_{32}	8.284	15.048	6.667
5_{33}	8.788	12.297	8.915
5_{23}	3.241	20.880	5.878
5_{24}	4.215	11.508	14.277
5_{14}	1.788	16.959	11.253
5_{15}	1.284	4.713	24.002
5_{05}	1.010	5.452	23.538
6_{60}	35.932	3.511	2.558
6_{61}	35.915	3.576	2.508
6_{51}	24.730	10.321	6.984
6_{52}	24.737	10.280	6.973
6_{42}	15.410	16.817	9.973
6_{43}	15.582	15.990	10.428
6_{33}	7.622	25.510	8.868
6_{34}	8.778	18.881	14.341
6_{24}	3.328	29.388	9.284
6_{25}	4.503	15.434	22.063
6_{15}	2.652	20.147	19.200
6_{16}	1.484	5.830	34.686
6_{06}	1.347	6.219	34.434
7_{70}	48.921	4.087	2.992

If we now use the correct energy difference combinations, we can isolate the ground state constants. Ground state energy differences are given by the difference between a P-branch and an R-branch transition which both terminate at the same excited state $J_{K_{-1}K_1}$. If we consider the principle sub-branch of a C-type transition , then each transition involves $\Delta K_{-1} = 1$ and $\Delta K_1 = 0$, and the ground state energy difference is given by

$$\Delta E = R_{(J-1,K_{-1}-1,K_1)} - P_{(J+1,K_{-1}+1,K_1)} \tag{81}$$

where ΔE represents the energy difference between two ground state levels appearing in the two different transitions.

From Equation (25) we get

$$\Delta E = (A + C)(2J + 1) + \left(\frac{A-C}{2}\right)\left[E_{\kappa(J+1,K_{-1}+1,K_1)} - E_{\kappa(J-1,K_{-1}-1,K_1)}\right] \tag{82}$$

and from Equation (80) we have

$$\Delta E = \left[\alpha_{(J+1,K_{-1}+1,K_1)} - \alpha_{(J-1,K_{-1}-1,K_1)}\right]A + \left[\beta_{(J+1,K_{-1}+1,K_1)} - \beta_{(J-1,K_{-1}-1,K_1)}\right]B$$

$$+ \left[\gamma_{(J+1,K_{-1}+1,K_1)} - \gamma_{(J-1,K_{-1}-1,K_1)}\right]C \tag{86}$$

Experimental values of ΔE can be used to check the values (to within rigid rotor accuracies) of A, B and C determined from microwave measurements, before inputing them into the least-squares fitting routine. The results are tabulated in the next chapter.

Chapter 5

RESULTS AND RECOMMENDATIONS

During the course of this experiment, we scanned over an interval of $15cm^{-1}$ covering roughly 46 P and R-branch transitions and thousands of lines. The 200 lines to which we could reliably assign quantum numbers were entered into the least squares program and used to perform the curve fitting. Over 4600 lines have been mapped using the S-Reduced hamiltonian to model the molecular vibration-rotation. Since a listing of all 4600 lines would be prohibitively long, graphical representations of experimental spectra and computer generated spectra (in the P and R-branches) are presented for visual comparison.

The measured excited state band constants and ν_8 band center are presented in Table 16.

Table 16

Measured Excited State Band Constants and ν_8 Band Center

Band Constant (cm^{-1})	Calculated value (cm^{-1})	Estimated Standard Deviation (cm^{-1})
ν_0	887.2185	$.2513 \times 10^{-3}$
A	1710	$.2376 \times 10^{-5}$
B	.1691	$.2624 \times 10^{-4}$
C	.1681	$.4281 \times 10^{-4}$
D_J	$.5809 \times 10^{-7}$	$.6425 \times 10^{-7}$
D_{JK}	$-.7969 \times 10^{-7}$	$.9017 \times 10^{-7}$
D_K	$.3439 \times 10^{-7}$	$.3033 \times 10^{-7}$

Table 16 (cont.)		
d_1	$.6288 \times 10^{-7}$	$.1067 \times 10^{-6}$
d_2	$-.2359 \times 10^{-6}$	$.4440 \times 10^{-7}$

The sextic distortion coefficients were also determined, but were found to be so small as to not contribute to the fit to a significant degree.

Appropriate energy difference combinations of the most reliable experimental low J transitions of the P and R-branches were used to check the values of the ground state inertial constants A, B and C determined in previous microwave experiments. Equation (85) was used to calculate A and C. B was calculated by using Equation (86) and the values of the energy derivatives from Table 15. The results are presented in Table 17.

Table 17

Calculated Ground State Inertial Constants

Inertial Constant	Calculated Value (cm^{-1})	Calculated Standard Deviation (cm^{-1})	Difference From Value given in [14] (Mhz)
A	.17138	.00018	1.8
B	.16983	.00080	17.1
C	.16762	.00221	-28.5

The values in the last column of Table 17 are a reflection of the fact that we are dealing exclusively with C-type transitions for this vibrational band. Because for the principle sub-branch of a C-type transition, $\Delta K_{-1} = 1$ and $\Delta K_1 = 0$, we should expect the transition energy differences to be primarily dependent on A for a molecule approaching the prolate symmetric

limit [see Equation (86)]. For more reliable information on B and C we would have to search for those C-type transitions for which $\Delta K_1 > 0$. These are the weaker transitions in a C-type spectra and would be correspondingly more difficult to isolate. That is why the error differences for B and C in Table 17 are so much greater than the error difference for A, and the estimated standard deviations in Table 16 are similarly skewed. Nevertheless, the differences are still within our experimental resolution, and we can use the values of the ground state inertial constants derived in Reference [14] in the fitting routine with full confidence.

RECOMMENDATIONS

The TDL is still a practical tool for high-resolution spectroscopy in the middle IR region. However, to reduce error, the sweep-integration method of data collection is preferable to the lock-in method. Since the data points are integrated simultaneously, even fast scans would be long enough to reduce the noise and prevent line smearing, thus giving spectra that are reproducible. Experimental setups using the multichannel integrator can be found in Reference [15].

The next logical step in studying SF_2O_2 should involve hetrodyning a CO_2 laser with the diode laser. The P(20) line of $^{13}CO_2$ (at 896.90947969 cm^{-1})is very close to the R-branch transition $J = 28 \rightarrow 29$ and can be used to pinpoint a line very exactly. This type of experiment would provide a very reliable method to independently confirm the results of our experiment.

The following 8 pages contain graphical output of experimental spectra (top of page) and corresponding computer generated spectra (bottom of page). The transitions depicted here are representative of the P-branch and R-branch transitions that were scanned during the course of the experiment. For the sake of clarity some transition quantum numbers and frequencies have been ommited in the experimental spectra.

J=3-4

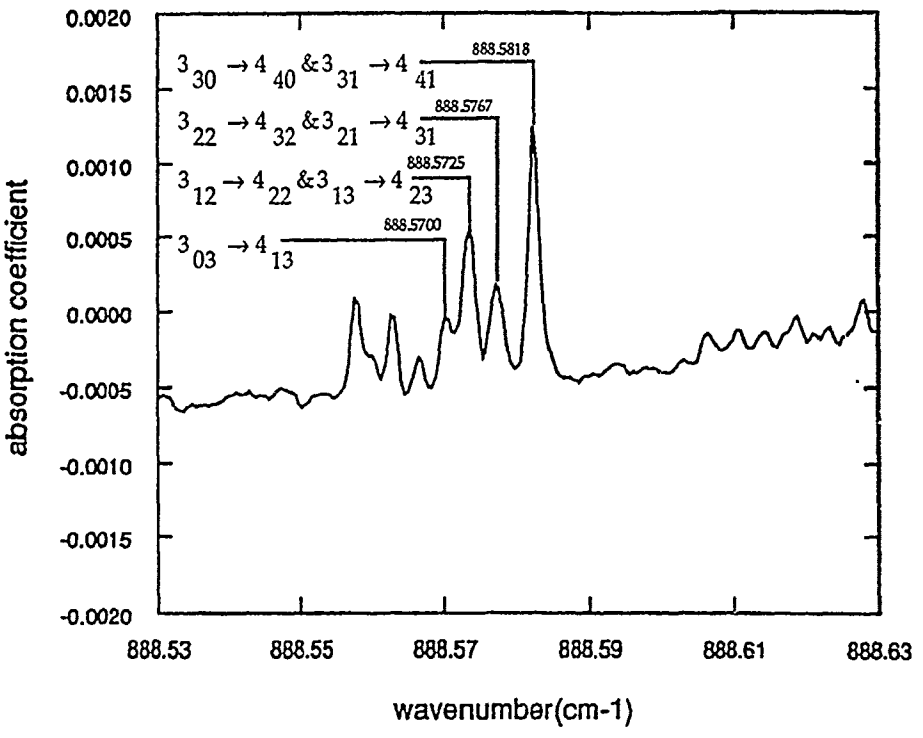
0.0020
0.0015
0.0010
0.0005
0.0000
-0.0005
-0.0010
-0.0015
-0.0020
absorption coefficient
888.53
888.55
888.57
888.59
888.61
888.63
wavenumber(cm-1)
$3_{30} \rightarrow 4_{40}$ &$3_{31} \rightarrow 4_{41}$
888.5818
$3_{22} \rightarrow 4_{32}$ &$3_{21} \rightarrow 4_{31}$
888.5767
$3_{12} \rightarrow 4_{22}$ &$3_{13} \rightarrow 4_{23}$
888.5725
$3_{03} \rightarrow 4_{13}$
888.5700

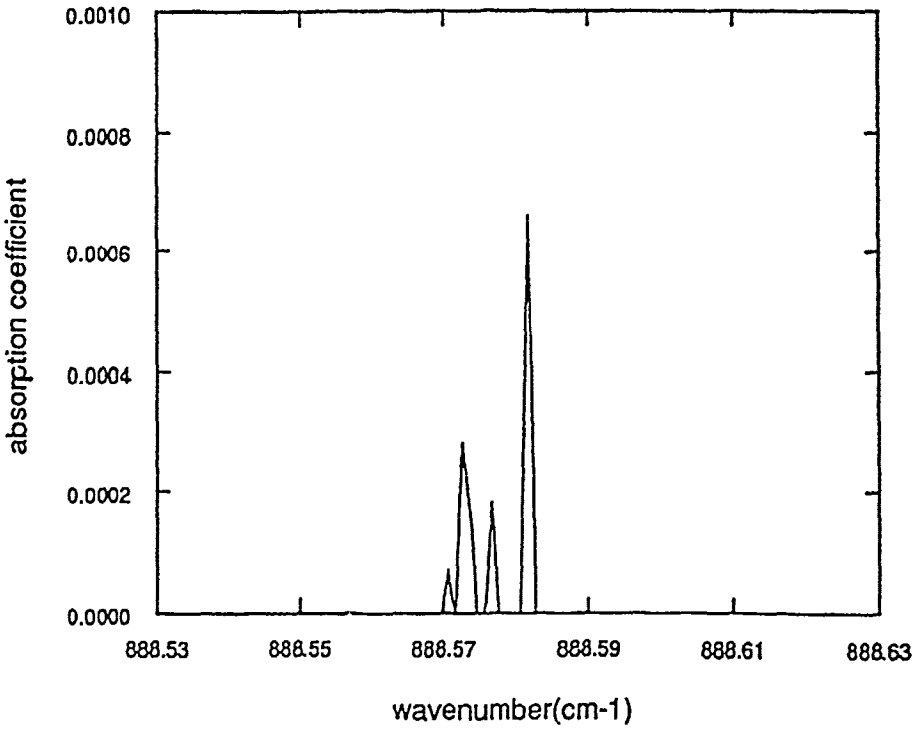
0.0010
0.0008
0.0006
0.0004
0.0002
0.0000
absorption coefficient
888.53
888.55
888.57
888.59
888.61
888.63
wavenumber(cm-1)

J=6-7

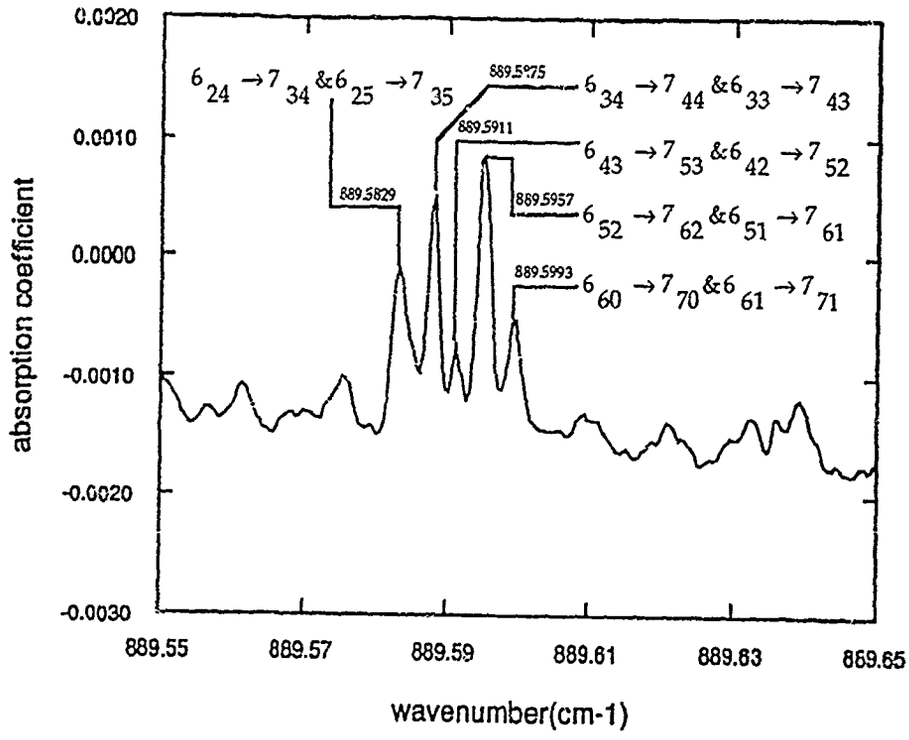
0.0020
0.0010
0.0000
-0.0010
-0.0020
-0.0030
absorption coefficient
889.55
889.57
889.59
889.61
889.63
889.65
wavenumber(cm-1)
$6_{24} \rightarrow 7_{34}$ &$6_{25} \rightarrow 7_{35}$
889.5829
889.5875
$6_{34} \rightarrow 7_{44}$ &$6_{33} \rightarrow 7_{43}$
889.5911
$6_{43} \rightarrow 7_{53}$ &$6_{42} \rightarrow 7_{52}$
889.5957
$6_{52} \rightarrow 7_{62}$ &$6_{51} \rightarrow 7_{61}$
889.5993
$6_{60} \rightarrow 7_{70}$ &$6_{61} \rightarrow 7_{71}$

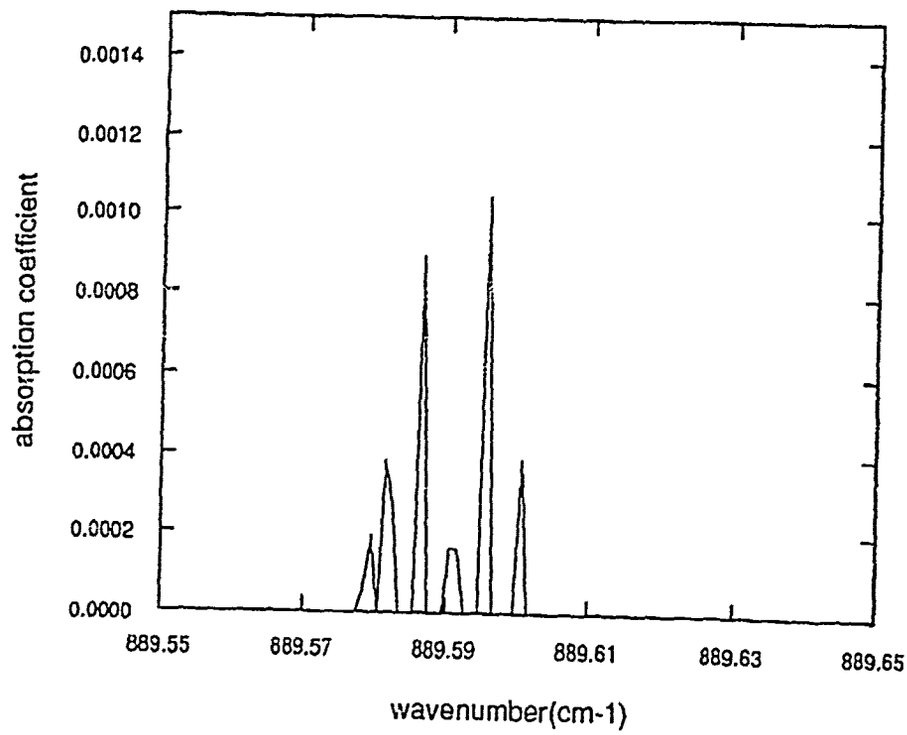
0.0014
0.0012
0.0010
0.0008
0.0006
0.0004
0.0002
0.0000
absorption coefficient
889.55
889.57
889.59
889.61
889.63
889.65
wavenumber(cm-1)

J=6-7

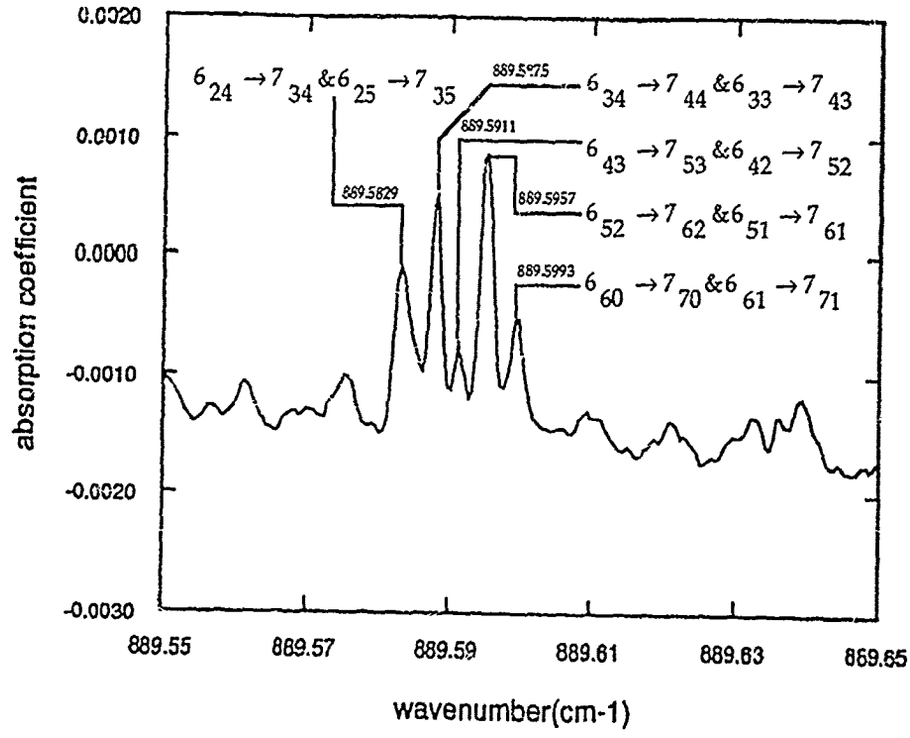
0.0020
0.0010
0.0000
-0.0010
-0.0020
-0.0030
absorption coefficient
889.55
889.57
889.59
889.61
889.63
889.65
wavenumber(cm-1)
$6_{24} \rightarrow 7_{34}$ &$6_{25} \rightarrow 7_{35}$
889.5829
889.5875
$6_{34} \rightarrow 7_{44}$ &$6_{33} \rightarrow 7_{43}$
889.5911
$6_{43} \rightarrow 7_{53}$ &$6_{42} \rightarrow 7_{52}$
889.5957
$6_{52} \rightarrow 7_{62}$ &$6_{51} \rightarrow 7_{61}$
889.5993
$6_{60} \rightarrow 7_{70}$ &$6_{61} \rightarrow 7_{71}$

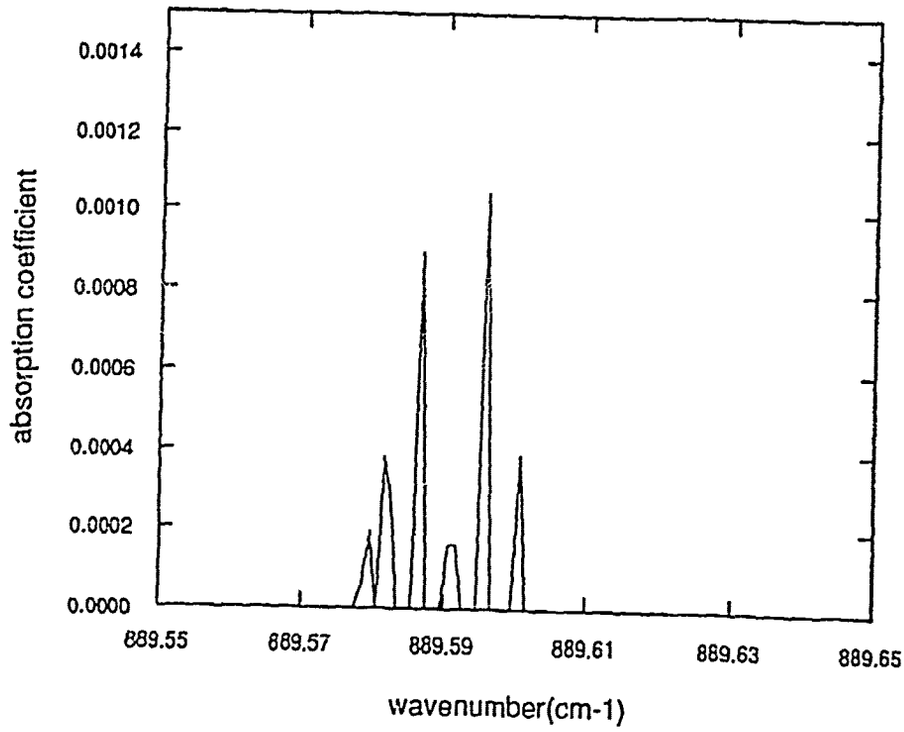
0.0014
0.0012
0.0010
0.0008
0.0006
0.0004
0.0002
0.0000
absorption coefficient
889.55
889.57
889.59
889.61
889.63
889.65
wavenumber(cm-1)

J=16-17

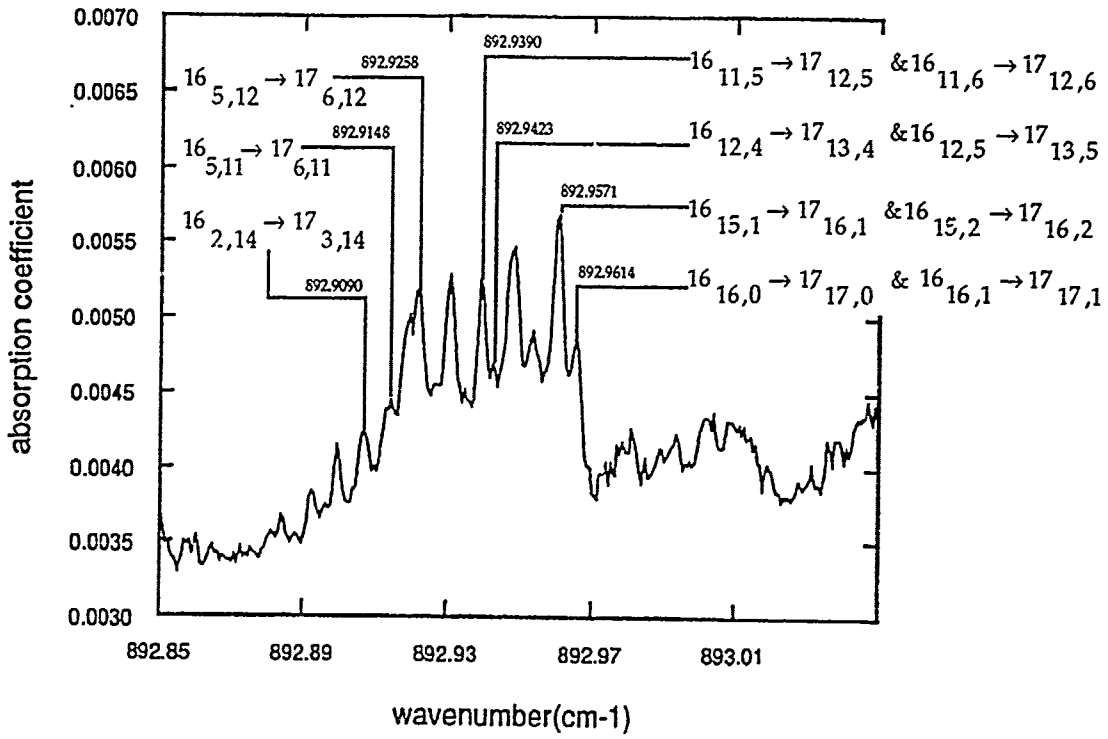
0.0070
0.0065
0.0060
0.0055
0.0050
0.0045
0.0040
0.0035
0.0030
absorption coefficient
892.85
892.89
892.93
892.97
893.01
wavenumber(cm-1)
892.9258
892.9148
892.9090
892.9390
892.9423
892.9571
892.9614
16 5,12 → 17 6,12
16 5,11 → 17 6,11
16 2,14 → 17 3,14
16 11,5 → 17 12,5 &16 11,6 → 17 12,6
16 12,4 → 17 13,4 &16 12,5 → 17 13,5
16 15,1 → 17 16,1 &16 15,2 → 17 16,2
16 16,0 → 17 17,0 & 16 16,1 → 17 17,1

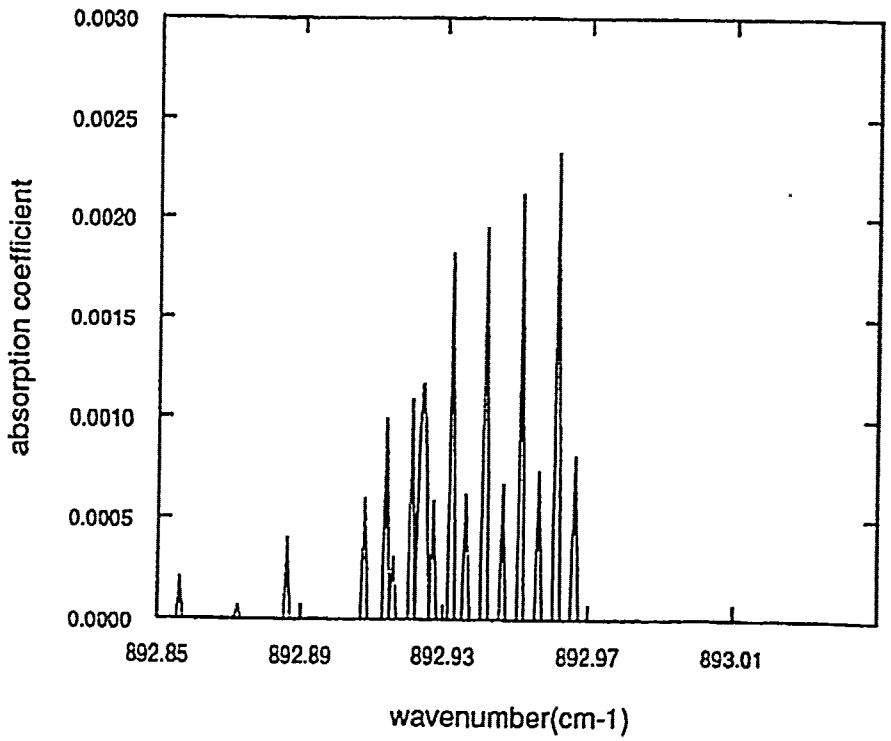
0.0030
0.0025
0.0020
0.0015
0.0010
0.0005
0.0000
absorption coefficient
892.85
892.89
892.93
892.97
893.01
wavenumber(cm-1)

J=28-29

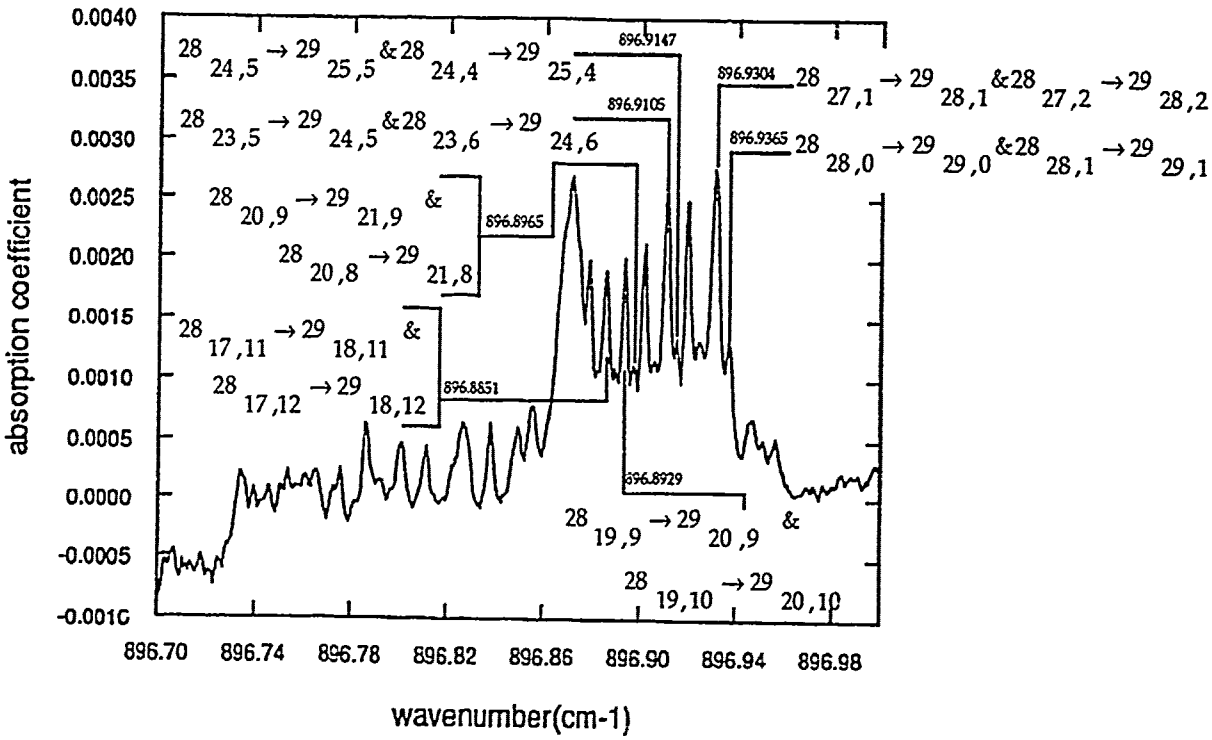
absorption coefficient
wavenumber(cm-1)
0.0040
0.0035
0.0030
0.0025
0.0020
0.0015
0.0010
0.0005
0.0000
-0.0005
-0.0010
896.70
896.74
896.78
896.82
896.86
896.90
896.94
896.98
896.9147
896.9304
896.9105
896.9365
896.8965
896.8851
896.8929
28 24,5 → 29 25,5 &28 24,4 → 29 25,4
28 27,1 → 29 28,1 &28 27,2 → 29 28,2
28 23,5 → 29 24,5 &28 23,6 → 29 24,6
28 28,0 → 29 29,0 &28 28,1 → 29 29,1
28 20,9 → 29 21,9 &
28 20,8 → 29 21,8
28 17,11 → 29 18,11 &
28 17,12 → 29 18,12
28 19,9 → 29 20,9 &
28 19,10 → 29 20,10

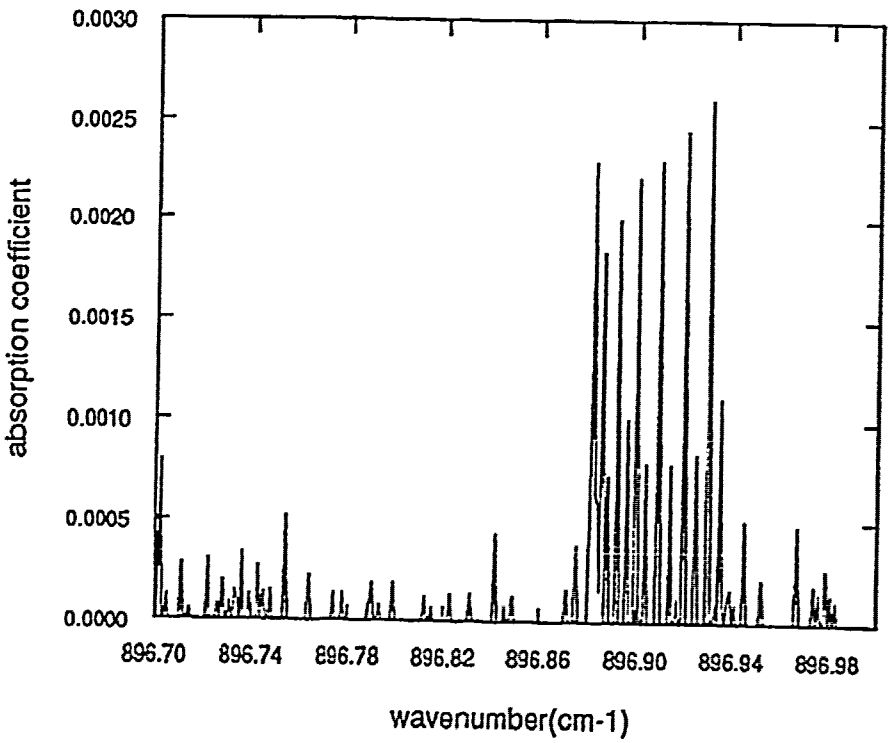
absorption coefficient
wavenumber(cm-1)
0.0030
0.0025
0.0020
0.0015
0.0010
0.0005
0.0000
896.70
896.74
896.78
896.82
896.86
896.90
896.94
896.98

J=5-4

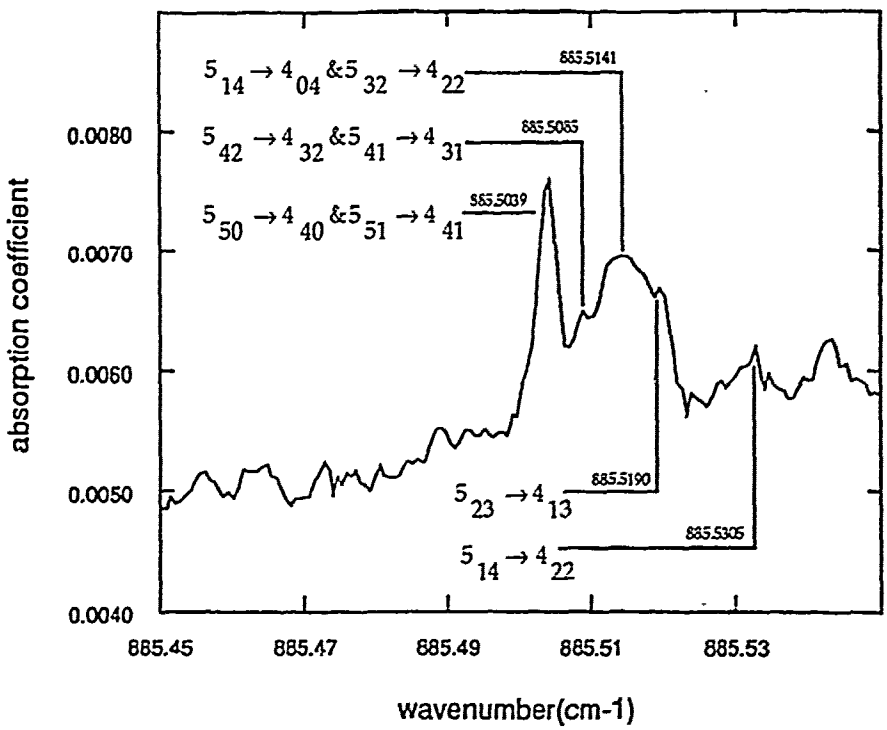
$5_{14} \rightarrow 4_{04}$ &$5_{32} \rightarrow 4_{22}$
885.5141
$5_{42} \rightarrow 4_{32}$ &$5_{41} \rightarrow 4_{31}$
885.5085
$5_{50} \rightarrow 4_{40}$ &$5_{51} \rightarrow 4_{41}$
885.5039
$5_{23} \rightarrow 4_{13}$
885.5190
$5_{14} \rightarrow 4_{22}$
885.5305
absorption coefficient
0.0080
0.0070
0.0060
0.0050
0.0040
885.45
885.47
885.49
885.51
885.53
wavenumber(cm-1)

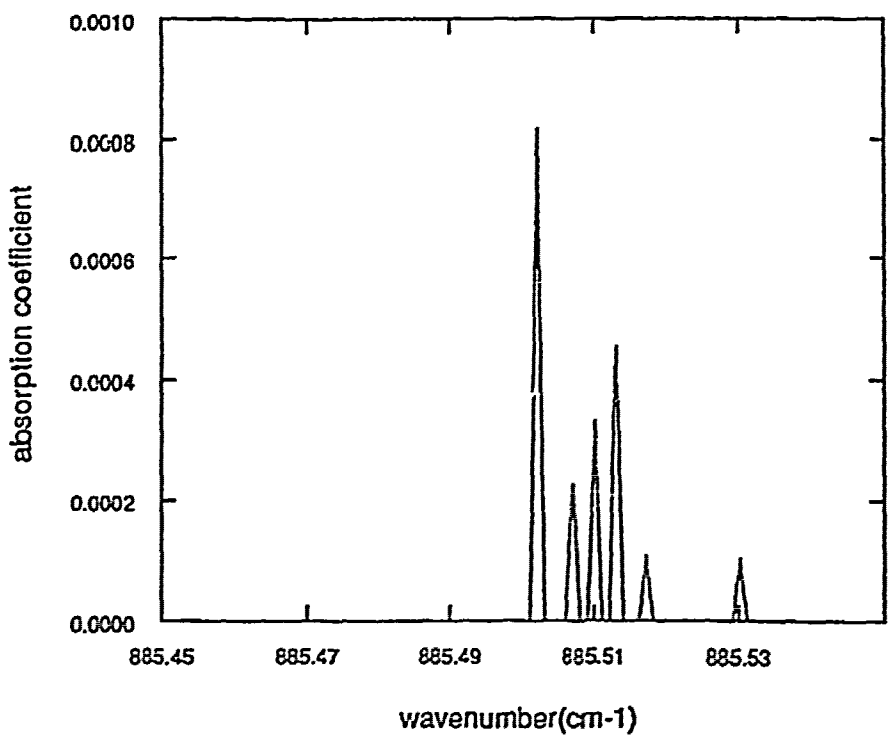
absorption coefficient
0.0010
0.0008
0.0006
0.0004
0.0002
0.0000
885.45
885.47
885.49
885.51
885.53
wavenumber(cm-1)

J=7-6

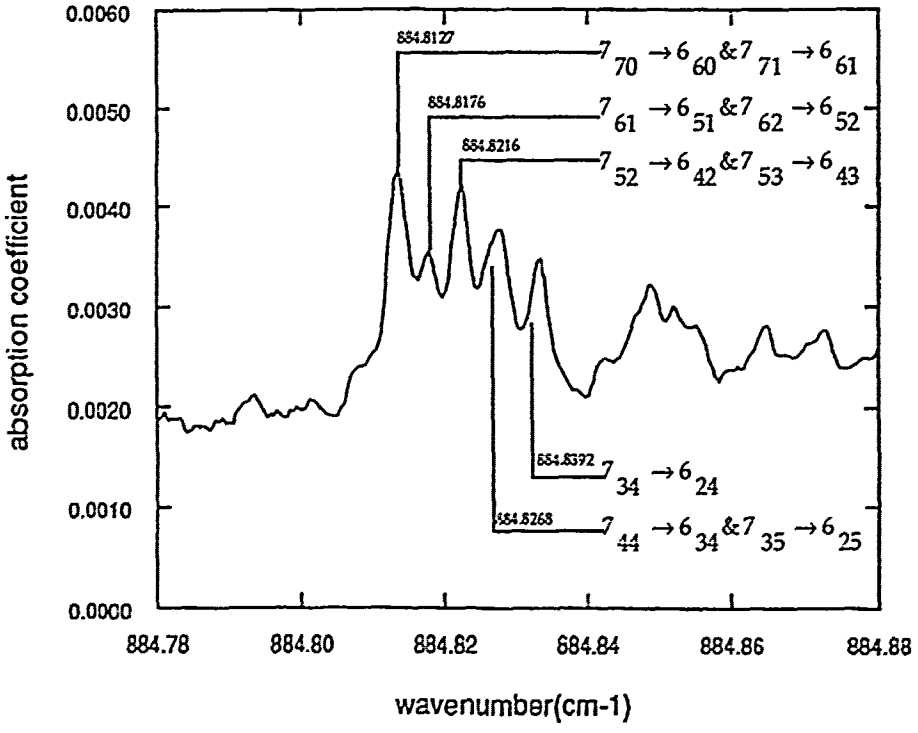
0.0060
0.0050
0.0040
0.0030
0.0020
0.0010
0.0000
absorption coefficient
884.8127
$7_{70} \rightarrow 6_{60}$ & $7_{71} \rightarrow 6_{61}$
884.8176
$7_{61} \rightarrow 6_{51}$ & $7_{62} \rightarrow 6_{52}$
884.8216
$7_{52} \rightarrow 6_{42}$ & $7_{53} \rightarrow 6_{43}$
884.8392
$7_{34} \rightarrow 6_{24}$
884.8268
$7_{44} \rightarrow 6_{34}$ & $7_{35} \rightarrow 6_{25}$
884.78
884.80
884.82
884.84
884.86
884.88
wavenumber(cm-1)

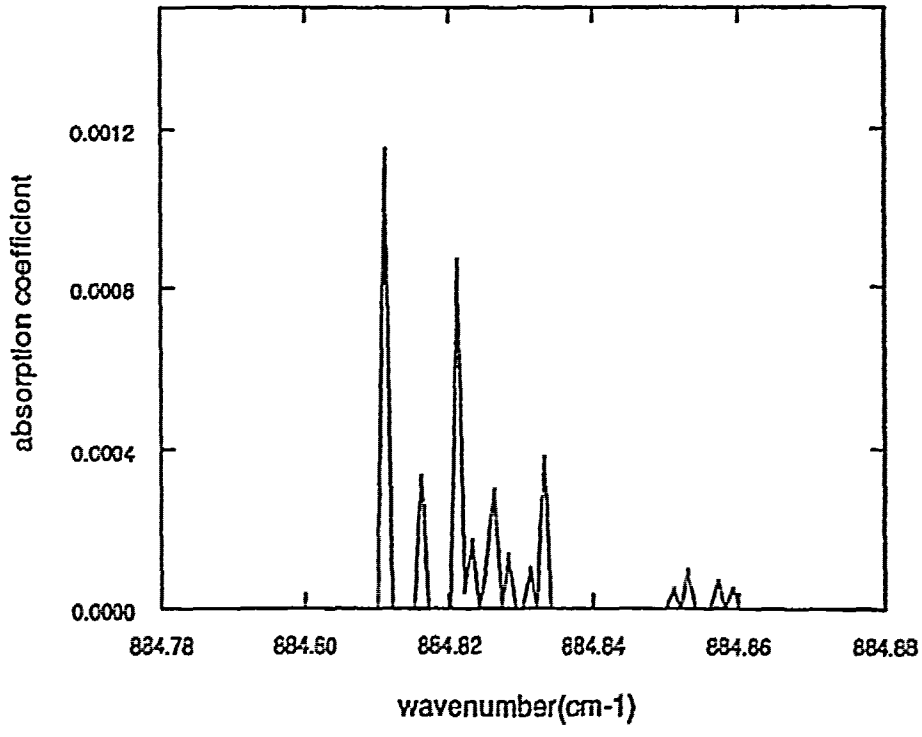
0.0012
0.0008
0.0004
0.0000
absorption coefficient
884.78
884.80
884.82
884.84
884.86
884.88
wavenumber(cm-1)

J=16-15

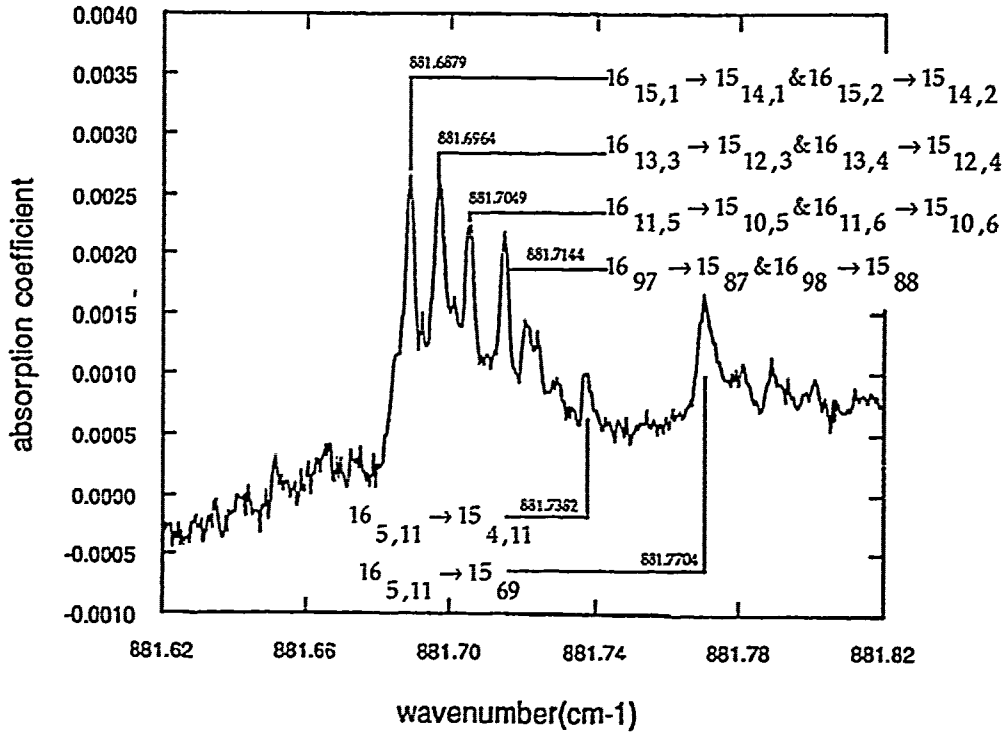
0.0040
0.0035
0.0030
0.0025
0.0020
0.0015
0.0010
0.0005
0.0000
-0.0005
-0.0010
absorption coefficient
881.62
881.66
881.70
881.74
881.78
881.82
wavenumber(cm-1)
881.6879
881.6964
881.7049
881.7144
881.7382
881.7704
16 15,1 → 15 14,1 &16 15,2 → 15 14,2
16 13,3 → 15 12,3 &16 13,4 → 15 12,4
16 11,5 → 15 10,5 &16 11,6 → 15 10,6
16 97 → 15 87 &16 98 → 15 88
16 5,11 → 15 4,11
16 5,11 → 15 69

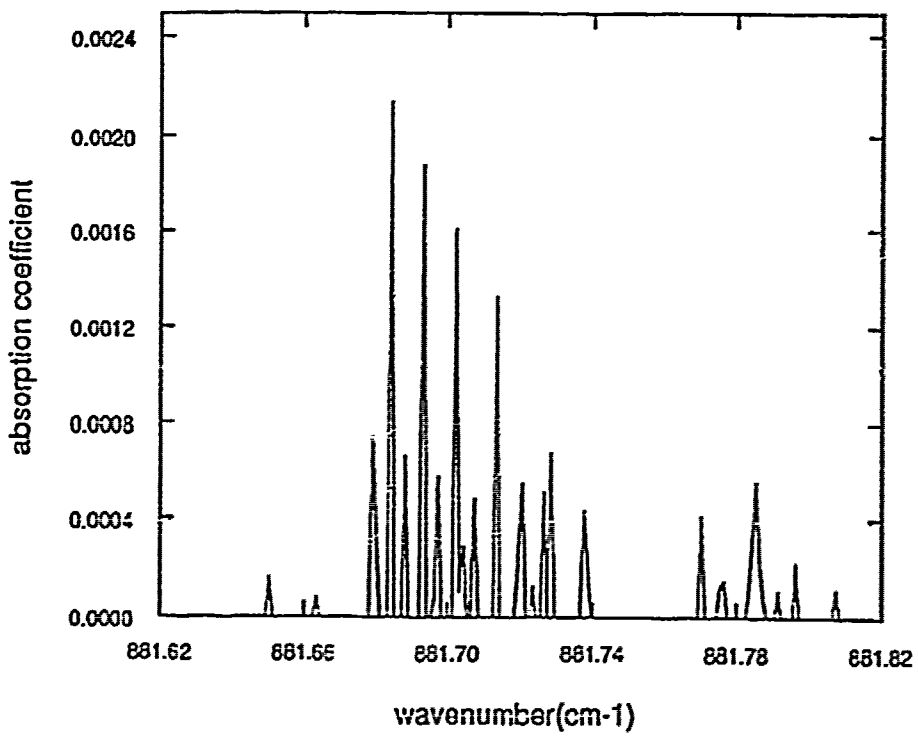
0.0024
0.0020
0.0016
0.0012
0.0008
0.0004
0.0000
absorption coefficient
881.62
881.66
881.70
881.74
881.78
881.82
wavenumber(cm-1)

Appendix A

Development of the Hamiltonian

To find the vibrational-rotational energies of an asymmetric molecular rotor we use a model which treats the nuclei as point masses moving through a potential field created by the average motion of the molecular electrons. The molecules are thought of as being held together by semi-rigid springs whose energies are eigenvalues of the Schroedinger equation.

$$H\Psi = E\Psi \qquad \text{(A-1)}$$

A-1 The Classical Hamiltonian[8]

The form of the hamiltonian is found by first considering the classical kinetic energy for the system of point masses. The most convenient set of coordinates to use consists of a set of axes fixed in space (X,Y,Z) and a set of axes (x,y,z) rotating with the molecule whose origin is at the molecular center of mass and whose orientation in space is described by the three Eularian angles (θ,ϕ,χ). The Eularian angles are discussed more fully in Appendix B.

Let the position of the α_{th} nuclei with respect to the molecular center of mass be $\vec{r}_\alpha$ with components $(x_\alpha, y_\alpha, z_\alpha)$. The center of mass is located at a distance $|\vec{R}|$ from the fixed axes. The equilibrium position of the α_{th} particle, which is fixed in the moving system, is given by $\vec{a}_\alpha$ (see Figure A-1).

---

[8]The theory of Section A-1 is taken from the following References: [3] [pp. 2-6]; [1] [pp. 14-17, 273-278]; [4] [pp. 260-264].

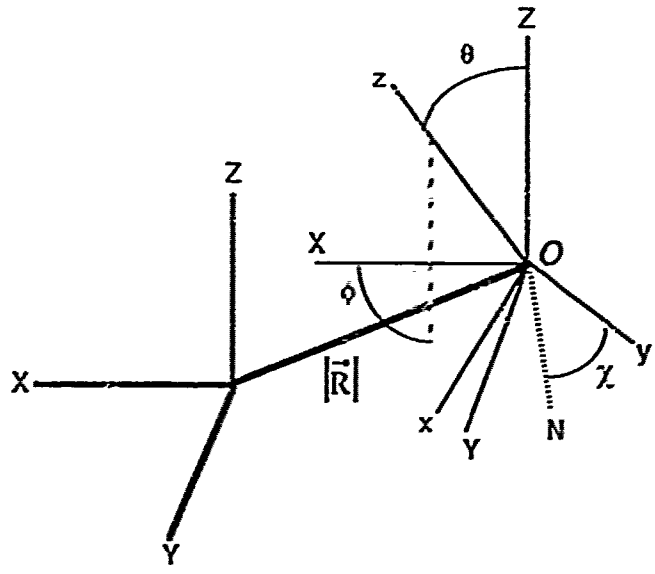

Figure A-1 – Molecular Coordinates. From [1] [p. 285]

We can now define the vector $\vec{\rho}$, the displacement vector ,as follows:

$$\vec{\rho}_\alpha = \vec{r}_\alpha - \vec{a}_\alpha \qquad \text{(A-2)}$$

If the instantaneous angular velocity of the rotation is ω, then the velocity of the α_{th} particle is described by:

$$\vec{v}_{tot} = \dot{\vec{R}} + (\vec{\omega} \times \vec{r}_\alpha) + \vec{v}_\alpha \qquad \text{(A-3)}$$

where

$$\vec{v}_\alpha = \dot{\vec{r}}_\alpha \qquad \text{(A-4)}$$

The first term represents translational velocity, the second the velocity of rotation, and the third the velocity of vibration about the equilibrium point. The kinetic energy of the molecule is

$$T = \frac{1}{2}\sum_{\alpha} m_{\alpha}\left(\vec{v}_{tot}\right)^2 = \frac{1}{2}\sum_{\alpha} m_{\alpha}\left[\dot{\vec{R}} + \left(\dot{\vec{\omega}} \times \vec{r}_{\alpha}\right) \cdot \left(\vec{\omega} \times \vec{r}_{\alpha}\right) + \dot{\vec{v}}_{\alpha} + 2\dot{\vec{R}} \cdot \left(\vec{\omega} \times \vec{r}_{\alpha}\right)\right.$$

$$\left. + 2\dot{\vec{R}} \cdot \vec{v}_{\alpha} + 2\vec{\omega} \cdot \left(\vec{r}_{\alpha} \times \vec{v}_{\alpha}\right)\right] \qquad \text{(A-5)}$$

Since we have defined the (x,y,z) axes to be a center of mass system, it is true by definition that

$$\sum_{\alpha} m_{\alpha}\vec{r}_{\alpha} = 0 \qquad \text{(A-6)}$$

Taking the total differential of $\vec{r}_{\alpha}$ ($\vec{r}_{\alpha}$ is a function of rotation and vibration) with respect to time gives

$$0 = \sum_{\alpha} m_{\alpha}\dot{\vec{r}}_{\alpha} = \sum_{\alpha} m_{\alpha}\left[\left(\vec{\omega} \times \vec{r}_{\alpha}\right) + \vec{v}_{\alpha}\right] = \vec{\omega} \times \sum_{\alpha} m_{\alpha}\vec{r}_{\alpha} + \sum_{\alpha} m_{\alpha}\vec{v}_{\alpha} = \sum_{\alpha} m_{\alpha}\vec{v}_{\alpha} = 0 \qquad \text{(A-7)}$$

Since the atoms in the molecule are all vibrating about their equilibrium positions, the rotating axes cannot be attached to the rotating coordinate system in a definite way. However, to ensure the rotating axes actually rotate with the molecule we can impose the condition

$$\sum_{\alpha} m_{\alpha}\left(\vec{a}_{\alpha} \times \vec{r}_{\alpha}\right) = 0 \qquad \text{(A-8)}$$

This is almost the same as stating that there must be no angular momentum with respect to the body-fixed, rotating system of axes. We take the total differential of Equation (A-8) with respect to time:

$$0 = \sum_{\alpha} m_{\alpha}\left[\left(\vec{a}_{\alpha} \times \dot{\vec{r}}_{\alpha} + \vec{v}_{\alpha}\right) + \left(\vec{a}_{\alpha} \times \dot{\vec{v}}_{\alpha}\right)\right] = \sum_{\alpha} m_{\alpha}\left(\dot{\vec{\omega}} \times \vec{a}_{\alpha}\right) \times \vec{r}_{\alpha} + \sum_{\alpha} m_{\alpha}\vec{a}_{\alpha} \times \left(\vec{\omega} \times \vec{r}_{\alpha}\right)$$

$$+ \sum_{\alpha} m_{\alpha}\left(\vec{a}_{\alpha} \times \vec{v}_{\alpha}\right) = \sum_{\alpha} m_{\alpha}\vec{a}_{\alpha} \times \vec{v}_{\alpha} \qquad \text{(A-9)}$$

Using Equation (A-3), Equation (A-6), Equation (A-7), and Equation (A-9) to modify Equation (A-5) leaves

$$2T = \dot{\vec{R}}^2 M + \sum_\alpha m_\alpha(\vec{\omega} \times \vec{r}_\alpha) \cdot (\vec{\omega} \times \vec{r}_\alpha) + \sum_\alpha m_\alpha(\vec{v}_\alpha)^2 + 2\vec{\omega}(\vec{\rho}_\alpha \times \vec{v}_c) \quad \text{(A-10)}$$

where $$M = \sum m_\alpha$$

Disregarding the translational term and noting that by expanding the determinant form of the cross product we get

$$\sum_\alpha m_\alpha(\vec{\omega} \times r_\alpha) \cdot (\vec{\omega} \times \vec{r}_\alpha) = I_{xx}\omega_x^2 + I_{yy}\omega_y^2 + I_{zz}\omega_z^2 - 2I_{xy}\omega_x\omega_y - 2I_{yz}\omega_y\omega_z$$

$$- 2I_{xz}\omega_x\omega_z \quad \text{(A-11)}$$

and the kinetic energy becomes

$$2T = I_{xx}\omega_x^2 + I_{yy}\omega_y^2 + I_{zz}\omega_z^2 - 2I_{yz}\omega_y\omega_z - 2I_{xy}\omega_x\omega_y - 2I_{xz}\omega_x\omega_z$$

$$+ \sum_\alpha m_\alpha \vec{v}_\alpha^2 + 2\omega_x \sum_\alpha m_\alpha(\vec{\rho}_\alpha \times \vec{v}_\alpha)_x + 2\omega_y \sum_\alpha m_\alpha(\vec{\rho}_\alpha \times \vec{v}_\alpha)_y + 2\omega_z \sum_\alpha m_\alpha(\vec{\rho}_\alpha \times \vec{v}_\alpha)_z$$

(A-12)

where I_{xx}, I_{yy}, I_{zz}, I_{xy}, I_{yz}, I_{xz} are the components of the inertia tensor

$$I = \begin{pmatrix} I_{xx} & I_{xy} & I_{xz} \\ I_{yx} & I_{yy} & I_{yz} \\ I_{zx} & I_{zy} & I_{zz} \end{pmatrix} \quad \text{(A-12a)}$$

To deal with the coupled terms in Equation (A-12), it is necessary to treat the vibrations of the atoms as small displacements about their equilibrium points. The kinetic energy is then given by

$$2T = \sum_{\alpha=1}^{N} m_\alpha \left[\left(\frac{d\Delta x_\alpha}{dt} \right)^2 + \left(\frac{d\Delta y_\alpha}{dt} \right)^2 + \left(\frac{d\Delta z_\alpha}{dt} \right)^2 \right] \qquad \text{(A-13)}$$

where Δx_α, etc. are the components of $\vec{\rho}$. Let us now replace the coordinates $\Delta x_1, \ldots, \Delta z_N$ by a set of mass - weighted coordinates $q_1, \ldots, q_{3n}$ defined by $q_1 = \sqrt{m_1}\,\Delta x_1$, $q_2 = \sqrt{m_1}\,\Delta y_1$, $q_3 = \sqrt{m_1}\,\Delta z_1$, $q_4 = \sqrt{m_2}\,\Delta x_2$, etc. The kinetic energy now becomes

$$2T = \sum_{i=1}^{3N} \dot{q}_i^2 \qquad \text{(A-14)}$$

The potential energy V, a function only of the small vibrational displacements, is now a function of the q's. We can, therefore, expand V as a power series in the q_i's.

$$2V = 2V_0 + 2\sum_{i=1}^{3N} \left(\frac{\partial V}{\partial q_i} \right)_{q_i=o} q_i + \sum_{i,j=1}^{3N} \left(\frac{\partial^2 V}{\partial q_i \partial q_j} \right)_{q_i=q_j=0} q_i q_j + \cdots \qquad \text{(A-15)}$$

Adjusting the zero point of the energy to be the equilibrium point and noting that, at equilibrium, $\left(\frac{\partial V}{\partial q_i} \right)_{q_i=0} = 0$, we have

$$2V = \sum_{i,j=1}^{3N} f_{ij} q_i q_j \;, \quad \text{where} \quad f_{ij} = \left(\frac{\partial^2 V}{\partial q_i \partial q_j} \right)_{q_i q_j = 0} \qquad \text{(A-16)}$$

In deriving Equation (A-16), the higher order terms have been neglected.

Newton's equations of motion are written

$$\frac{d}{dt}\frac{\partial T}{\partial \dot{q}_j} + \frac{\partial V}{\partial q_j} = 0 \qquad ,j=1,2,...,3N \tag{A-17}$$

since T is a function of the velocities only, and V is a function of the coordinates only.

Substituting T and V from Equation (A-14) and Equation (A-16) into Equation (A-17) gives

$$\ddot{q}_j + \sum_{i=1}^{3N} f_{ij} q_i = 0 \qquad , j=1,2,\ldots,3N \tag{A-18}$$

A solution to this set of 3N simultaneous second-order differential equations is

$$q_i = A_i \cos\left(\lambda^{\frac{1}{2}} + \varepsilon\right) \tag{A-19}$$

By substituting Equation (A-19) into Equation (A-18), the following set of equations result

$$\sum_{i=1}^{3N}\left(f_{ij} - \delta_{ij}\lambda\right)A_i = 0 \qquad , j=1,2,\ldots,3N \tag{A-20}$$

where δ_{ij} is the Kronecker delta. Non-trivial solutions for A_i correspond only to those values λ for which the following secular equation is satisfied

$$\begin{vmatrix} (f_{1,1}-\lambda), f_{1,2}, f_{1,3}, \cdots, & f_{1,3N} \\ f_{2,1}, (f_{2,2}-\lambda), f_{2,3} \cdots, & f_{2,3N} \\ \vdots & \\ f_{3N,1}, f_{3N,2}, f_{3N,3}, \cdots, (f_{3N,3N}-\lambda) & \end{vmatrix} = 0 \tag{A-21}$$

When we choose a certain value $\lambda = \lambda_k$ so as to make the above determinant vanish, the coefficients $A_i = A_{ik}$ are determined for that particular value λ_k. Since the above system of equations does not determine A_{ik} uniquely, but gives only their ratios, arbitrary solutions

(which are unique) can be designated by the quantities l_{ik} which are defined in terms of an arbitrary solution A'_{ik} as follows

$$l_{ik} = \frac{A'_{ik}}{\left[\sum_i \left(A'_{ik}\right)^2\right]^{\frac{1}{2}}} \qquad \text{(A-22)}$$

The advantage to this is that the amplitudes are normalized such that

$$\sum_i l_{ik} = 1 \qquad \text{(A-23)}$$

Note the secular equation (A-21) consists of 3N rows and 3N columns corresponding to 3N unknown A_i's and 3N unknown eigenvalues λ_k. There are however six roots which are zero, corresponding to the three normal coordinates of translation, and three normal coordinates of rotation, leaving only 3N-6 non-zero roots (corresponding to the 3N-6 normal vibrational modes). This fact, along with the normalization relation (A-22), allows us to define

$$\sqrt{m_\alpha}\,\Delta x_\alpha = \sum_{k=1}^{3N-6} l_{\alpha k} Q_k$$

$$\sqrt{m_\alpha}\,\Delta y_\alpha = \sum_{k=1}^{3N-6} r_{\alpha k} Q_k \qquad \text{(A-24)}$$

$$\sqrt{m_\alpha}\,\Delta z_\alpha = \sum_{k=1}^{3N-6} n_{\alpha k} Q_k$$

$$\sum m_\alpha \vec{v}_\alpha^{\,2} = \sum_\alpha \sqrt{m_\alpha}\left(\Delta \dot{x}_\alpha^2 + \Delta \dot{y}_\alpha^2 + \Delta \dot{z}_\alpha^2\right) = \sum_k \dot{Q}_k^2$$

Now the coupling terms become

$$\sum_\alpha m_\alpha(\vec{\rho}_\alpha \times \vec{v}_\alpha)_x = \sum_\alpha m_\alpha\left(\Delta y_\alpha \Delta \dot{z}_\alpha - \Delta z_\alpha \Delta \dot{y}_\alpha\right) = \sum_{k=1}^{3N-6} \Im_k \dot{Q}_k$$

$$\sum_\alpha m_\alpha(\vec{\rho}_\alpha \times \vec{v}_\alpha)_y = \sum_{k=1}^{3N-6} \Re_k \dot{Q}_k \qquad \text{(A-25)}$$

$$\sum_\alpha m_\alpha(\vec{\rho}_\alpha \times \vec{v}_\alpha)_z = \sum_{k=1}^{3N-6} \aleph_k \dot{Q}_k$$

where $$\Im_k = \sum_{\alpha,l} m_\alpha\left(r_{\alpha l} n_{\alpha k} - n_{\alpha l} r_{\alpha k}\right) Q_l$$

$$\Re_k = \sum_{\alpha,l} m_\alpha\left(n_{\alpha l} l_{\alpha k} - l_{\alpha l} n_{\alpha k}\right) Q_l \qquad \text{(A-26)}$$

and $$\aleph_k = \sum_{\alpha,l} m_\alpha\left(l_{\alpha l} r_{\alpha k} - r_{\alpha l} l_{\alpha k}\right) Q_l$$

The kinetic energy is now

$$2T + I_{xx}\omega_x^2 + I_{yy}\omega_y^2 + I_{zz}\omega_z^2 - 2I_{xy}\omega_x\omega_y - 2I_{yz}\omega_y\omega_z - 2I_{xz}\omega_x\omega_z$$

$$+ 2\omega_x \sum_k \Im_k \dot{Q}_k + 2\omega_y \sum_k \Re_k \dot{Q}_k + 2\omega_z \sum_k \aleph_k \dot{Q}_k + \sum_k \dot{Q}_k \qquad \text{(A-27)}$$

We will find it convenient to have the kinetic energy expressed in terms of angular momenta, rather than angular velocities. The total angular momentum is a vector whose properties arise from its definition

$$\vec{P} = \sum_{\alpha} m_{\alpha} \vec{r}_{\alpha} \times \dot{\vec{r}}_{\alpha} = \sum_{\alpha} m_{\alpha} [\vec{r}_{\alpha} \times (\vec{\omega} \times \vec{r}_{\alpha})] + \sum_{\alpha} m_{\alpha} (\vec{r}_{\alpha} \times \vec{v}_{\alpha}) \qquad \text{(A-28)}$$

By expanding Equation (A-28) or by noting $P_x = \frac{\partial T}{\partial \omega_x}$,etc., we have

$$P_x = I_{xx}\omega_x - I_{xy}\omega_y - I_{xz}\omega_z + \sum \Im_k \dot{Q}_k$$

$$P_y = -I_{xy}\omega_x + I_{yy}\omega_y - I_{yz}\omega_z + \sum \Re_k \dot{Q}_k \qquad \text{(A-29)}$$

$$P_z = -I_{xz}\omega_x - I_{yz}\omega_y + I_{zz}\omega_z + \sum \aleph_k \dot{Q}_k$$

The momentum conjugate to Q_k is

$$p_k = \frac{\partial T}{\partial \dot{Q}_k} = \dot{Q}_k + \Im_k \omega_x + \Re_k \omega_y + \aleph_k \omega_z \qquad \text{(A-30)}$$

Solving Equation (A-30) for $\dot{Q}_k$ and substituting the result into Equation (A-29) yields

$$P_x = I_{xx}\omega_x - I_{xy}\omega_y - I_{xz}\omega_z + \sum \Im_k (p_k - \Im_k \omega_x - \Re_k \omega_y - \aleph_k \omega_z) \text{ , etc.} \qquad \text{(A-31)}$$

It is now convenient to introduce the following definitions

$$I'_{xx} = I_{xx} - \sum \Im_k^2 ; \; I'_{xy} = I_{xy} + \sum \Im_k \Re_k ; \; p_x = \sum \Im_k p_k$$

$$I'_{yy} = I_{yy} - \sum \Re_k^2 ; \; I'_{yz} = I_{yz} + \sum \Re_k \aleph_k ; \; p_y = \sum \Re_k p_k \qquad \text{(A-32)}$$

$$I'_{zz} = I_{zz} - \sum \aleph_k^2 ; \; I'_{xz} = I_{xz} + \sum \aleph_k \Im_k ; \; p_z = \sum \aleph_k p_k$$

We can see from their definitions that p_x, p_y, p_z are functions of the vibrations alone. As a result they are often called components of internal or vibrational angular momentum.

Substituting Equation (A-32) into Equation (A-31) gives

$$(P_x - p_x) = I'_{xx}\omega_x - I'_{xy}\omega_y - I'_{xz}\omega_z$$

$$(P_y - p_y) = -I'_{xy}\omega_x + I'_{yy}\omega_y - I'_{yz}\omega_z \qquad \text{(A-33)}$$

$$(P_z - p_z) = -I'_{xz}\omega_x - I'_{yz}\omega_y + I'_{zz}\omega_z$$

The inverse transformation of Equation (A-33) is

$$\omega_x = \mu_{xx}(P_x - p_x) + \mu_{xy}(P_y - p_y) \div \mu_{xz}(P_z - p_z)$$

$$\omega_y = \mu_{yx}(P_x - p_x) + \mu_{yy}(P_y - p_y) + \mu_{yz}(P_z - p_z) \qquad \text{(A-34)}$$

$$\omega_z = \mu_{zx}(P_x - p_x) + \mu_{zy}(P_y - p_y) + \mu_{zz}(P_z - p_z)$$

where $\mu_{xx} = \dfrac{I'_{yy}I'_{zz} - I'^{2}_{yz}}{\Delta}$; $\mu_{xy} = \dfrac{I'_{zz}I'_{xy} + I'_{yz}I'_{xz}}{\Delta}$; $\mu_{xz} = \dfrac{I'_{xy}I'_{yz} + I'_{yy}I'_{xz}}{\Delta}$

$$\mu_{yz} = \frac{I'_{xx}I'_{yz} + I'_{xy}I'_{xz}}{\Delta} \; ; \; \mu_{yy} = \frac{I'_{xx}I'_{zz} - I'^{2}_{xz}}{\Delta} \; ; \; \mu_{zz} = \frac{I'_{xx}I'_{yy} - I'^{2}_{xy}}{\Delta} \qquad \text{(A-35)}$$

and

$$\Delta = \begin{vmatrix} I'_{xx}, -I'_{xy}, -I'_{xz} \\ -I'_{xy}, I'_{yy}, -I'_{yz} \\ -I_{xz}, -I'_{yz}, I'_{zz} \end{vmatrix}$$

Substituting Equation (A-32), Equation (A-33), and Equation (A-34) into Equation (A-27) shows the kinetic energy as

$$2T = \mu_{xx}(P_x - p_x)^2 + \mu_{yy}(P_y - p_y)^2 + \mu_{zz}(P_z - p_z)^2 + 2\mu_{xy}(P_x - p_x)(P_y - p_y)$$

$$+ 2\mu_{yz}(P_y - p_y)(P_z - p_z) + 2\mu_{zx}(P_z - p_z)(P_x - p_x) = \sum p_k^2 \qquad \text{(A-36)}$$

Note that the $\mu_{gg'}$ are functions of the normal (vibrational) coordinates only. The classical hamiltonian is complete when V is added to Equation (A-36).

A-2 The Quantum Mechanical Hamiltonian[9]

Because the total angular momenta P_x, P_y, P_z, in Equation. (A-36) were not derived with respect to any conjugal coordinate system, we cannot transform directly from classical to quantum mechanical hamiltonian. Thus we must derive the quantum mechanically correct form of the hamiltonian in an arbitrary coordinate system.

In most normalized coordinate systems, an element of differential length in n dimensions is characterized by the expression

$$ds^2 = h_{11}dq_1^2 + h_{22}dq_2^2 + \cdots + h_{nn}dq_n^2 \qquad \text{(A-37)}$$

For an arbitrary coordinate system of n dimensions, a differential element of length is given by

$$ds^2 = g_{11}du_1^2 + 2g_{12}du_1du_2 + \cdots + g_{22}du_2^2 + 2g_{23}du_2du_3 + \cdots + g_{nn}du_n^2$$

$$= \sum_{i,j}^{n} g_{ij}du_r du_s,\ g_{ij} = g_{ji} \qquad \text{(A-38)}$$

where the coefficients g_{ij} may be functions of the coordinates. The transformation of the Schroedinger equation for a sing'e particle from the n-dimensional coordinate system

---

[9]The theory of Section A-2 is taken from the following References: [5]; [1] [pp. 279-283]; [6] [pp.262-263].

represented by Equation (A-37), to the n-dimensional coordinate system given in Equation (A-38) is

$$\sum_{i,j=1}^{n} g^{\frac{1}{2}} \frac{\partial}{\partial u_i}\left(g^{\frac{-1}{2}} g^{ij} \frac{\partial \psi_q}{\partial u_j} \right) + \frac{2m}{h^2}\left(E - V_q\right)\psi_q = 0 \qquad \text{(A-39)}$$

where

$$\iint \cdots \int \psi_q \psi_q^* g^{\frac{-1}{2}} du_1 du_2 \cdots du_n = 1 \quad \text{and} \quad g = \begin{vmatrix} g_{11}, g_{12} \cdots ; g_{1n} \\ g_{21}, g_{22} \cdots g_{2n} \\ \\ g_{n1}, g_{n2}, \cdots, g_{nn} \end{vmatrix} \qquad \text{(A-40)}$$

The corresponding normalization for ψ_u is

$$\iint \cdots \int \psi_u \psi_u^* du_1 du_2 \cdots du_n = 1 \qquad \text{(A-41)}$$

Equation (A-40) and Equation (A-41) imply

$$\psi_q = g^{\frac{1}{4}} \psi_u \qquad \text{(A-42)}$$

Substituting from Equation (A-42) into Equation (A-39) and multiplying through by $-\frac{h^2 g^{\frac{-1}{4}}}{2m}$ gives

$$\frac{1}{2} m \sum_{i,j=1}^{n} g^{\frac{1}{4}} \frac{h}{i} \frac{\partial}{\partial u_i}\left(g^{\frac{-1}{2}} g^{ij} \frac{h}{i} \frac{\partial}{\partial u_j} g^{\frac{1}{4}} \psi_u \right) + V_u \psi_u - E\psi_u = 0 \qquad \text{(A-43)}$$

Replacing the differential operators $\frac{h}{i}\frac{\partial}{\partial u}$ by the corresponding momenta and absorbing the m into the determinant gives the hamiltonian in the correct form for arbitrary coordinates

$$H = \frac{1}{2} g^{\frac{1}{4}} \sum_{i,j}^{n} p_i g^{\frac{-1}{2}} g^{ij} p_j g^{\frac{1}{4}} + V \qquad \text{(A-44)}$$

Notice that the potential V is unchanged from its classical form because it is a function of the coordinates and not of the momenta.

For the hamiltonian in Equation (A-44) the kinetic energy is given by

$$2T = \sum_{i,j} g_{ij} \dot{q}_i \dot{q}_j \qquad \text{(A-45)}$$

or in terms of the momenta

$$2T = \sum_{i,j} g^{ij} p_i p_j \qquad \text{(A-46)}$$

The coefficients g^{ij} are elements of the matrix which is the inverse of the matrix formed by the g_{ij}, and the momenta p_i are, of course, conjugate to the generalized coordinates q_i.

Transforming now to a set of momenta P'_m which are not conjugate to any set of coordinates, but are instead defined by the expression

$$P_i = \sum_m s_{im} P'_m \qquad \text{(A-47)}$$

$$2T = \sum_{m,n} G^{mn} P'_m P'_n \qquad \text{(A-48)}$$

now

$$G^{mn} = \sum_{k,l} s_{km} g^{kl} s_{ln} \qquad \text{(A-49)}$$

where we define

We must now determine under what conditions a quantum mechanical hamiltonian may be written in a form analogous to equation Equation (A-44), but in terms of the momenta P'_m, namely

$$H = \frac{1}{2} G^{\frac{1}{4}} \sum_{m,n} P'_m G^{mn} G^{\frac{-1}{2}} P'_n G^{\frac{1}{4}} + V \qquad \text{(A-50)}$$

where $G = |G^{mn}|$.

To find these conditions, substitute Equation (A-49) into Equation (A-50) and the expression

$$P'_m = \sum_i s^{mi} p_i \qquad \text{(A-51)}$$

which is the inverse of the transformation Equation (A-47).

We derive the result

$$H = \frac{1}{2} g^{\frac{1}{4}} s^{\frac{1}{2}} \sum_{ijkm} s^{mi} p_i s_{km} g^{kj} g^{\frac{-1}{2}} s^{-1} p_j g^{\frac{1}{4}} s^{\frac{1}{2}} + V \qquad \text{(A-52)}$$

by noting that $G = s^2 g$ and $\sum_n s_{ln} s^{nj} = \delta_{lj}$; where $s = |s_{im}|$.

For Equation (A-51) to reduce to Equation (A-44) the condition

$$s^{\frac{1}{2}} \sum_{i,m} s^{mi} p_i s_{km} s^{-1} = s^{\frac{-1}{2}} p_k \qquad \text{(A-53)}$$

must be fulfilled.

If the kinetic energy of the rotating-vibrating molecule was expressed in terms of the Eularian angles, θ, ϕ, χ and the normal coordinates Q_k, together with the conjugate momenta p_θ, p_ϕ, p_χ and p_k; the hamiltonian operator could immediately assume the form of Equation (A-44). But the kinetic energy is expressed in terms of $(P_x - p_x), (P_y - p_y), (P_z - p_z)$ and p_k. We therefore need to apply the condition Equation (A-53) to the transformation of the momenta p_θ, p_ϕ, p_χ and p_k to the momenta found in Equation (A-36).

To achieve this transformation, we first note that the total angular velocity vector can be written as (see Figure A-2)

$$\vec{\omega} = \dot{\vec{\theta}} + \dot{\vec{\phi}} + \dot{\vec{\chi}} = \omega_x i + \omega_y j + \omega_z k = \omega_X i' + \omega_Y j' + \omega_Z k' \qquad \text{(A-54)}$$

where the components of $\vec{\omega}$ are

$$\omega_x = i \cdot \vec{\omega} = i \cdot \dot{\vec{\theta}} + i \cdot \dot{\vec{\phi}} + i \cdot \dot{\vec{\chi}} \text{ ,etc.} \qquad \text{(A-55)}$$

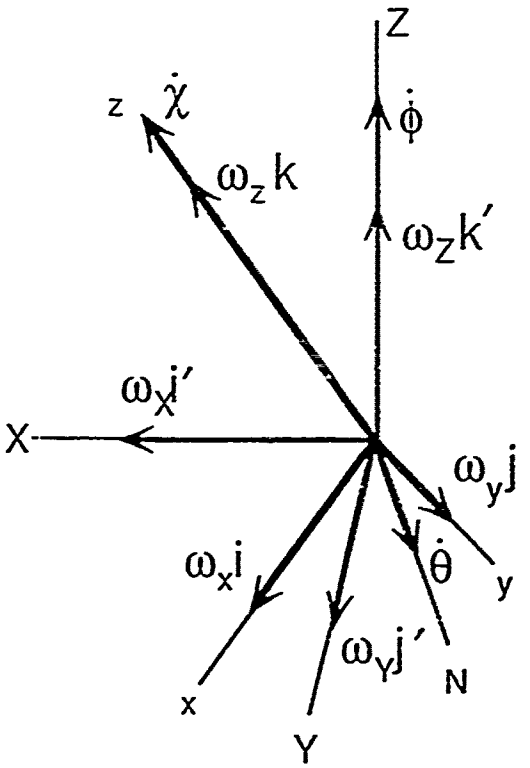

Figure A-2 -- Components of Total Angular Velocity . From [1] [p. 281]

From Figure A-2 we see

$$\omega_x = \sin\chi \cdot \dot{\theta} - \sin\theta\cos\chi \cdot \dot{\varphi}$$

$$\omega_y = \cos\chi \cdot \dot{\theta} + \sin\theta\cos\chi \cdot \dot{\varphi} \qquad \text{(A-56)}$$

$$\omega_z = \cos\dot{\theta} \cdot \dot{\varphi} + \chi$$

with the inverse transformation

$$\dot{\theta} = \sin\chi \cdot \omega_x + \cos\chi \cdot \omega_y$$

$$\dot{\varphi} = -\csc\theta\cos\chi \cdot \omega_x + \csc\theta\sin\chi \cdot \omega_y \qquad \text{(A-57)}$$

$$\dot{\chi} = \cot\theta\cos\chi \cdot \omega_x - \cot\theta\sin\chi \cdot \omega_y + \omega_z$$

Recall that

$$P_x = \frac{\partial T}{\partial \omega_x} = \frac{\partial T}{\partial \dot{\theta}}\frac{\partial \dot{\theta}}{\partial \omega_x} + \frac{\partial T}{\partial \dot{\varphi}}\frac{\partial \dot{\varphi}}{\partial \omega_x} + \frac{\partial T}{\partial \dot{\chi}}\frac{\partial \dot{\chi}}{\partial \omega_x} = \frac{\partial \dot{\theta}}{\partial \omega_x}p_\theta + \frac{\partial \dot{\varphi}}{\partial \omega_x}p_\varphi + \frac{\partial \dot{\chi}}{\partial \omega_x}p_\chi \qquad \text{(A-58)}$$

From Equation (A-57) we can find $\frac{\partial \dot{\theta}}{\partial \omega_x}$, etc. resulting in

$$P_x = \sin\chi p_\theta - \csc\theta\cos\chi p_\varphi + \cot\theta\cos\chi p_\chi$$

$$Py = \cos\chi p_\theta + \csc\theta\sin\chi p_\varphi - \cot\theta\sin\chi p_\chi \qquad \text{(A-59)}$$

$$P_z = p_\chi$$

From the definitions of p_x, p_y, p_z in Equation (A-32) we have

$$P'_x = (P_x - p_x) = \sin\chi p_\theta - \csc\theta\cos\chi p_\phi + \cot\theta\cos\chi p_\chi - \sum \Im_k p_k$$

$$P'y = (P_y - py) = \cos\chi p_\theta + \csc\theta\sin\chi p_\phi - \cot\theta\sin\chi p_\chi - \sum \Re_k p_k$$

$$P'_z = (P_z - p_z) = p_\chi - \sum \aleph_k p_k \qquad \text{(A-60)}$$

$$p_k = p_k$$

We have now found the coefficients s_{mi} of the transformation Equation (A-51). The inverse equations are

$$p_\theta = \sin\chi P'_x + \cos\chi P'_y + \sum(\sin\chi \Im_k + \cos\chi \Re_k) p_k$$

$$p_\phi = -\sin\theta\cos\chi P'_x + \sin\theta\sin\chi P'_y + \cos\theta P'_z$$

$$+ \sum(-\sin\theta\cos\chi \Im_k + \sin\theta\sin\chi \Re_k + \cos\theta \aleph_k) p_k$$

$$p_\chi = P'_z + \sum \aleph_k p_k \qquad \text{(A-61)}$$

$$p_k = p_k$$

giving the coefficients s^{im} of the inverse transformation Equation (A-47). Rewriting the condition (A-53) as

$$\sum_{ikm} s^{mi} p_i s_{km} s^{-1} = 0 \qquad \text{(A-62)}$$

and noting that p_i is a differential operator allows us to write

$$\sum_{ikm} s^{mi} s_{km} \left(p_i s^{-1} \right) + s^{-1} \sum_{ikm} s^{mi} \left(p_i s_{km} \right) = \sum_{i} \left(p_i s^{-1} \right) + s^{-1} \sum_{im} s^{mi} \left(p_i \sum_{k} s_{km} \right) = 0 \tag{A-63}$$

It has been shown that the above condition is satisfied for the case in hand, allowing us to write the quantum mechanical hamiltonian in the form of Equation (A-50)

$$H = \frac{1}{2} \mu^{\frac{1}{4}} \sum_{gg'} \left(P_g - p_g \right) \mu_{gg'} \mu^{\frac{-1}{2}} \left(P_{g'} - p_{g'} \right) \mu^{\frac{1}{4}} + \frac{1}{2} \mu^{\frac{1}{4}} \sum_{k} p_k \mu^{\frac{-1}{2}} p_k \mu^{\frac{1}{4}} + V \tag{A-64}$$

As an aside, we stop here for a moment and quickly derive the hamiltonian used as a starting point in the rigid rotor-harmonic oscillator approximation presented in Chapter 2. This approximation begins with the hamiltonian (A-64), which is completely general and contains no approximations. The first approximation we make is to neglect the dependence of μ and $\mu_{gg'}$ on the normal coordinates [see Equation(A-35)]. This means they are now constant, and are not affected by any operators. Thus Equation (A-64) reduces to

$$H = \frac{1}{2} \sum_{gg'} \mu_{gg'} \left(P_g - p_g \right) \left(P_{g'} - p_{g'} \right) + \frac{1}{2} \sum_{k} p_k^2 + V \tag{A-64a}$$

Next we perform a unitary transformation to ensure the axes moving with the molecule coincide with the principle inertial axes of the molecule at equilibrium, thereby causing the off-diagonal terms of the inertia tensor to vanish. We also neglect the terms of the form $\sum_{k} \Im_k \Re_k$ since, by definition, they depend on the squares of the small vibrational displacements [see Equation (A-26)]. Then the terms I'_{xy}, I'_{yz} and I'_{xz} are zero, and $I'_{xx} = I_{xx}$, $I'_{yy} = I_{yy}$ and $I'_{zz} = I_{zz}$ [see Equation. (A-32)]. The terms μ_{gg} now become reciprocals of the principle rigid moments of inertia and the hamiltonian is now as shown in Equation (1).

A-3 Perturbation Treatment[10]

A more convenient form of Equation (A-64) is

$$H = \frac{1}{2}\sum_{gg'}\mu_{gg}P_gP_{g'} - \sum_g h_gP_g + \frac{1}{2}\sum_{gg'}\mu^{\frac{1}{4}}p_g\mu_{gg'}\mu^{\frac{1}{2}}p_{g'}\mu^{\frac{1}{4}} + \frac{1}{2}\sum_k \mu^{\frac{1}{4}}p_k\mu^{\frac{-1}{2}}p_k\mu^{\frac{1}{4}} + V \tag{A-65}$$

where

$$h_g = \frac{1}{2}\sum_{g'}\left(\mu^{\frac{-1}{4}}\mu_{gg'}p_{g'}\mu^{\frac{1}{4}} + \mu^{\frac{1}{4}}p_{g'}\mu_{g'g}\mu^{\frac{-1}{4}}\right)$$

The hamiltonian in Equation (A-65) can be divided into three terms: H_o, a purely vibrational term consisting of the last three terms of Equation (A-65); H_R^o, which consists of those parts of the first term which are diagonal in the vibrational quantum numbers; and the perturbing hamiltonian H', which includes the second term and those parts of the first term which are not included in H_R^o.

We now make the following approximations: the wave function Ψ_{VR} can be written as the product of the two independent functions Ψ_V and Ψ_R, where Ψ_V are the orthonormal solutions to the harmonic oscillator hamiltonian, and Ψ_R depends only on the rotational coordinates. In this manner, H_o and H_R^o are diagonal in V, but not necessarily in R. If we expand Ψ_R for an asymmetric rotor in terms of the symmetric rotor basis functions (see Appendix B), we see Ψ_R is not diagonal in K.

Before we apply a perturbation treatment to H we must take care of the off-diagonal elements of H' in the vibrational matrix. We do this by performing a unitary transformation

---

[10]The theory of Section A-3 is taken from the following References: [3] [pp.33-37]; [6] [pp. 263-266]; [25] [pp. 277-281].

which will remove to first order in λ the off-diagonal matrix elements of H', while preserving to first order in λ the matrix elements of H' that lie inside the diagonal blocks (see Figure A-3).

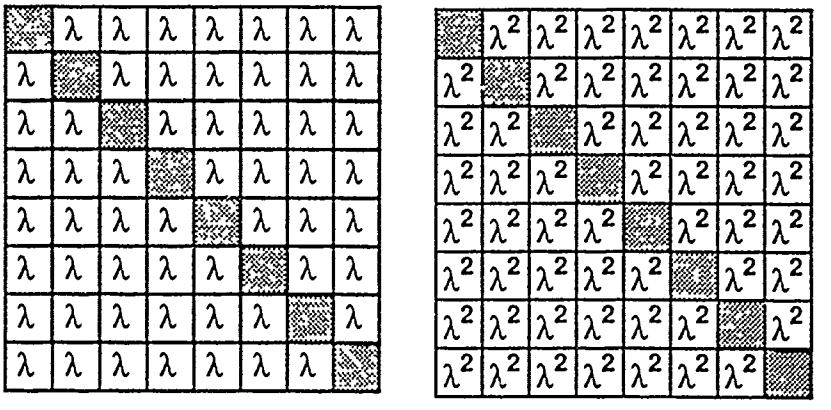

Figure A-3 -- Matrix Representation Of H'. From [3] [p. 34].

Thus the elements of H' which are outside the diagonal blocks are of the order λ^2 and contribute to the energy only to fourth order in λ. These elements can be neglected in second order perturbation theory. This unitary transformation is known as the Van Vleck transformation.

A unitary operator can be expressed as

$$U = \exp(i\lambda S) \tag{A-66}$$

where S is hermitian. We transform H as follows

$$G = U^{-1}HU = \left[I - i\lambda s - \frac{\lambda^2 s^2}{2} + \frac{i\lambda^3 s^3}{6} + \cdots\right]\left[H_o + H_R^o + H'\right]\left[I + i\lambda s - \frac{\lambda^2 s^2}{2} - \cdots\right]$$

$$= G_o + \lambda G_1 + \lambda^2 G_2 + \lambda^3 G_3 + \cdots \tag{A-67}$$

Equating like powers of λ gives

$$G_o = H_o + H_R^o$$

$$G_1 = H' + i\left[\left(H_o + H_R^o\right)S - S\left(H_o + H_R^o\right)\right]$$

$$G_2 = i(H'S - SH') + S\left(H_o + H_R^o\right)S - \frac{1}{2}\left[\left(H_o + H_R^o\right)S^2 + S^2\left(H_o + H_R^o\right)\right] \quad \text{(A-68)}$$

Now let the rotational sub-block of interest be labeled by $|V;JKM\rangle$ and indexed by j, k, l etc. , and the levels of the other rotational sub- blocks by α, β, γ and so forth. The Van Vleck transformation must satisfy two requirements. Requirement one is that $\langle j|G_1|k\rangle = \langle j|H'|k\rangle$ or

$$0 = \langle j|i\left[\left(H_o + H_R^o\right)S - S\left(H_o + H_R^o\right)\right]|k\rangle = \left(E_j - E_k\right)\langle j|S|k\rangle \quad \text{(A-69)}$$

This requirement is satisfied by

$$\langle j|S|k\rangle = 0 \quad \text{(A-70)}$$

Requirement two is that $\langle j|G_1|\alpha\rangle$ vanishes, or

$$0 = \langle j|H'|\alpha\rangle + i\langle j|\left[\left(H_o + H_R^o\right)S - S\left(H_o + H_R^o\right)\right]|\alpha\rangle = \langle j|H'|\alpha\rangle + i\left(E_j - E_\alpha\right)\langle j|S|\alpha\rangle \quad \text{(A-71)}$$

which implies

$$\langle j|S|\alpha\rangle = \frac{i\langle j|H'|\alpha\rangle}{E_j - E_\alpha} \quad \text{(A-72)}$$

Thus we have determined the nature of the hermitian operator S that generates the unitary transformation. Now by applying Equation (A-70) and Equation (A-72) to Equation (A-67) we

can determine the matrix elements of G within the same $(2j \times 1) \times (2j \times 1)$ block $|V;JKM\rangle$ to second order

$$\langle j|G_o|k\rangle = \langle j|H_o + H_R^o|k\rangle = E_j \delta_{jk}$$

$$\langle j|G_1|k\rangle = \langle j|H'|k\rangle \tag{A-73}$$

$$\langle j|G_2|k\rangle = \sum_\alpha \frac{\left[\frac{1}{2}(E_j+E_k)-E_\alpha\right]\langle j|H'|\alpha\rangle\langle\alpha|H'|k\rangle}{(E_j-E_\alpha)(E_k-E_\alpha)}$$

Now the off-diagonal sub-blocks contain terms only of order λ^2 and higher and can be neglected in second order perturbation theory. If more accuracy is desired, G can always be subjected to another Van Vleck transformation.

If we now neglect the off-diagonal elements of H in the matrix V, the remaining diagonal terms each factor into smaller matrices, one for each vibrational state, whose elements $\langle R,V|H|R',V\rangle$ are labeled by the rotational quantum numbers only.

Using standard perturbation theory, we can write

$$H = H_o + H_R + H' \tag{A-74}$$

where we can expand the perturbing hamiltonian H' to second order in a power series in λ (λ small), that is

$$H' = \lambda H'_1 + \lambda^2 H'_2 \tag{A-75}$$

The zeroeth and first order terms are given by

$$\langle RV|H_o + H_R^o + \lambda H'|R'V\rangle = \langle RV|H_o|RV'\rangle + \langle RV|H_R^o + \lambda H|R'V\rangle =$$

$$E_v + \frac{1}{2}\sum_{gg'}\langle\mu_{gg'}\rangle\langle RV|P_gP_{g'}|R'V\rangle - \lambda\sum_g\langle h_g\rangle\langle RV|P_g|R'V\rangle \qquad \text{(A-76)}$$

E_V is the vibrational energy, diagonal in R and V, whose diagonal elements are E_v. The last two terms come from the fact that $\mu_{gg'}$ and h_g are functions only of the vibrational coordinates [see Equation (A-33) and Equation (A-65)] plus the approximation $\Psi_{VR} = \Psi_V\Psi_R$.

We can further simplify Equation (A-76) by noting that, since h_g is pure imaginary (each operator p_g carries one term of -ih and all other terms are real), and because H and P_g are hermitian, the matrix $\langle V|h_g|V'\rangle$ is hermitian. Also for a non-degenerate asymmetric rotor, the Ψ_V are real. Hence the diagonal term

$$\langle V|h_g|V\rangle = \langle V|h_g^{\dagger}|V\rangle = \langle V|h_g^*|V\rangle = -\langle V|h_g|V\rangle = 0 \qquad \text{(A-77)}$$

The second order term is given by

$$\lambda^2 H_2' = \lambda^2 \sum_{\substack{R'V'' \\ V''\neq V}} \frac{\langle VR|H|V''R''\rangle\langle V''R''|H|VR\rangle}{E_v - E_{v''}} \qquad \text{(A-78)}$$

Here we have assumed the rotational spacing is small compared to the vibrational levels so that $E_{RV}^o - E_{R''V''}^o$ can be replaced by $E_V^o - E_{V''}^o$. Equation (A-78), when multiplied out will give us the quartic, cubic and quadratic terms of P_x, P_y and P_z. The coefficients of the terms P_x^3, P_y^3 and P_z^3 are of the form

$$\frac{1}{2}\sum_{\substack{V'' \\ V\neq V''}} \frac{\langle V|\mu_{gg'}|V''\rangle\langle V''|h_g|V\rangle + \langle V|h_{g'}|V''\rangle\langle V''|\mu_{gg'}|V\rangle}{E_v - E_{v''}} \qquad \text{(A-79)}$$

They can be shown to vanish by noting that, since h_g is pure imaginary, $\langle V|h_g|V''\rangle = -\langle V|h_g|V''\rangle$; and since μ_{gg} is a real operator, $\langle V|\mu_{gg}|V''\rangle = \langle V''|\mu_{gg}|V\rangle$. The rest of the cubic terms are of the type $P_x^2 P_y - P_y P_x^2$, etc. These can likewise be eliminated by use of the commutation rules $[P_i, P_j] = \varepsilon_{ijk} P_k$ at the cost of introducing extra quadratic terms.

Thus, as a result of the perturbation treatment, the rotational matrix $H = H_o + H_R^c + H'$, which corresponds to a single vibrational state can be written as a polynomial in P_x, P_y and P_z

$$H = E_v + \frac{1}{2}\sum_{gg'} \alpha_{gg'} P_g P_{g'} + \frac{1}{4}\sum_{gg'jj'} \tau_{gg'jj'} P_g P_{g'} P_j P_{j'} \qquad \text{(A-80)}$$

where $\alpha_{gg'}$ and $\tau_{gg'jj'}$ are functions of the vibrational state only. Note also that

$$\tau_{gg'jj'} = \sum_{\substack{V'' \\ V \neq V''}} \frac{\langle V|\mu_{gg'}|V''\rangle\langle V''|\mu_{jj'}|V\rangle}{E_v - E_{v''}} \qquad \text{(A-81)}$$

A-4 The Reduced Hamiltonian[11]

The form of the hamiltonian in Equation (A-80) has several drawbacks. First, if further accuracy is desired, higher order perturbation must be considered, which could become extremely cumbersome. Also, not all the coefficients $\alpha_{gg'}$ and $\tau_{gg'jj'}$ are determinable. If all the constants in Equation (A-80) were known, it would be a straightforward process, in principle, to determine the energy levels from them. However, the situation that we are faced with experimentally is the reverse of this; we wish to determine, from observed energy levels, the

[11]The theory of Section A-4 is taken from the following References: [4] [pp. 2-80]; [18]; [17] [pp. 1935-1947].

values of the rotational and centrifugal constants. The problem in carrying out this reverse calculation is that not all constants or combination of constants contribute to the energy levels and are therefore not determinable from them. For example, neglecting the quartic distortion terms in Equation (A-80) allows us to write the rotational hamiltonian as

$$H_{rot} = \frac{1}{2}\sum_{gg'} \alpha_{gg'} J_g J_{g'} \qquad \text{(A-82)}$$

where $\alpha_{gg'}$ are related to the values in Equation (A-35) , for the particular vibrational state and the symbol J now represents the total angular momentum. We can reduce the matrix $\alpha_{gg'}$ to diagonal form by a simple rotation of axes (to a principle axes system) giving us the reduced form of the hamiltonian

$$H_{rot} = XJ_x^2 + YJ_y^2 + ZJ_z^2 \qquad \text{(A-83)}$$

where X, Y, Z are the principle values of $\frac{1}{2}\alpha_{gg'}$. It is obvious that the rotational energies depend only on the principle values of $\frac{1}{2}\alpha_{gg'}$ and all the other coefficients $\frac{1}{2}\alpha_{gg'}$ are not determinable from those energies. Therefore, to obtain increased accuracy and to determine all the coefficients in the hamiltonian, it is necessary to write the hamiltonian in another form.

The hamiltonian in Equation (A-80) contains such terms as $J_x J_z J_x J_y$ with individual terms appearing in any order. By using the commutation relations $\left[J_i, J_j\right] = \varepsilon_{ijk} J_k$ we can rewrite such these terms in the form $\frac{1}{2}\left(J_x^p J_y^q J_z^r + J_z^r J_y^q J_x^p\right)$ + terms to lower degree in J. For example

$$J_x J_z J_x J_y = \frac{1}{2}\left(J_x^2 J_y J_z + J_z J_y J_x^2\right) + \frac{i}{2}J_x^3 - \frac{i}{2}\left(J_x J_z^2 + J_z^2 J_x\right) - \frac{1}{2}\left(J_y J_z + J_z J_y\right) \qquad \text{(A-84)}$$

The terms of lower degree can then be changed in the same way, and the process can be repeated resulting in a sum of terms of the following form

$$H_{rot} = \sum_{pqr} h_{pqr} \left(J_x^p J_y^q J_z^r + J_z^r J_y^q J_x^p \right) \tag{A-85}$$

where the coefficients h_{pqr} may or may not be complex.

To simplify further, we note that the rotational hamiltonian, of a given vibrational state, is invariant to both operations of hermitian conjugation and time reversal. That is

$$H_{rot} = H_{rot}^{\Downarrow} + TH_{rot}T^{-1} = \left(TH_{rot}T^{-1} \right) \tag{A-86}$$

where the symbol $\Downarrow$ represents the adjoint of the operator. In addition, the operators J and the coefficients h_{pqr} have the following properties

$$J^{\Downarrow} = J, \quad TJT^{-1} = -J, \quad h_{pqr}^{\Downarrow} = h_{pqr}^{*}, \quad Th_{pqr}T^{-1} = h_{pqr}^{*} \tag{A-87}$$

Equation (A-86) and Equation (A-87) together give us

$$H_{rot}^{\Downarrow} = \sum_{pqr} h_{pqr}^{*} \left(J_x^p J_y^q J_z^r + J_z^r J_y^q J_x^p \right)$$

$$TH_{rot}T^{-1} = \sum_{pqr} (-1)^{p+q+r} h_{pqr}^{*} \left(J_x^p J_y^q J_z^r + J_z^r J_y^q J_x^p \right) \tag{A-88}$$

$$\left(TH_{rot}T^{-1} \right)^{\Downarrow} = \sum_{pqr} (-1)^{p+q+r} h_{pqr}^{*} \left(J_x^p J_y^q J_z^r + J_z^r J_y^q J_x^p \right)$$

The last equation of (A-88) shows that since terms of odd degree in p+q+r change sign under operations of time reversal and hermitian conjugation, they do not satisfy the invariance relation (A-86). The first two equations of (A-88) show that the remaining terms of even degree satisfy the invariance relation only if the h_{pqr} are real. We now have a simplified rotational hamiltonian

$$H_{rot} = \sum_{\substack{p+q+r \\ even}} h_{pqr}\left(J_x^p J_y^q J_z^r + J_z^r J_y^q J_x^p\right) \qquad \text{(A-89)}$$

where h_{pqr} are real. Note that the coefficients of the terms of degree greater than two are the centrifugal distortion coefficients for a particular vibrational state of the molecule. One further simplification can be made by noting that for molecules of C_{2v} (orthorhombic) symmetry the only non-zero terms in Equation (A-89) are those with p, q, and r all even, giving us

$$H_{rot} = \sum_{\substack{p,q,r \\ even}} h_{pqr}\left(J_x^p J_y^q J_z^r + J_z^r J_y^q J_x^p\right) \quad ,h_{pqr} \text{ real} \qquad \text{(A-90)}$$

If further accuracy is desired, we can just extend the power series to any degree in J that we want. For the purposes of this experiment, expansion of the power series (A-90) to the sixth power in J is needed. With a slight change in notation we have

$$H_{rot} = \sum_{\alpha} B_\alpha J_\alpha^2 + \sum_{\alpha,\beta} T_{\alpha\beta} J_\alpha^2 J_\beta^2 + \sum_{\alpha} \Phi_{\alpha\alpha\alpha} J_\alpha^6 + \sum_{\alpha\neq\beta} \Phi_{\alpha\alpha\beta}\left(J_\alpha^4 J_\beta^2 + J_\beta^2 J_\alpha^4\right) +$$

$$\Phi_{xyz}\left(J_x^2 + J_y^2 + J_z^2 + J_z^2 J_y^2 J_x^2\right) \qquad \text{(A-91)}$$

where the coefficients are real and $T_{\alpha\beta} = T_{\beta\alpha}$. In terms of J^2, J_z and $J_\pm$ we have

$$H_{rot} = \left[B_{200} J^2 + B_{020} J_z^2 + T_{400}\left(J^2\right)^2 + T_{220} J^2 J_z^2 + T_{040} J_z^4 + \Phi_{600}\left(J^2\right)^3 + \Phi_{420}\left(J^2\right)^2 J_z^2\right]$$

$$+ \Phi_{240} J^2 J_z^4 + \Phi_{060} J_z^6 + \tfrac{1}{2}\left[B_{002} + T_{202} J^2 + T_{022} J_z^2 + \Phi_{420}\left(J^2\right)^2 + \Phi_{222} J^2 J_z^2 + \Phi_{042} J_z^4 ,\right.$$

$$\left. J_+^2 + J_-^2\right]_+ + \tfrac{1}{2}\left[T_{004} + \Phi_{204} J^2 + \Phi_{024} J_z^2, J_+^4 + J_-^4\right]_+ + \Phi_{006}\left(J_+^6 + J_-^6\right) \qquad \text{(A-92)}$$

where $[A,B]_+$ represents the anti-commutator $AB + BA$ and the subscripts on the coefficients now refer to the powers of J, J_z and $J_\pm$ respectively. To go from the form of the

H_{rot} in Equation (A-91) to H_{rot} in Equation (A-92) requires repeated use of the commutation relations $\left[J_i, J_j\right] = \varepsilon_{ijk} J_k$. For each constant, terms of higher degree are negligible therefore neglected. With this in mind the relations between the constants in Equation (A-91) and Equation (A-92) are given in Table A-1.

TABLE A-1
Relationship among constants in Equation (A-91) and Equation (A-92). From [4] [p. 21].

$$B_{200} = \tfrac{1}{2}(B_x + B_y) - 4T_{004} \qquad \Phi_{024} = \tfrac{1}{8}(\Phi_{xxz} + \Phi_{yyz} - \Phi_{xyz}) - \Phi_{204}$$

$$B_{002} = \tfrac{1}{4}(B_x - B_y) \qquad \Phi_{006} = \tfrac{1}{64}(\Phi_{xxx} - \Phi_{yyy}) - \tfrac{1}{32}(\Phi_{xxy} - \Phi_{yyx})$$

$$B_{020} = B_z - B_{200} + 6T_{004}$$

$$T_{400} = \tfrac{1}{8}(3T_{xx} + 3T_{yy} + 2T_{xy})$$

$$T_{220} = (T_{xz} + T_{yz}) - 2T_{400}$$

$$T_{040} = T_{zz} - T_{220} - T_{400}$$

$$T_{202} = \tfrac{1}{4}(T_{xx} - T_{yy})$$

$$\Phi_{600} = \tfrac{5}{16}(\Phi_{xxx} + \Phi_{yyy}) + \tfrac{1}{8}(\Phi_{xxy} + \Phi_{yyx})$$

$$\Phi_{420} = \tfrac{3}{4}(\Phi_{xxz} + \Phi_{yyz}) + \tfrac{1}{4}\Phi_{xyz} - 3\Phi_{600}$$

$$\Phi_{240} = (\Phi_{zzx} + \Phi_{zzy}) - \Phi_{240} - 3\Phi_{600}$$

$$\Phi_{060} = \Phi_{zzz} - \Phi_{240} - \Phi_{420} - \Phi_{600}$$

$$\Phi_{402} = \tfrac{15}{64}(\Phi_{xxx} - \Phi_{yyy}) + \tfrac{1}{32}(\Phi_{xxy} - \Phi_{yyx})$$

$$\Phi_{222} = \tfrac{1}{2}(\Phi_{xxz} - \Phi_{yyz}) - 2\Phi_{402}$$

$$\Phi_{042} = \tfrac{1}{2}(\Phi_{zzx} - \Phi_{zzy}) - \Phi_{222} - \Phi_{402}$$

$$\Phi_{204} = \tfrac{3}{32}(\Phi_{xxx} + \Phi_{yyy}) - \tfrac{1}{16}(\Phi_{xxy} + \Phi_{yyx})$$

We still have the problem of which constants or combination of constants contribute to the energy levels and can therefore be determined from them. We can solve this problem by noting that the eigenvalues of the rotational hamiltonian are unaltered when the hamiltonian

is transformed by an arbitrary unitary operator [the transformation from Equation (A-82) to Equation (A-83) is an example of such a unitary transformation]. If we construct the unitary operator as a power series in the total angular momentum J and other parameters, then the transformed hamiltonian will be a power series similar to the original hamiltonian, but with coefficients depending on the parameters in the unitary transformation. Because these parameters are arbitrary, we can choose the unitary operator in such a way as to eliminate as many terms as possible from the transformed hamiltonian. The coefficients of the remaining terms are the maximum number of terms which can be determined from the experimental data. The situation is not quite as simple as described above, but we can still make a meaningful transformation by considering orders of magnitudes of various coefficients involved, and discarding terms which may be negligible. Details of this process can be found in Reference [4]. A hamiltonian subjected thus to a unitary operation is called a reduced hamiltonian.

We wish to construct a reduced hamiltonian H'_{rot} with the same eigenvalues as H_{rot}. The reduced hamiltonian is given by

$$H'_{rot} = UH_{rot}U^{-1} \tag{A-93}$$

Recall that the most convenient form for a unitary operator is

$$U = \exp(iS) \tag{A-94}$$

where S is hermitian. To make H'_{rot} invariant under time reversal, we must make U invariant, which requires that S change sign under time reversal. Therefore, if we express S as a power series similar in form to Equation (A-85), we see it has real coefficients and contains powers of p+q+r=odd only.

$$S = \sum_{\substack{p+q+r \\ odd}} s_{pqr}\left(J_x^p J_y^q J_z^r + J_z^r J_y^q J_x^p\right) \tag{A-95}$$

The exact structure of S, and therefore of U,depends on the symmetry of the molecule in question. Details of the arguments and exact forms of U and S can be found in Reference [4].

As a result of these arguments it has been shown that for molecules of orthorhombic symmetry, the hamiltonian of Equation (A-91) can be transformed to an analogous form H'_{rot} by the following changes in coefficients

$$B'_x = B_x - 4(B_y - B_z)s_{111}$$

$$T'_{xx} = T_{xx}$$

$$T'_{xy} = T_{xy} - 2(B_x - B_y)s_{311}$$

$$\Phi'_{xxx} = \Phi_{xxx}$$

$$\Phi'_{xxy} = \Phi_{xxy} - 2(B_x - B_y)s_{311} - 4(T_{xx} - T_{xy})s_{111} - 4(B_x - B_y)s^2_{111} \qquad \text{(A-96)}$$

$$\Phi'_{xxz} = \Phi_{xxz} + 2(B_x - B_z)s_{311} + 4(T_{xx} - T_{xz})s_{111} - 4(B_x - B_z)s^2_{111}$$

$$\Phi'_{xyz} = \Phi_{xyz} - 6[(B_y - B_z)s_{311} + (B_z - B_x)s_{131} + (B_x - B_y)s_{113}]$$

where s_{111}, s_{311}, s_{131}, and s_{113} are coefficients from Equation (A-95)

H_{rot} of Equation (A-92) can also be transformed to an analogous form H'_{rot} by making the coefficient transformations indicated in Table A-2. Note the coefficients s_{111}, s_{311}, s_{131} and s_{113} have been replaced by the parameters ρ, λ, μ and ν which are also defined in Table A-2.

TABLE A-2
Coefficients of the Transformed Hamiltonian. From [4] [p. 33].

$$B'_{200} = B_{200} + 4\rho \qquad B'_{020} = B_{020} - 14\rho \qquad B'_{002} = B_{002} + 4\sigma\rho$$

$$T_{400}' = T_{400} - 2\rho \qquad T_{220}' = T_{220} + 12\rho \qquad T'_{040} = T_{040} + \rho$$

$$T'_{202} = T_{202} \qquad T'_{022} = T_{022} - 4\sigma\rho \qquad T'_{004} = T_{004} + \rho$$

$$\Phi'_{600} = \Phi_{600} - \lambda$$

$$\Phi'_{420} = \Phi_{420} + 6\lambda - 3\mu$$

$$\Phi'_{240} = \Phi_{240} - 5\lambda = 10\mu$$

$$\Phi'_{060} = \Phi_{060} - 7\mu$$

$$\Phi'_{402} = \Phi_{402} - \nu$$

$$\Phi'_{222} = \Phi_{222} - 2\sigma\lambda + 10\nu + \frac{(-2T_{220} + 4\sigma T_{202} - 8T_{004} - 16\rho)\rho}{B_{002}}$$

$$\Phi'_{042} = \Phi_{042} - 2\sigma\mu - 9\nu + \frac{\left[-4T_{040} + 4\sigma T_{022} + 8T_{004} - 8(\sigma^2 - 3)\rho\right]\rho}{B_{002}}$$

$$\Phi'_{204} = \Phi_{204} + \frac{\lambda}{2}$$

$$\Phi'_{024} = \Phi_{024} - 8\sigma\nu = \frac{3\mu}{2} + \frac{(-4T_{022} + 16\sigma T_{004} + 16\sigma\rho)\rho}{B_{002}}$$

$$\Phi'_{006} = \Phi_{006} + \nu$$

$$\rho = B_{002} s_{111} \qquad \mu = B_{002}(2s_{113} - s_{311} - s_{131}) + 2T_{022} s_{111} - 2B_{020} s_{111}^2$$

$$\lambda = B_{002}(s_{311} + s_{131}) + 2T_{202} s_{111}$$

$$\nu = \frac{1}{4} B_{002}(s_{311} - s_{131}) + 2T_{004} s_{111} + B_{002} s_{111}^2 \qquad \sigma = \frac{B_{020}}{B_{002}}$$

The reduction of the rotational hamiltonian is completed by making appropriate reductions of certain coefficients which will fix the parameters ρ, λ, μ and ν. Because SF_2O_2 approaches the symmetric prolate limit, we need to consider a reduction that stays finite in this limit. The choice we make is called the asymmetric top reduction or the S-reduction. This reduction is obtained by the conditions

$$T'_{022} = \Phi'_{022} = \Phi'_{042} = \Phi'_{024} = 0 \qquad \text{(A-97)}$$

These conditions are solved to give the values of ρ, λ, μ and ν given in Table A-3.

The form of the S-reduced hamiltonian is

$$H'^{S}_{rot} = B_x^{(s)} J_x^2 + B_y^{(s)} J_y^2 + B_z^{(s)} J_z^2 - D_j (J^2)^2 J_z^2 - D_k J_z^4$$

$$+ d_1 J^2 (J_+^2 + J_-^2) + d_2 (J_+^4 + J_-^4) + H_J (J^2)^3 + H_{JK} (J^2)^2 J_z^2 + H_{KJ} J^2 J_z^4$$

$$+ H_K J_z^6 + h_1 (J^2)^2 (J_+^2 + J_-^2) + h_2 J^2 (J_+^4 + J_-^4) + h_3 (J_+^6 + J_-^6) \qquad \text{(A-98)}$$

The relationship of the coefficients in Equation (A-98) to coefficients from previous expressions of H'_{rot} is given in Table A-3.

TABLE A-3

Constants of the S-Reduced Hamiltonian. From [4] [p. 35].

$$B_x^{(s)} = B_x - 4T_{004} + (2+\sigma^{-1})T_{022}$$

$$B_y^{(s)} = B_y - 4T_{004} - (2-\sigma^{-1})T_{022}$$

$$B_z^{(s)} = B_z + 6T_{004} - \tfrac{5}{2}\sigma^{-1}T_{002}$$

$$-D_J = T_{004} - \tfrac{1}{2}\sigma^{-1}T_{002} \qquad -D_{JK} = T_{220} + 3\sigma^{-1}T_{002} \qquad -D_K = T_{040} - \tfrac{5}{2}\sigma^{-1}T_{022}$$

$$d_1 = T_{202} \qquad d_2 = T_{004} + \tfrac{1}{4}\sigma^{-1}T_{022} \qquad H_J = \Phi_{600} - \lambda$$

$$H_{JK} = \Phi_{420} + 6\lambda - 3\mu \qquad H_{KJ} = \Phi_{240} - 5\lambda + 10\mu \qquad H_K = \Phi_{060} - 7\mu$$

$$h_1 = \Phi_{402} - \nu \qquad h_2 = \Phi_{204} + \tfrac{\lambda}{2} \qquad h_3 = \Phi_{006} + \nu$$

$$\rho = \tfrac{1}{4}\sigma^{-1}T_{022}$$

$$\mu = \left(2\sigma^2 + \tfrac{27}{16}\right)^{-1}\left\{\sigma\Phi_{042} - \tfrac{9}{8}\Phi_{024} + \left[-2\sigma T_{040} + (\sigma^2+3)T_{022} - 5\sigma T_{004}\right]\frac{T_{022}}{B_{020}}\right\}$$

$$\nu = \tfrac{3}{16}\sigma^{-1}\mu + \tfrac{1}{8}\sigma^{-1}\Phi_{024} + \frac{T_{004}\,T_{022}}{B_{020}}$$

$$\lambda = 5\sigma^{-1} + \tfrac{1}{2} + \sigma^{-1}\Phi_{222} + \left(-\tfrac{1}{2}\sigma^{-1}T_{220} + T_{202} - \sigma^{-2}T_{022} - 2\sigma^{-1}T_{004}\right)\frac{T_{022}}{B_{020}}$$

Appendix B
Wave Equation Solution For The Symmetric Top[12]

The motion of a symmetric top is usually described by the Euler angles (see Figure B-1).

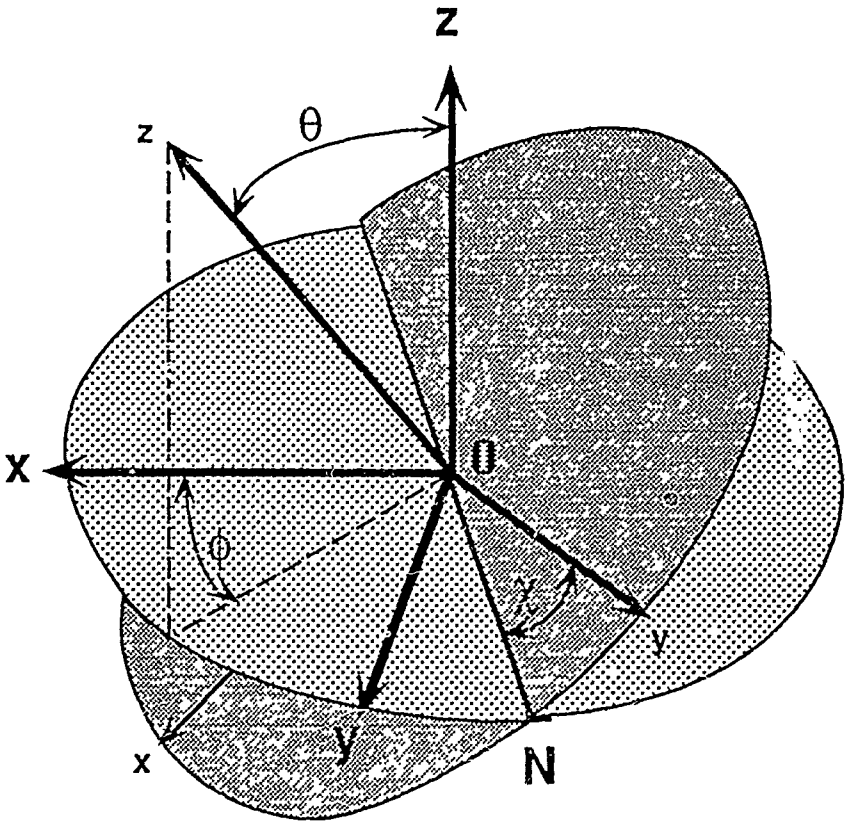

Figure B-1 --The Euler angles. From [25] [p. 78].

Now let $\vec{r}$ be an arbitrary vector having Cartesian components $r_F = (r_X, r_Y, r_Z)$ in the space-fixed (lab) frame and the Cartesian components $r_g = (r_x, r_y, r_z)$ in the body-fixed

---

[12]The theory of Appendix B is taken from the following references: [2] [pp. 60-61]; [25] [pp.77-83]; [1] [pp. 285-286].

(molecular) frame. Since we are describing the rotation of the symmetric top by the Euler angles, the two representations of the vector $\vec{r}$ are related by the unitary transformation Φ

$$r_F = \sum_g \Phi_{Fg(\theta,\phi,\chi)} r_g$$

$$r_g = \sum_F \Phi_{gF(\theta,\phi,\chi)} r_F \qquad \text{(B-1)}$$

where Φ is called the direction cosine matrix. Naturally we express the operator Φ by the product of the three Euler angle rotations (see Figure B-2)

$$\Phi_{(\theta,\phi,\chi)} = R_{z(\chi)} R_{N(\theta)} R_{Z(\phi)} \qquad \text{(B-2)}$$

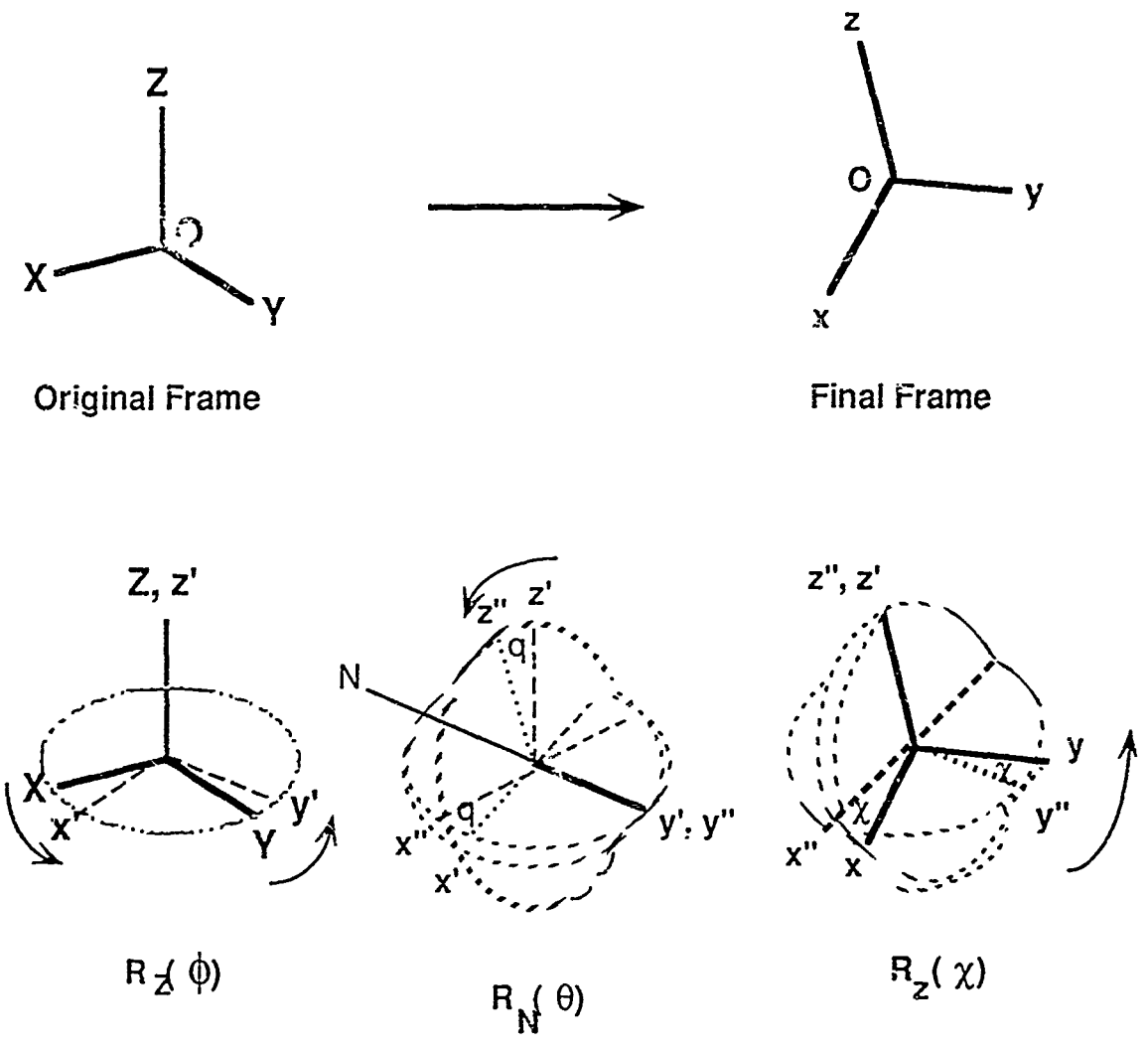

Figure B-2 – Components of Euler Angle Rotations. From [25] [p. 79].

Since we can represent the Euler angles as the product of three rotations, we can find the relationship between r_F and r_g to be as depicted in Table B-1. Because the Φ_{gF} are the real elements of a unitary transformation, $\Phi_{gF}^{-1} = \Phi_{Fg}$. That means the transformation is orthonormal, i.e.

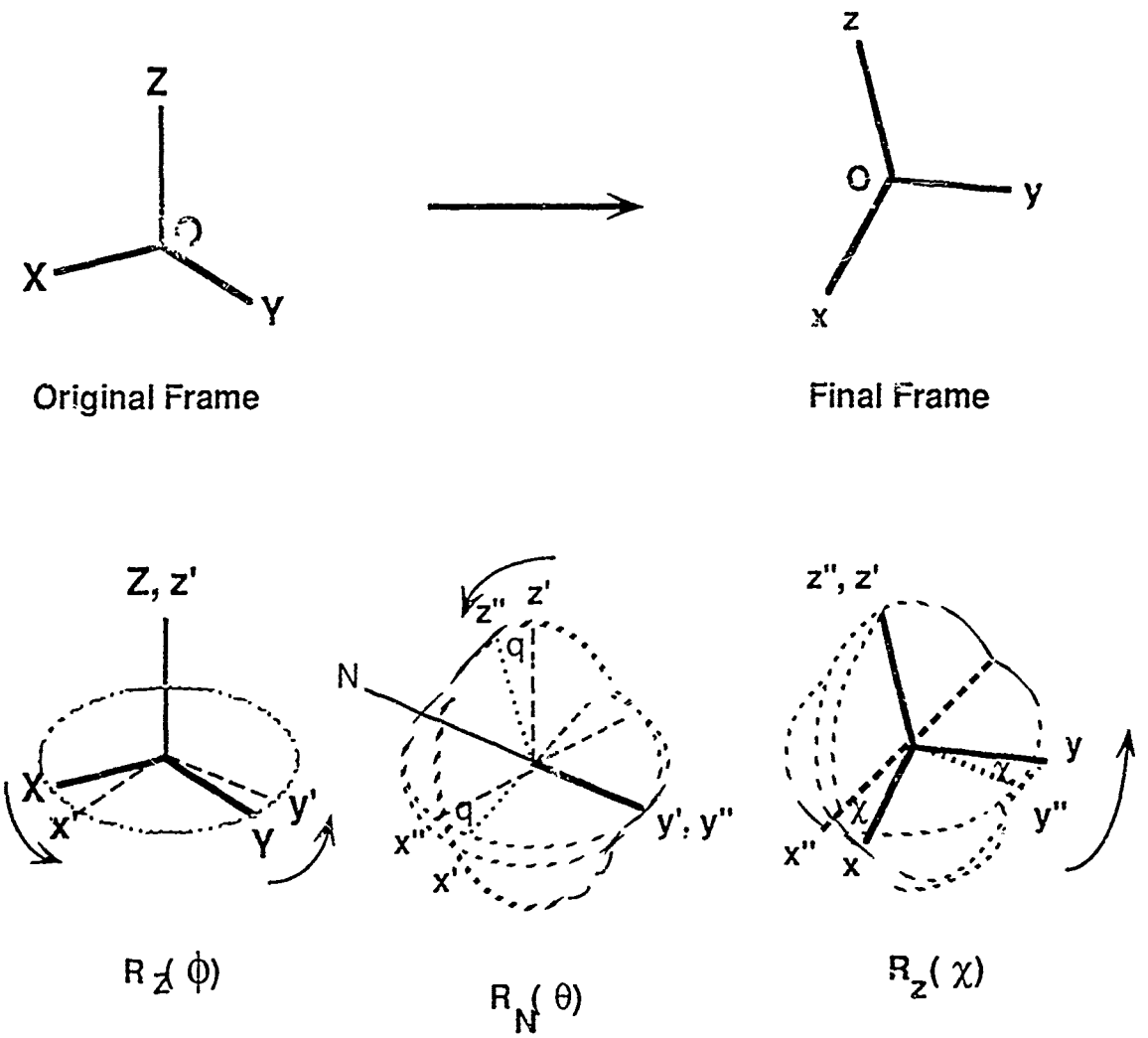

Figure B-2 – Components of Euler Angle Rotations. From [25] [p. 79].

Since we can represent the Euler angles as the product of three rotations, we can find the relationship between r_F and r_g to be as depicted in Table B-1. Because the Φ_{gF} are the real elements of a unitary transformation, $\Phi^{-1}_{gF} = \Phi_{Fg}$. That means the transformation is orthonormal, i.e.

$$\sum_{g} \Phi_{Fg} \Phi_{F'g} = \delta_{FF'}$$

$$\sum_{F} \Phi_{Fg} \Phi_{Fg'} = \delta_{gg'} \qquad \text{(B-3)}$$

and Table B-1 can be read either across or down. The entries in Table B-1 are the cosines of the angles between the various pairs of axes.

Table B-1

Direction Cosines Relating Rotating to Nonrotating Axes as Functions Of Eularian Angles.

From [1] [p. 286].

	X	Y	Z
x	$\cos\theta\cos\varphi\cos\chi - \sin\phi\sin\chi$	$\cos\theta\sin\phi\cos\chi + \cos\phi\sin\chi$	$-\sin\theta\cos\chi$
y	$-\cos\theta\cos\phi\sin\chi - \sin\phi\cos\chi$	$-\cos\theta\sin\phi\sin\chi + \cos\phi\cos\chi$	$\sin\theta\sin\chi$
z	$\sin\theta\cos\varphi$	$\sin\theta\sin\phi$	$\cos\theta$

By examining Figure B-1 we deduce the following relations

$$\hat{n}_{\phi} = \hat{n}_{Z}$$

$$\hat{n}_{\theta} = -\hat{n}_{X}\sin\phi + \hat{n}_{Y}\cos\phi \qquad \text{(B-4)}$$

$$\hat{n}_{\chi} = \hat{n}_{X}\sin\theta\cos\varphi + \hat{n}_{Y}\sin\theta\sin\phi + \hat{n}_{Z}\cos\theta$$

By noting that the projection of the angular momentum J on an arbitrary axis $\hat{n}$ is the operator which generates an infinitesimal rotation α_n about $\hat{n}$, that is

$$\sum_{g} \Phi_{Fg} \Phi_{F'g} = \delta_{FF'}$$

$$\sum_{F} \Phi_{Fg} \Phi_{Fg'} = \delta_{gg'} \qquad \text{(B-3)}$$

and Table B-1 can be read either across or down. The entries in Table B-1 are the cosines of the angles between the various pairs of axes.

Table B-1

Direction Cosines Relating Rotating to Nonrotating Axes as Functions Of Eularian Angles.

From [1] [p. 286].

	X	Y	Z
x	$\cos\theta\cos\phi\cos\chi - \sin\phi\sin\chi$	$\cos\theta\sin\phi\cos\chi + \cos\phi\sin\chi$	$-\sin\theta\cos\chi$
y	$-\cos\theta\cos\phi\sin\chi - \sin\phi\cos\chi$	$-\cos\theta\sin\phi\sin\chi + \cos\phi\cos\chi$	$\sin\theta\sin\chi$
z	$\sin\theta\cos\phi$	$\sin\theta\sin\phi$	$\cos\theta$

By examining Figure B-1 we deduce the following relations

$$\hat{n}_{\phi} = \hat{n}_{Z}$$

$$\hat{n}_{\theta} = -\hat{n}_{X}\sin\phi + \hat{n}_{Y}\cos\phi \qquad \text{(B-4)}$$

$$\hat{n}_{\chi} = \hat{n}_{X}\sin\theta\cos\phi + \hat{n}_{Y}\sin\theta\sin\phi + \hat{n}_{Z}\cos\theta$$

By noting that the projection of the angular momentum J on an arbitrary axis $\hat{n}$ is the operator which generates an infinitesimal rotation α_n about $\hat{n}$, that is

$$A = \frac{h}{8\pi^2 I_a}, \quad B = \frac{h}{8\pi^2 I_b}, \quad C = \frac{h}{8\pi^2 I_c} \tag{B-10}$$

Equation (B-10) implies

$$A > B > C \tag{B-11}$$

For a symmetric prolate top we identify the symmetry axis (z-axis) as the a-axis, and the other two axes as the b-axes. This gives us the hamiltonian

$$H = BJ^2 + J_Z^2(A - B) \tag{B-12}$$

We use the hamiltonian (B-12) in the Schroedinger equation. We can calculate J^2 and J_Z^2 from Equation (B-7)

$$J^2 = -\frac{1}{\sin\theta}\frac{\partial}{\partial\theta}\left(\sin\theta\frac{\partial}{\partial\theta}\right) + \frac{1}{\sin^2\theta}\frac{\partial^2}{\partial\phi^2} - \frac{2\cos\theta}{\sin^2\theta}\frac{\partial^2}{\partial\chi\partial\phi}\left(\frac{1}{\sin^2\theta}\right)\frac{\partial^2}{\partial\chi^2}$$

$$J_Z^2 = -\frac{\partial^2}{\partial\phi^2} \tag{B-13}$$

Upon substitution into Schroedinger's equation we get

$$\left[\frac{1}{\sin^2\theta}\frac{\partial}{\partial\phi}\left(\sin\theta\frac{\partial}{\partial\theta}\right) + \frac{1}{\sin^2\theta}\frac{\partial^2}{\partial\phi^2} + \left(\frac{\cos^2\theta}{\sin^2\theta} + \frac{A}{B}\right)\frac{\partial^2}{\partial\chi^2} - \frac{2\cos\theta}{\sin^2\theta}\frac{\partial^2}{\partial\chi\partial\phi} + \frac{E}{hB}\right]\psi = 0 \tag{B-14}$$

We assume a solution of the form

$$\psi = \Theta_{(\theta)} e^{iM\phi} e^{iK\chi} \tag{B-15}$$

where M and K must be integers to preserve the periocity of the solution. $\Theta_{(\theta)}$ must now satisfy the equation

$$\left(\frac{1}{\sin\theta}\right)\frac{d}{d\theta}\left(\sin\theta\frac{d\Theta_{(\theta)}}{d\theta}\right)+\left[-\frac{M^2}{\sin\theta}-\left(\frac{\cos^2\theta}{\sin^2\theta}+\frac{A}{B}\right)K^2+\left(\frac{2\cos\theta}{\sin^2\theta}\right)KM+\frac{E}{hB}\right]\Theta_{(\theta)}=0 \tag{B-16}$$

By letting

$$x=\frac{1}{2}(1-\cos\theta) \tag{B-17}$$

we get

$$\Theta_{(\theta)}=x^{\frac{1}{2}|K-M|}(1-x)^{\frac{1}{2}|K+M|}F_{(x)} \tag{B-18}$$

where $F_{(x)}$ is a polynomial in x.We find the equation for $F_{(x)}$ to be

$$x(1-x)F''_{(x)}+(\alpha-\beta x)F'_{(x)}+\gamma F_{(x)}=0 \tag{B-19}$$

where

$$\alpha=|K-M|+1$$

$$\beta=|K+M|+|K-M|+2 \tag{B-20}$$

$$\gamma=\frac{E}{hB}-\frac{AK^2}{B}+K^2-\left(\frac{1}{2}|K+M|+\frac{1}{2}|K-M|\right)\left(\frac{1}{2}|K+M|+\frac{1}{2}|K-M|+1\right)$$

Equation (B-19) can be solved by normal power series methods. By letting $F_{(x)}=\sum_{n=0}^{\infty}a_n x^n$ we get the recurrence relation

$$a_{n+1}=\left[\frac{n(n+1)+\beta n-\gamma}{(n+1)(n+\alpha)}\right]a_n \tag{B-21}$$

For a physical solution the recurrence relation must terminate which means we get for the energy

$$E = BJ(J+1) + (A - B)K^2 \tag{B-22}$$

where

$$J = n_{max} + \frac{1}{2}|K + M| + \frac{1}{2}|K - M| \tag{B-23}$$

and n_{max} is the largest value of the integer n for which the recurrence relation (B-21) does not vanish. Note from Equation (B-23) that J (the total angular momentum) must be a positive integer such that

$$J = 0,1,2,\ldots$$

$$K = 0,\pm 1,\pm 2,\ldots,\pm J \tag{B-24}$$

$$M = 0,\pm 1,\pm 2,\ldots,\pm J$$

Finally , note that K and M represent the projection of the total angular momentum J onto the space-fixed (lab) axis and the molecule-fixed Z axis (axis of symmetry) respectively.

Bibliography

[1] E. Bright Wilson, Jr., J.C. Decius and Paul C. Cross, *Molecular Vibrations*, (Dover Publications,Inc., New York, 1980)

[2] C.H. Townes and A.L. Schawlow, *Microwave Spectroscopy*, (Dover Publications, Inc., New York, 1975)

[3] Harry C. Allen, Jr. and Paul C. Cross, *Molecular Vib-Rotors*, (John Wiley and Sons, Inc., New York, 1963)

[4] James K.G. Watson,"Aspects of Quartic and Sextic Centrifugal Effects on Rotational Energy Levels" in *Vibrational Spectra and Structure VI*, Ed. James R. Durig, (Elsevier Scientific Publishing Co., New York, 1977)

[5] Boris Podolsky, "Quantum-Mechanically Correct Form of Hamiltonian Function For Conservative Systems", Phys. Rev. 32, 812-816 (1928)

[6] E. Bright Wilson, Jr. and J.B. Howard, "The Vibration-Rotation Energy Levels of Polyatomic Molecules", J. Chem. Phys. 4, 260-268 (1936)

[7] Gilbert W. King, R.M. Hainer and Paul C. Cross, "The Asymmetric Rotor", J. Chem. Phys. 11, 27-42 (1943)

[8] Gilbert W. King, R.M. Hainer and Paul C. Cross, "The Asymmetric Rotor II: Calculation of Dipole Intensities and Line Classifications", J. Chem Phys. 12, 210-222 (1944)

[9] Daniel Kivelson and E. Bright Wilson, Jr., "Approximate Treatment of the Effect of Centrifugal Distortion on the Rotational Energy Levels of Asymmetric-Rotor Molecules", J. Chem. Phys. 20, 1575-1579 (1952)

[10] Daniel Kivelson and E. Bright Wilson, Jr., "Theory of Centrifugal Distortion Constants of Polyatomic Rotor Molecules", J. Chem Phys. 21, 1229-1236 (1953)

[11] W.D. Perkins and M. Kent Wilson, "The Infrared Spectrum of SF_2O_2", J. Chem. Phys. 20, 1791-1794 (1952)

[12] G.R. Hunt and M.K. Wilson, "The Infrared Spectrum of Sulfuryl Flouride", Spectrochimica Acta 16,570-574 (1960)

[13] Arlan W. Mantz, "Advances in Tunable-Diode-Laser Spectroscopy", Laser Focus, March,1987

[14] Robert M. Fristrom, "The Microwave Spectrum of a Slightly Aspherical Top - The Structure and Dipole Moment of Sulfuryl Flouride", J. Chem. Phys. 20, 1-5 (1952)

[15] D.E. Jennings, "Absolute Line Strengths in ν_4, $^{12}CH_4$: A Dual-Beam diode Laser Spectrometer With Sweep Integration", Applied Optics 19,2695-2700 (1980)

[16] R.S. King, J.F. Butler and K.J. Linden, "Tunable Diode Laser Spectroscopy: An Invited Review", Optical Engineering 19, 945-959 (1980)

[17] James K.G. Watson, "Determination of Centrifugal Distortion Coefficients of Asymmetric-Top Molecules", J. Chem. Phys. 46, 1935-1949 (1966)

[18] James K.G. Watson, "Determination of Centrifugal Distortion Coefficients of Asymmetric-Top Molecules III: Sextic Coefficients", J. Chem. Phys. 48, 4517-4524 (1967)

[19] M.R. Aleiv and James K.G. Watson, "Calculated Sextic Centrifugal Distortion Constants of Polyatomic Molecules", J. Mol. Spec. 61, 29-52 (1976)

[20] James K.G. Watson, "Centrifugal Corrections for Asymmetric-Top Molecules", J. Chem. Phys. 45, 1360-1361 (1966)

[21] B.P. Van Eijck, "Reformulation of Quartic Centrifugal Distortion Hamiltonian", J. Mol. Spec. 53, 246-249 (1974)

[22] James K.G. Watson, " A Planarity Relation for Sextic Centrifugal Distortion Constants", J. Mol. Spec. 65, 123-133 (1977)

[23] Phillip R. Bevington, *Data Reduction and Error Analysis for the Physical Sciences*, (McGraw Hill, New York, 1969)

[24] E. Bright Wilson, "The Vibration-Rotation Energy Levels of Polyatomic Molecules III: Effect of Centrifugal Distortion", J. Chem. Phys, 5, 617-620 (1937)

[25] Richard N. Zare, *Angular Momentum*, (John Wiley and Sons, Inc., New York, 1988)

[26] Gerard Herzberg, F.R.S.C., *Molecular Spectra and Molecular Structure, Vol II, Infrared and Raman Spectra of Polyatomic Molecules*, (Krieger Publishing Co., Malabar, Fla., 1991)

[27] Werner Brugel, *An Introduction to Infrared Spectroscopy*, (John Wiley and Sons, Inc., New York, 1962)

[28] G. Pierre, A.Valentin and L. Henry, "The Ground State of Silane Obtained From the Study of the Fourier Transform Spectroscopy of the ν_2 and ν_4 modes ", Can. J. Phys. 62, 254-259 (1984)

[29] J.K. Bragg and S. Golden, "The Interaction of Nuclear Electric Quadropole Moments With Molecular Rotation in Asymmetric Top Molecules II. Approximate Methods for First Order Coupling", Phys. Rev. 75, 735-738 (1949)

[30] S. Carter, "Asymvib, the computer program", (unpublished pamphlet), Dept. of Chemistry, Whitenights University, Reading RG6 2AD, England